Assembly and Arrangement of the Type Three Secretion System of *Yersinia enterocolitica*

Inauguraldissertation

zur

Erlangung der Würde eines Doktors der Philosophie

vorgelegt der Philosophisch-Naturwissenschaftlichen Fakultät

der Universität Basel

von

Marlise Amstutz

aus Sigriswil BE, Schweiz

Basel, 2014

Namensnennung-Keine kommerzielle Nutzung-Keine Bearbeitung 3.0 Schweiz
(CC BY-NC-ND 3.0 CH)

Sie dürfen: **Teilen** — den Inhalt kopieren, verbreiten und zugänglich machen

Unter den folgenden Bedingungen:

Namensnennung — Sie müssen den Namen des Autors/Rechteinhabers in der von ihm festgelegten Weise nennen.

Keine kommerzielle Nutzung — Sie dürfen diesen Inhalt nicht für kommerzielle Zwecke nutzen.

Keine Bearbeitung erlaubt — Sie dürfen diesen Inhalt nicht bearbeiten, abwandeln oder in anderer Weise verändern.

Wobei gilt:

- **Verzichtserklärung —** Jede der vorgenannten Bedingungen kann **aufgehoben** werden, sofern Sie die ausdrückliche Einwilligung des Rechteinhabers dazu erhalten.
- **Public Domain (gemeinfreie oder nicht-schützbare Inhalte) —** Soweit das Werk, der Inhalt oder irgendein Teil davon zur Public Domain der jeweiligen Rechtsordnung gehört, wird dieser Status von der Lizenz in keiner Weise berührt.
- **Sonstige Rechte —** Die Lizenz hat keinerlei Einfluss auf die folgenden Rechte:
    - Die Rechte, die jedermann wegen der Schranken des Urheberrechts oder aufgrund gesetzlicher Erlaubnisse zustehen (in einigen Ländern als grundsätzliche Doktrin des **fair use** bekannt);
    - Die **Persönlichkeitsrechte** des Urhebers;
    - Rechte anderer Personen, entweder am Lizenzgegenstand selber oder bezüglich seiner Verwendung, zum Beispiel für **Werbung** oder Privatsphärenschutz.
- **Hinweis —** Bei jeder Nutzung oder Verbreitung müssen Sie anderen alle Lizenzbedingungen mitteilen, die für diesen Inhalt gelten. Am einfachsten ist es, an entsprechender Stelle einen Link auf diese Seite einzubinden.

Quelle: http://creativecommons.org/licenses/by-nc-nd/3.0/ch/ Datum: 12.11.2013

Genehmigt von der Philosophisch-Naturwissenschaftlichen Fakultät auf Antrag von

Prof. Dr. Guy R. Cornelis und Prof. Dr. Henning Stahlberg

Basel, den 22.05.2012

Prof. Dr. Martin Spiess

Table of Contents

1 Summary

The type three secretion system (T3SS) is a bacterial weapon found in many Gram-negative bacteria. It consists out of a needle like structure called injectisome, which enables bacteria to inject effector proteins into eukaryotic cells. The injectisome is a very complex molecular machine, inserted in the inner and outer bacteria membrane, passing the periplasm with the peptidoglycan layer. We used an approach with fluorescent hybrid proteins to study the assembly order of the injectisome in *Yersinia enterocolitica*. First the outer membrane protein YscC was genetically fused to the red fluorescent protein mCherry. This construct was able to build fluorescent foci in the bacterial membrane by itself, without any other components of the T3SS. Then we engineered fusions between the green fluorescent protein EGFP and the inner membrane protein YscD, the putative C-ring protein YscQ or the ATPase YscN. All three constructs showed fluorescent foci at the bacterial membrane. Comparison of the different EGFP constructs with the YscC-mCherry construct in double mutants showed that the proteins co-localize. Thus we considered the foci to be a read out for injectisome assembly. By combining the EGFP constructs with different deletion mutants we found that the assembly occurs from the outside to the inside. Starting with the outer membrane protein YscC to the inner membrane. Then the ATPase and C-ring assemble together and finally the needle is formed.

Different single particle structures of T3SS, needle complexes, purified from *Shigella flexneri* and *Salmonella enterica* are available. But in the course of purification the inner membrane export apparatus, the ATPase complex and the C-ring were lost. As well no such complex has been purified from *Y. enterocolitica*. Thus we investigated the *Y. enterocolitica* injectisomes *in situ* by cryo electron tomography (cryo-ET). Unfortunately, the 1-µm diameter of *Y. enterocolitica* is too large to obtain optimal resolution with cryo-ET. Thus we engineered a *minD* mutant that forms so called minicells, due to asymmetric septum placement. We collected tomograms of particles from wild type and minicells and constructed an average structure with a resolution of 3.7 nm. In addition the 6 nm resolution *in situ* structure of the injectisome of *S. flexneri* was made. We saw significant stretching of the *in situ* structure compared to the isolated particles. Moreover we saw flexibility of the basal body. We can only speculate that such flexibility might increase the stability of the structure and protect it of mechanical forces. In addition for the first time we could visualize a mass in cytoplasm just below the middle of the injectisome. Due to homology to the flagellum we can assume, that this is the ATPase. But to conclusively assign proteins to masses seen in the *in situ* structure we would need to label them.

A question mark in the *Y. enterocolitica* injectisome assembly is, how the structure can pass the peptidoglycan layer. The flagellum, which is evolutionary closely related to the injectisome, as well as other types of injectisomes have a muramidase or more specifically lytic transglycosylase (LT) encoded within their loci. No gene encoding for a LT, can be found on the pYV plasmid that encodes otherwise for the entire T3SS. Thus we tested several genomic LT for their involvement in the assembly of the T3SS. It is possible that the injectisome assembles through temporary gaps

generated during the synthesis of new peptidoglycan strands. This theory is very intriguing, as the pattern of the fluorescent foci resembled closely the arrangement of the bacterial cytoskeleton protein MreB, which is assumed to be involved in placing the peptidoglycan synthesis machinery. Comparing the localization of MreB and the injectisome showed that both constructs seem to be arranged on two different helical paths. This convinced us that injectisome arrangement is not stochastic but rather controlled. To find the underlying structure responsible for this arrangement, we compared the localization of other proteins with similar arrangement as MreB. In *Bacillus subtilis* different membrane compositions were shown to be helically distributed. Unfortunately staining of the inner membrane is difficult in Gram-negative bacteria. Therefore we compared injectisome location with a potential bacterial lipid raft marker, which showed injectisomes do not insert into the lipid rafts.

Thus although our knowledge about the assembly, the structure and the function of the T3SS is improving enormously, the question of how injectisomes are localized remains to be answered.

2 General Introduction

In pathogenic bacteria several systems have evolved, allowing bacteria to survive the challenges of the host immune defence. Among these systems we find the type three secretion system (T3SS) of Gram-negative bacteria. The T3SS consists of a needle like structure, the injectisome, that allows bacteria to inject so called effector proteins, into the cytosol of eukaryotic cells (Cornelis & Wolf-Watz, 1997; Galan & Collmer, 1999). Some parts of the injectisome are comparable to components of the flagellum, which contains an export apparatus to export hook and filament proteins (Cornelis, 2006; Macnab, 2003). The effector function varies largely in the different bacteria. In *Yersinia* the effectors lead to impairment of the cytoskeleton dynamics and to apoptosis of macrophages, preventing phagocytosis and the onset of an inflammatory reaction, whereas e.g. in *Shigella* the effectors rearrange the cytoskeleton promoting *Shigella* uptake by non-phagocytic cells. The effectors are often difficult to identify as they share low identity and their genes can be spread over the entire genome. In contrast, the machinery proteins are rather well conserved and encoded together in pathogenicity islands or even on individual plasmids, as it is the case for *Yersinia*.

2.1 The *Yersinia* Ysc Injectisome

In *Yersinia enterocolitica* a 70 kb virulence plasmid termed pYV (for plasmid involved in *Yersinia* virulence) encodes the T3SS called “Ysc” (for Yop secretion) (Fig. 2.1). The over 30 proteins needed to assemble a fully functional injectisome are encoded in a few operons in close proximity of each other. The injectisome can very roughly be separated into four parts. First there is the basal body, which spans the inner and outer membrane, second the cytosolic part with the ATPase complex, third the inner membrane export apparatus, which presumably allows export through the inner membrane and last but not least the extracellular part consisting out of a hollow tube with a tip structure at its distal end (Fig. 2.2).

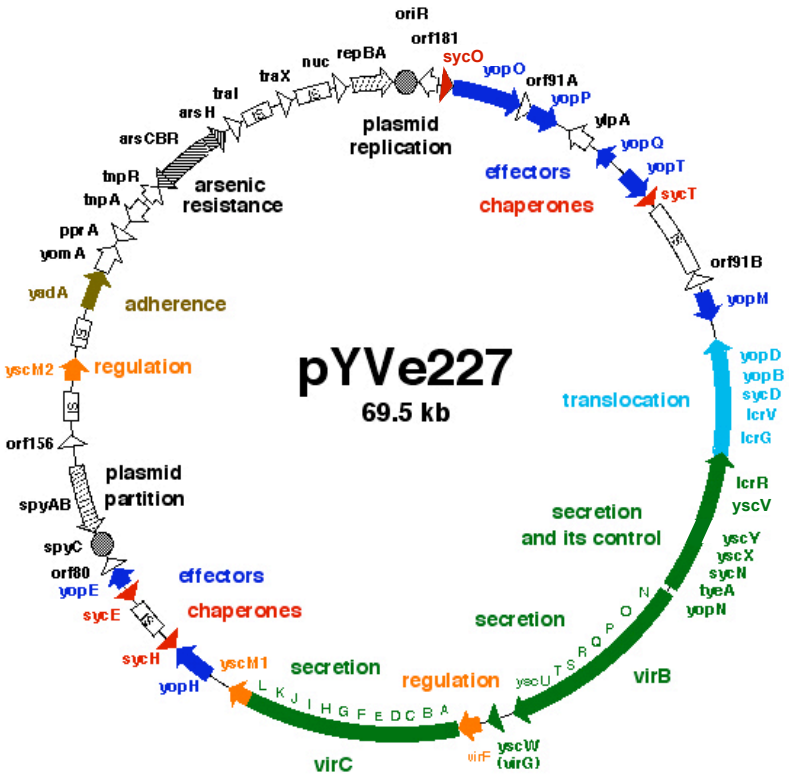

Fig. 2.1: Genetic Map of pYVe227; (adapted from (Iriarte & Cornelis, 1999))

Detailed genetic map of the pYVe227. The genes are coloured according to their function. Green: Ysc secretion machinery and control genes; light blue: tip and pore; dark blue: effectors; red: effector chaperones; orange: gene expression regulators; khaki: an adhesin; different patterns: plasmid replication, arsenic resistance, plasmid partition

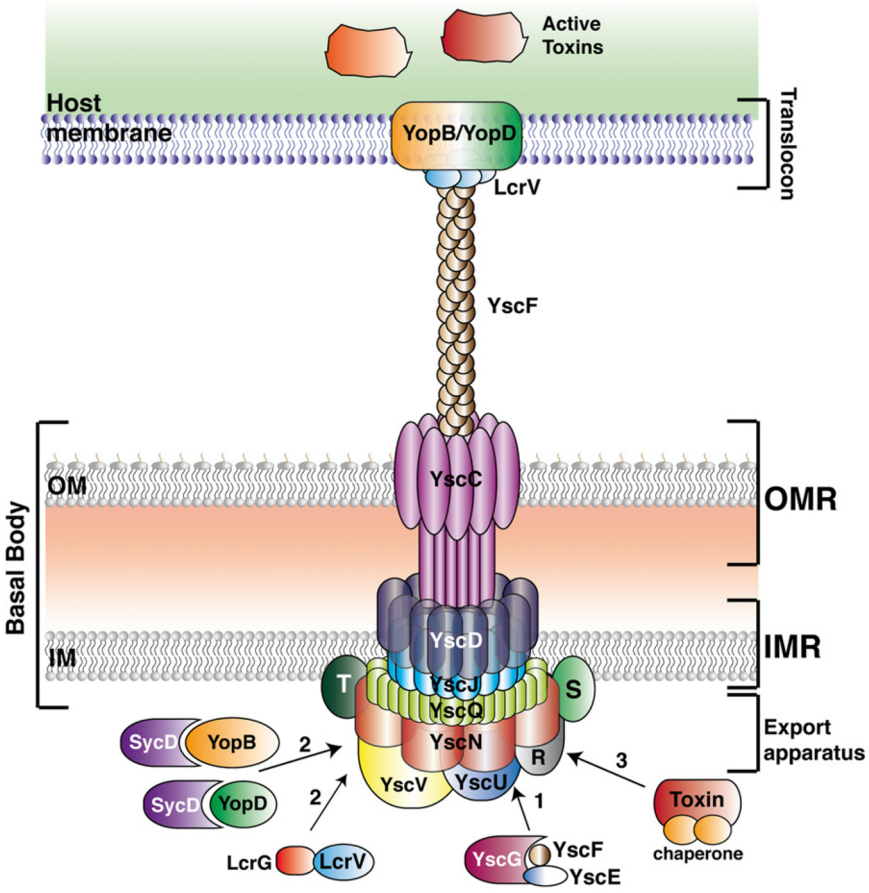

Basal body			
Yersinia	YscC	YscD	YscJ
Pseudomonas	PscC	PscD	PscJ
Shigella	MxiD	MxiG	MxiJ
Salmonella	InvG	PrgH	PrgK
E. coli	EscC	EscD	EscJ

Export apparatus						
YscQ	YscN	YscR	YscS	YscT	YscU	YscV
PscQ	PscN	PscR	PscS	PscT	PscU	PcrD
Spa33	Spa47	Spa24	Spa9	Spa29	Spa40	MxiA
SpaO	InvC	SpaP	SpaQ	SpaR	SpaS	InvA
SepQ	EscN	EscR	EscS	EscT	EscU	EscV

Translocon			
Yersinia	YopB	YopD	LcrV
Pseudomonas	PopB	PopD	PcrV
Shigella	IpaB	IpaC	IpaD
Salmonella	SipB	SipC	SipD
E. coli	EspD	EspB	EspA

Needle
YscF
PscF
MxiH
PrgI
EscF

Chaperones			
SycD	LcrG	YscG	YscE
PcrH	PcrG	PscG	PscE
IpgC	n.i.	n.i.	n.i.
SicA	n.i.	n.i.	n.i.
CesD	n.i.	n.i.	n.i.

Fig. 2.2: The *Yersinia* Ysc Injectisome (Izoré et al, 2011)

Schematic illustration of the *Yersinia* Ysc injectisome. The basal body spans the inner and outer bacterial membrane. The hollow needle bridges the distance to the eukaryotic cell, allowing the tip to insert the pore into the host membrane. The table lists homologous proteins in *Pseudomonas*, *Shigella*, *Salmonella* and pathogenic *E. coli* spp; n.i.: molecules that were not yet identified. Note: in this table is no separation between the transmembrane proteins of the export apparatus and the cytoplasmic proteins and effectors are called toxins.

2.1.1 Basal Body

The basal body consists of three proteins (Kimbrough & Miller, 2000; Marlovits & Stebbins, 2009), an outer membrane protein and two inner membrane proteins. The outer membrane protein (YscC, MxiD, InvG in *Yersinia*, *Shigella* and *Salmonella*[1]) belongs to the secretin family. Secretins are found in type 2 secretion systems, type IV pili and filamentous phages. They contain an N-terminal sec signal sequence, followed by a large periplasmic domain, called N-terminal domain. This N-terminal domain can vary depending on its direct function but is conserved between secretins of related systems. The C-terminal domain is conserved over the entire secretin family

[1] For simplicity the *Yersinia* protein and its homologues in *Shigella* and *Salmonella* will in future always be mentioned in this order. When homologues of other systems are mentioned it will be specified.

and is the part that is inserted into the membrane (Genin & Boucher, 1994). The very C-terminus is variable and differs even between the different secretins of the T3SS (Daefler & Russel, 1998). This C-terminus is the interaction part to the corresponding pilotin (Daefler et al, 1997), YscW (formally known as VirG) in *Yersinia*. The pilotin is a lipoprotein needed for the correct targeting of the secretin to the outer membrane (Hardie et al, 1996). Secretins form stable rings, which for YscC was suggested to contain 13 subunits (Koster et al, 1997).

YscJ/MxiJ/PrgK homologues are Sec dependant lipoproteins placed in the periplasmic leaflet of the inner membrane. In addition to their lipid anchor they contain a C-terminal transmembrane domain (Michiels et al, 1991). Structural studies of EscJ, the YscJ homologue in enteropathogenic *E. coli* (EPEC), showed that it consists out of two subdomains connected by a linker. Crystal packing and molecular modelling are suggesting EscJ forms a 24-subunit ring (Crepin et al, 2005; Yip et al, 2005).

Proteins forming the second inner membrane protein, YscD/MxiG/PrgH, are less conserved. They contain a N-terminal cytoplasmic domain that shares high sequence similarity to a forkhead-associated domain, a transmembrane part and a large C-terminal periplasmic domain (Allaoui et al, 1995; McDowell et al, 2011; Pallen et al, 2002). The crystal structure of the periplasmic domain of PrgH reveals 3 subdomains with analogous folds; a wedge-shaped structure with two α-helices folding against a 3 stranded β-sheet, called ring-building motif. This same fold is found in the two domains of EscJ and in the structure of the periplasmic part of the EPEC secretin, EscC (Spreter et al, 2009).

2.1.2 The Cytosolic Components: ATPase Complex

Four cytosolic proteins, which are essential to build a functional T3SS, are thought to be structural parts of the injectisome: YscN, YscK, YscL and YscQ. Interactions between these proteins, shown in yeast two and three hybrid assays, suggest that these four proteins form a complex (Jackson & Plano, 2000). YscN/Spa47/InvC show homology to the F_0F_1 ATPase. The ATPase function is activated by oligomerization to a hexameric (or double hexameric) ring (Akeda & Galan, 2004; Andrade et al, 2007; Eichelberg et al, 1994; Müller et al, 2006; Pozidis et al, 2003; Woestyn et al, 1994; Zarivach et al, 2007). YscL/MxiN/OrgB, which seem to be evolutionary linked to the stalk of the F_0F_1 ATPase, has been shown to be a negative regulator of the ATPase activity (Blaylock et al, 2006; Pallen et al, 2006). YscK/MxiK/OrgA, which have no obvious analogue in the flagellum, interact with the ATPase (Jouihri et al, 2003; Morita-Ishihara et al, 2006). In *S. flexneri* Spa47, MxiN, Spa33 and MxiK were purified as a complex (Johnson & Blocker, 2008). YscQ/Spa33/SpaO show some homology to the flagellar C-ring protein FliN. FliG, FliM and FliN build a cup like structure in the cytoplasm co-purifying with the flagellum (Francis et al, 1994; Khan et al, 1992; Schuster & Baeuerlein, 1992). This C-ring is responsible for the switching of the rotation direction of the flagellum (Macnab, 2003). There is no evidence for rotation of the T3S needle and the

function of YscQ and its homologues are not elucidates, yet. In *Pseudomonas syringae* two interacting proteins $HrcQ_A$ and $HrcQ_B$, which are encoded in genes next to each other, are the homologues of the flagellar C-ring proteins FliN/FliM (Fadouloglou et al, 2004). Immuno-gold staining placed Spa33 at the base of purified *Shigella* needle complexes but no ring like structure as in flagella could be visualized (Morita-Ishihara et al, 2006). The ATPase, the stalk-like protein and the C-ring protein build complexes at least in *Shigella* and EPEC (Biemans-Oldehinkel et al, 2011; Johnson & Blocker, 2008; Jouihri et al, 2003).

2.1.3 The Export Apparatus

YscR, YscS, YscT, YscU and YscV are essential transmembrane proteins, which share high sequence homology to flagellar proteins. YscR (24 kDa), YscS (10 kDa) and YscT (28 kDa) are believed to consist almost entirely of transmembrane domains (Fig. 2.3) (for a review see Ghosh 2004). YscV (also called LcrD) and YscU contain in addition to the transmembrane domains a large C-terminal cytoplasmic domain.

By fusions of PhoA at different places of YscU four transmembrane helices were demonstrated (Allaoui et al, 1994). The cytoplasmic domain of YscU/Spa40/SpaS and the flagellar homologue FlhB contain an auto-cleavage site, but after cleavage the two parts stay attached (Ferris & Minamino, 2006; Fraser et al, 2003; Lavander et al, 2002; Minamino & Macnab, 2000). Mutations in the auto-cleavage site of YscU prevent export of the translocators (Sorg et al, 2007). Specific point mutations in *flhB* can restore motility in mutants lacking the flagellar filament due to a mutation in *fliK* (Kutsukake et al, 1994; Williams et al, 1996). Analogous point mutations in *yscU* can partially restore secretion in an *yscP* deletion strain (Edqvist et al, 2003). This suggests that YscU is involved in substrate specificity.

YscV/MxiA/InvA and their flagellar homologue FlhA contain eight transmembrane helices (Plano et al, 1991). The crystal structures of the C-terminal domain of FlhA and InvA show the same ring-building motif as seen in the basal body proteins (Bange et al, 2010; Lilic et al, 2010; Moore & Jia, 2010; Worrall et al, 2010), but still the function of YscV is unknown.

EscR, the EPEC homologue of YscR/Spa24/InvL, interacted in a yeast two-hybrid screen with EscS, EscU and with itself (Creasey et al, 2003). In *Clostridium* the flagellar genes for *fliR* (*yscT*) and *flhB* are fused. Analogue to this an engineered fusion between these two proteins can restore swimming in a fliR flhB double mutant (Van Arnam et al, 2004). This suggests a proximity or even interaction of YscU and YscT.

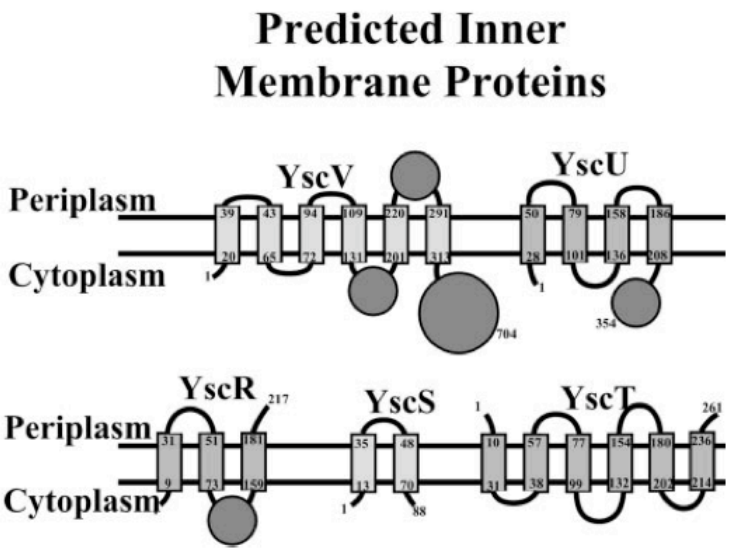

Fig. 2.3: Predicted Inner Membrane Proteins (Ghosh, 2004)
Schematic illustration of the predicted inner membrane proteins. YscR, YscS, YscT consist almost completely of transmembrane helices. YscV and YscU contain appart of the transmembrane helices also a large cytosolic domain.

2.1.4 The Needle, the Tip and the Pore

The needle is a hollow tube made by helical polymerization of a small protein YscF/MxiH/PrgI (Cordes et al, 2003; Hoiczyk & Blobel, 2001; Kubori et al, 2000; Tamano et al, 2000). In the *Yersinia* Ysc and *Pseudomonas aeruginosa* Psc, two chaperones YscE/PscE and YscG/PscG build a complex with the needle subunit YscF/PscF preventing it to polymerize in the cytoplasm (Quinaud et al, 2005; Quinaud et al, 2007; Sun et al, 2008). The needle has an outer and inner diameter of 7 and 2 nm, respectively and is about 60 nm long (Hoiczyk & Blobel, 2001). In *Yersinia* the needle length can be varied by sequence insertion or deletion into repeat regions of *yscP*; the longer the amino acid sequence of the YscP repeat region the longer the needle (Journet et al, 2003). Even more, if the length of YscP is varied by breaking α-helices, the needle length changes accordingly (Wagner et al, 2009). Thus YscP can be seen as a molecular ruler. This is similar to the hook length control in flagella, which is mediated by FliK (Kawagishi et al, 1996; Williams et al, 1996). Interestingly in the T3SS of *S. enterica* a deletion of the *yscP* homologue *invJ* does not only make long deregulated needles, it also misses the inner rod made by PrgJ (Marlovits et al, 2006).

A pentameric tip made by LcrV/IpaD/SipD is concluding the needle (Mueller et al, 2005). The tip is the scaffold for the pore, which is formed upon contact with the host cell. This pore is made by two hydrophobic proteins YopB/IpaB/SipB and YopD/IpaC/SipC (Blocker et al, 1999; Cornelis & Wolf-Watz, 1997; Hakansson et al, 1993; Ménard et al, 1993). The tip and pore proteins are often referred to as translocators, as they are required for effector translocation into the eukaryotic cell, but not for secretion into the culture media.

2.2 Different Injectisome Families

Gene clusters encoding T3SS are found in many proteobacteria and in *Chlamydiales* (Pallen et al, 2005). Phylogenetic analysis allows classification of the T3SS in seven different families; Ysc, Inv-Mxi-Spa, Ssa-Esc, Rhizobiales, Chlamydiales, Hrc-Hrp1 and Hrc-Hrp2 (Fig. 2.4) (Troisfontaines & Cornelis, 2005). Injectisomes of the Ysc family can be found e.g. in *P. aeruginosa*, *Aeromonas* spp. and *Bordetella* spp. Injectisomes of the Inv-Mxi-Spa family can be found e.g. in *S. enterica*, *S. flexneri* and as well in *Y. enterocolitica*. The high-virulence *Y. enterocolitica* biotype 1B (or American strains) contain, apart from the Ysc system, also a second T3SS, the Ysa system, which is encoded in a pathogenicity island on the genome and belongs to the family of Inv-Mxi-Spa T3SS (Haller et al, 2000). The archetype of the Ssa-Esc family is the Esc T3SS of enteropathogenic and enterohemorrhagic *E. coli* (EPEC and EHEC). It contains a filament made by EspA expanding the needle (Knutton et al, 1998; Sekiya et al, 2001). Hrc-Hrp1 and Hrc-Hrp2 T3SS can be found in plant pathogens. Plant cells are structural different of animal cells. They have a cell wall protecting them. To account for these special conditions the Hrc-Hrp1 and 2 systems replaced the needle with a pilus of up to 3 µm length (Cornelis & Van Gijsegem, 2000).

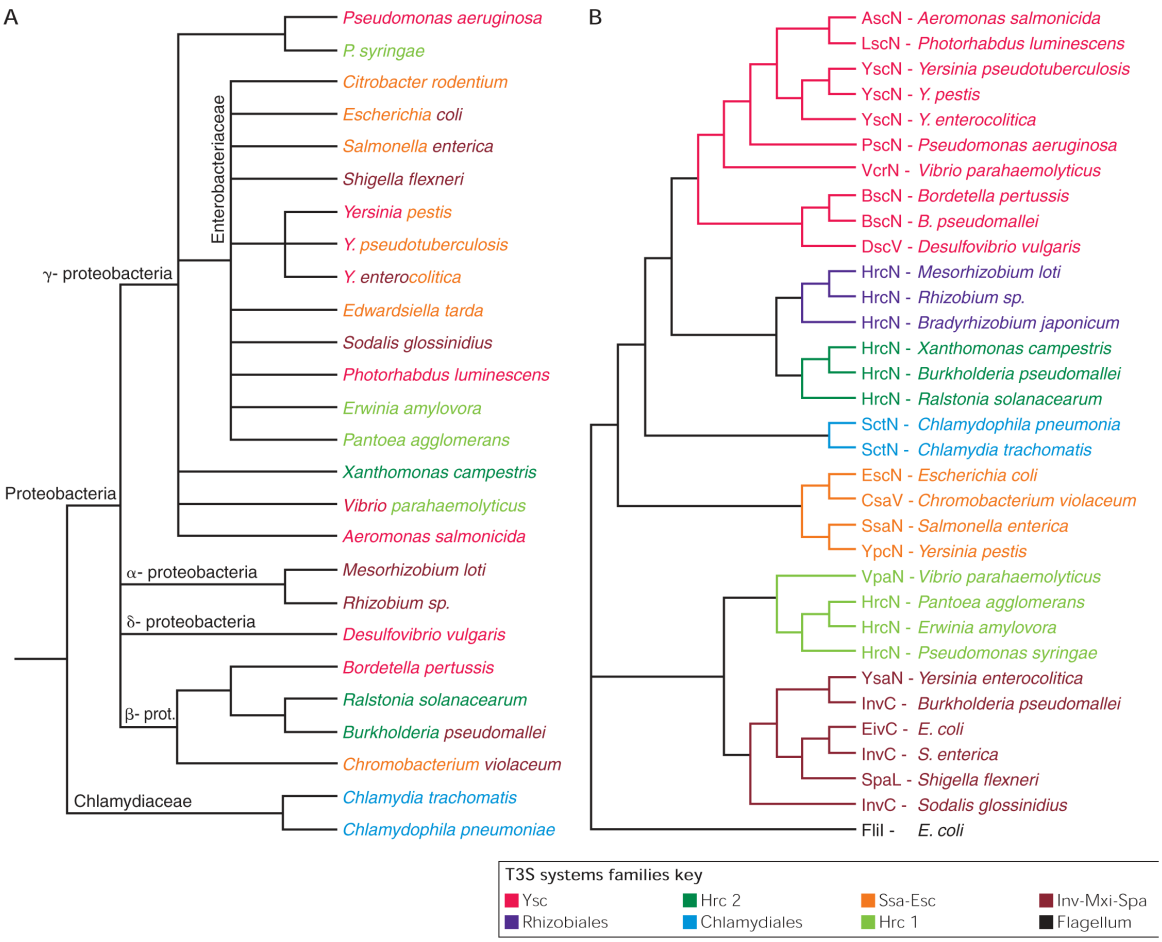

Fig. 2.4: Phylogenetic Tree of Bacteria T3SS (Troisfontaines & Cornelis, 2005)

A: rRNA tree made with aligned sequences from the Ribosomal Database Project II.

B: relationship phylogram of the ATPases of injectisomes and the ATPase of the *E. coli* flagellum. The seven T3S families are represented in different colours; the same colours are used in the rRNA tree to illustrate the lack of correlation between the two trees. The bacteria with mixed colours in the rRNA tree contain 2 or 3 T3SS of different families.

2.2.1 The Inv-Mxi-Spa Family: a Structural Insight

The most extensive structural studies have been done on the T3SS of *S. flexneri* and *S. enterica* encoded on the *Salmonella* pathogenicity island 1 (SPI1) both archetypes of the Inv-Mxi-Spa family. One of the milestones in the structural understanding of T3SS is the purification of those two machines (Blocker et al, 2001; Kubori et al, 1998; Tamano et al, 2000). The EPEC complex from the Ssa-Esc family has been purified as well (Sekiya et al, 2001), but much less follow up work has been done on this structure. The export apparatus and the cytosolic components are not co-purifying with these structures, which are often referred to as needle complexes. Mainly five proteins could be found to make up these needle complexes: the secretin MxiD/InvG, the two inner membrane proteins MxiJ/PrgK and MxiG/PrgH, the needle subunit MxiH/PrgI and MxiI/PrgJ which is thought to form an inner rod (Marlovits et al, 2004). By now reconstruction of these purified needle complexes show a resolution of around 2.5 nm for *S. flexneri* (Hodgkinson et al, 2009) and about 1 nm for *S. enterica* (Schraidt & Marlovits, 2011). In *S. enterica* a 15 fold symmetry is seen for the outer membrane ring and a 24 fold symmetry for the inner membrane ring (Schraidt & Marlovits, 2011), while in *S. flexneri* a 12 fold symmetry is reported for inner and outer membrane rings (Hodgkinson et al, 2009). These EM structures allow fitting of structures retrieved from X-ray and NMR analysis (see Fig. 2.5). The fitting of the crystal structure of the N-terminal part of EscC suggests that the secretin reaches deep down in the periplasm (Spreter et al, 2009). But it can only be guessed where structures like the ATPase and c-ring have to be placed.

Functional component	Characterized homologues	Available structures
Translocon	EspB, EspD[1]	AFM
	PopD(CBD):PcrH[2]	X-ray
	IpaB(CBD):IpgC[3]	X-ray
Tip	**LcrV[4]**	X-ray
	IpaD[3]	X-ray
	BipD[5]	X-ray
	EspA[1]	X-ray
Needle	YscF[4]	X-ray
	PrgI[6]	X-ray; NMR
	MxiH[3]	X-ray; EM
	BsaL[5]	NMR
	PscF[2]	X-ray
OM - Secretin	**EscC[1]**	X-ray
	InvG[6]	EM
	YscC[4]	EM
OM - Pilotin	**MxiM[3]**	X-ray
	MxiM:secretin[3]	NMR
Inner membrane	**PrgH[6]**	X-ray
	EscJ[1]	X-ray
	EscJ[1]	NMR
Export apparatus	**EscN[1]**	X-ray
	EscU[1]	X-ray
	YscU[4]	X-ray
	SpaS[6]	X-ray
	Spa40[3]	X-ray
	InvA[6]	X-ray
	HrcQ (C-ring)[2]	X-ray

[1]EPEC, [2]*Pseudomonas*, [3]*Shigella*, [4]*Yersinia*, [5]*Burkholdiria*, [6]*Salmonella*; CBD – chaperone binding domain.

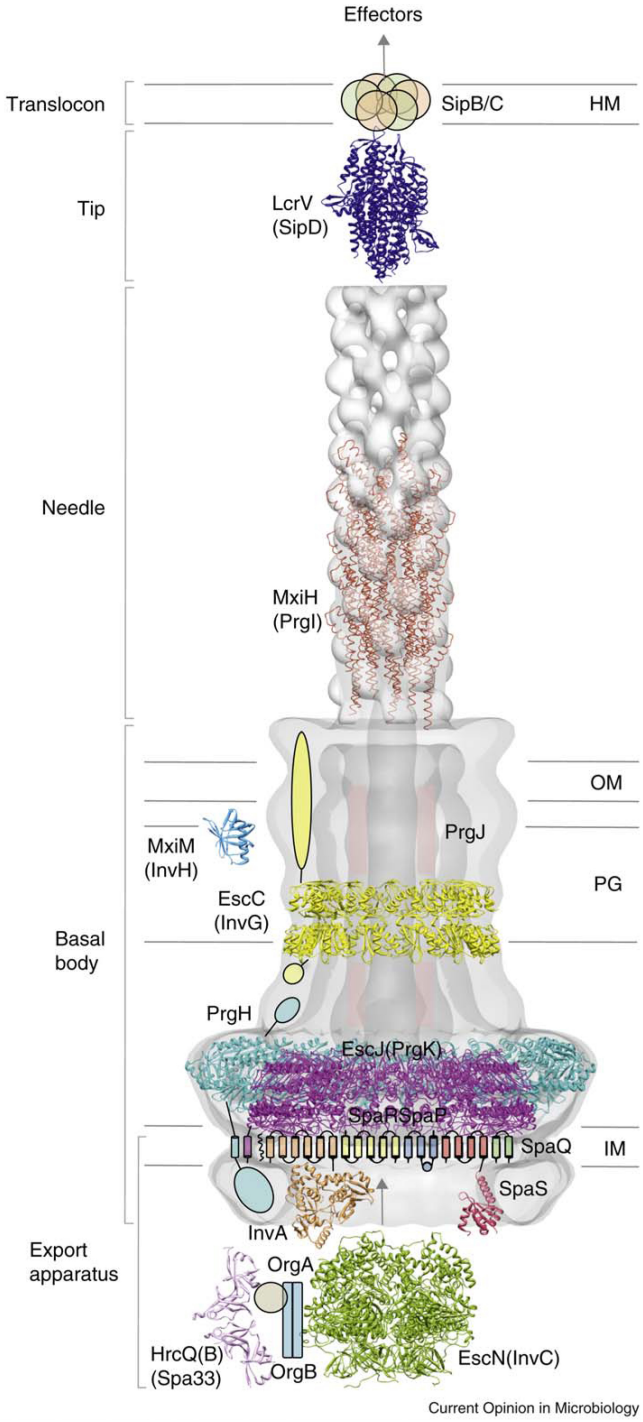

Fig. 2.5: Structural Overview of T3SS Injectisomes (Worrall et al, 2011)

Molecular structures of the individual components are modelled into the 3D electron micrograph reconstructions of both *Salmonella* needle-complex (Marlovits et al, 2004) and *Shigella* needle (Quinaud et al, 2007). Modelled positions of EscC, PrH and EscJ placed according to (Sanowar et al, 2010) and MxiH according to (Zhang et al, 2006). Position of remaining structures for illustration only. All available structures listed in table including species and method used, the structures highlighted in bold are shown in the figure. IM: inner-membrane, PG: peptidoglycan, OM: outer-membrane, and HM: host-membrane.

3 Aim of the Thesis

In the frame of this work, we tried to study the steps needed for the assembly of the *Y. enterocolitica* Ysc injectisome. In which order are the different subunits arranged? Why are they building up at this place in the bacterium and not somewhere else? How can the injectisome pass the peptidoglycan layer?

4 Assembly of the *Y. enterocolitica* Injectisome

4.1 Introduction

The flagellum and the injectisomes are evolutionary closely related. But the flagellar research has started much earlier than the injectisome research and thus it is also more advanced in several points. For example the flagellum can be purified since more than half a century (Koffler & Kobayashi, 1957) while the first injectisome was purified in 1998 (Kubori et al, 1998). The possibility to purify the flagellum and substructures of the flagellum allowed assessment of the flagellar assembly order. In an array of deletion mutants it was checked at which point flagellar assembly stalled. It was found, that flagellar assembly starts at the MS-ring in the inner membrane, then continues with the C-ring after this it grows from inside out, crossing the peptidoglycan and the outer membrane (Fig. 4.1) (Kubori et al, 1992; Suzuki et al, 1978). When the MS-ring components of the *S. enterica* T3SS are overexpressed they can form a ring (Kimbrough & Miller, 2000), this speaks for an assembly start in the inner membrane, same as in flagella. But the outer membrane secretin is well known to form stable rings on its own as well (Crago & Koronakis, 1998; Koster et al, 1997). This would mean that the assembly starts with the inner and outer rings, which then somehow join and allow the rest of the structure to assemble (Fig. 4.2) (Kimbrough & Miller, 2002). Here we studied the assembly of the *Y. enterocolitica* Ysc T3SS with an approach that is not depending on purification of substructures. This allows us to evaluate the assembly of the C-ring protein YscQ and the ATPase YscN, which are lost in purified particles.

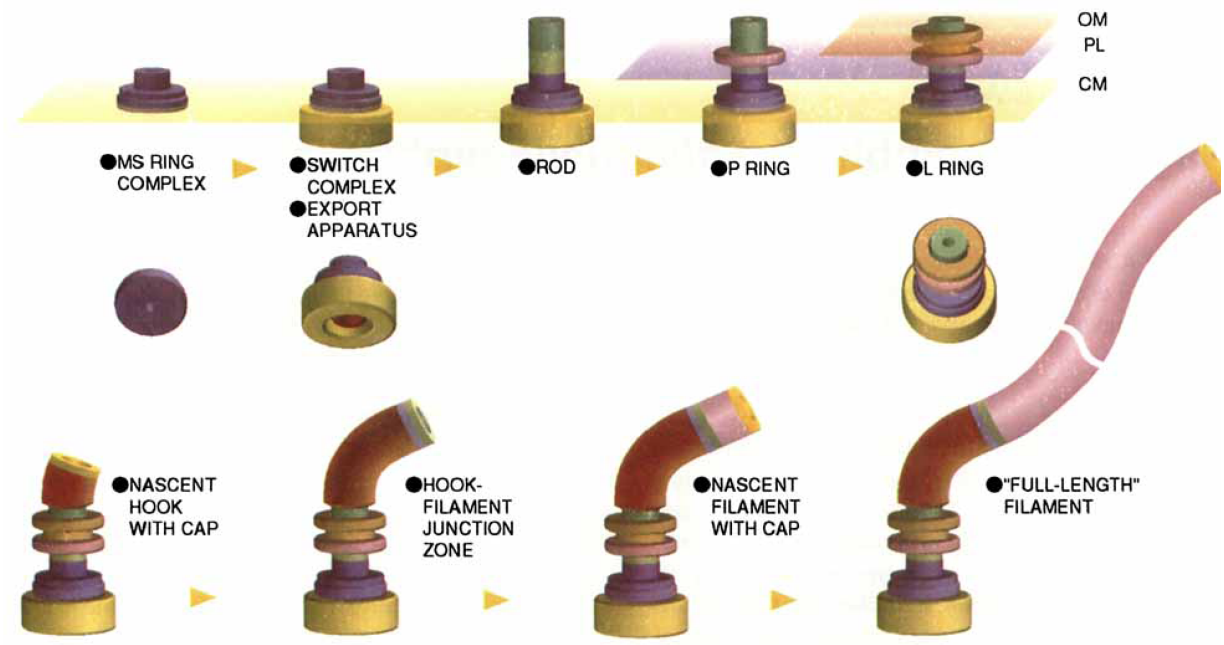

Fig. 4.1: Schematic illustration of flagellar assembly (Aizawa, 1996)

Flagellar assembly starts with the MS-ring (top left), and then it continues with the cytoplasmic ring. This inner membrane complex grows then through the peptidoglycan and the outer membrane (top right). Then the hook (bottom left) is formed and finally the filament can grow (bottom right).

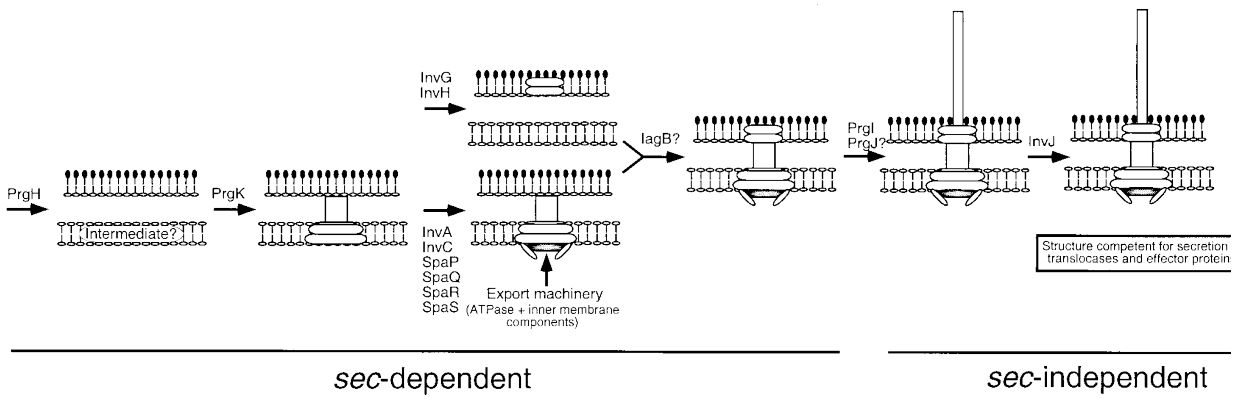

Fig. 4.2: Schematic illustration of *S. enterica* T3SS assembly (Sukhan et al, 2001)

In *S. enterica* first the MS-ring and the outer membrane secretin ring form independently of each other. Both rings join and the rest of the injectisome is formed in a sec-independent manner.

4.2 Statement of Personal Contribution

I contributed to this manuscript in designing, performing and analyzing experiments. I generated the plasmids and strains labelled with pMA…, together with Andreas Diepold I generated the fluorescence microscopy images and helped writing the paper.

4.3 Original Publication

The EMBO Journal (2010), 1–13 | © 2010 European Molecular Biology Organization | All Rights Reserved 0261-4189/10
www.embojournal.org

THE
EMBO
JOURNAL

Deciphering the assembly of the *Yersinia* type III secretion injectisome

Andreas Diepold, Marlise Amstutz, Sören Abel, Isabel Sorg, Urs Jenal and Guy R Cornelis*

Infection Biology, Biozentrum der Universität Basel, Basel, Switzerland

The assembly of the *Yersinia enterocolitica* type III secretion injectisome was investigated by grafting fluorescent proteins onto several components, YscC (outer-membrane (OM) ring), YscD (forms the inner-membrane (IM) ring together with YscJ), YscN (ATPase), and YscQ (putative C ring). The recombinant injectisomes were functional and appeared as fluorescent spots at the cell periphery. Epistasis experiments with the hybrid alleles in an array of injectisome mutants revealed a novel outside-in assembly order: whereas YscC formed spots in the absence of any other structural protein, formation of YscD foci required YscC, but not YscJ. We therefore propose that the assembly starts with YscC and proceeds through the connector YscD to YscJ, which was further corroborated by co-immunoprecipitation experiments. Completion of the membrane rings allowed the subsequent assembly of cytosolic components. YscN and YscQ attached synchronously, requiring each other, the interacting proteins YscK and YscL, but no further injectisome component for their assembly. These results show that assembly is initiated by the formation of the OM ring and progresses inwards to the IM ring and, finally, to a large cytosolic complex.

The EMBO Journal advance online publication, 7 May 2010; doi:10.1038/emboj.2010.84
Subject Categories: microbiology & pathogens
Keywords: microbial pathogenesis; nanomachine; protein complex assembly; protein transport

Introduction

The type III secretion (T3S) apparatus, also called injectisome, allows bacteria to export effector proteins on contact with eukaryotic cell membranes (Cornelis and Wolf-Watz, 1997; Galan and Collmer, 1999; Cornelis and Van Gijsegem, 2000). Effectors (called Yops in *Yersinia*) display a large repertoire of biochemical activities and modulate the function of crucial host regulatory molecules to the benefit of the bacterium (Alfano and Collmer, 2004; Mota and Cornelis, 2005; Grant *et al*, 2006). In *Yersinia spp.*, the injectisome is built when temperature reaches 37°C and export of the Yops can be artificially triggered, in the absence of cell contact, by Ca^{2+} chelation (Cornelis, 2006).

About 25 proteins (called Ysc in *Yersinia*) are needed to build the injectisome. Most of these are structural components, but some are ancillary components that are only involved during the assembly process and are either shed afterwards (e.g. the molecular ruler) or kept in the cytosol (e.g. chaperones). In contrast to the large diversity observed among effectors, the core proteins forming the injectisome (YscC, J, N, Q, R, S, T, U, V, and, to a lesser extent, YscD in *Yersinia*) are well conserved (Van Gijsegem *et al*, 1995; Cornelis, 2006).

A number of injectisome proteins copurify as a complex cylindrical structure, resembling the flagellar basal body. This structure, called the needle complex, consists of two pairs of rings that span the inner membrane (IM) and outer membrane (OM) of bacteria, joined together by a narrower cylinder and terminated by a needle, a filament, or a pilus (Kubori *et al*, 1998; Blocker *et al*, 1999; Kimbrough and Miller, 2000; Daniell *et al*, 2001; Jin and He, 2001; Sekiya *et al*, 2001; Morita-Ishihara *et al*, 2006; Sani *et al*, 2007; Hodgkinson *et al*, 2009; Schraidt *et al*, 2010). The needle is a hollow tube assembled through helical polymerization of a small protein (around 150 copies of YscF in *Yersinia*) (Cordes *et al*, 2003; Deane *et al*, 2006). It terminates with a tip structure serving as a scaffold for the formation of a pore in the host cell membrane (Mueller *et al*, 2005). The ring spanning the OM (hereafter called OM ring) and protruding into the periplasm consists of a 12–14mer of a protein from the YscC family of secretins (Koster *et al*, 1997; Kubori *et al*, 2000; Tamano *et al*, 2000; Blocker *et al*, 2001; Marlovits *et al*, 2004; Burghout *et al*, 2004b; Spreter *et al*, 2009). The lower ring spanning the IM is called MS ring and made of a lipoprotein (YscJ in *Yersinia*, MxiJ in *Shigella*, PrgK in *Salmonella enterica* SPI-1) proposed to form a 24-subunit ring (Kimbrough and Miller, 2000; Crepin *et al*, 2005; Yip *et al*, 2005; Silva-Herzog *et al*, 2008; Hodgkinson *et al*, 2009). A protein from the less-conserved YscD family (MxiG in *Shigella*, PrgH in *S. enterica* SPI-1), which has the same general fold as the components of the two rings, is proposed to participate in MS ring formation and possibly connect the rings in the two membranes (Spreter *et al*, 2009).

Besides these proteins forming a rigid scaffold, the injectisome contains five essential integral membrane proteins (YscR, S, T, U, V), which are believed to recognize export substrates (Sorg *et al*, 2007) and form the export channel across the IM. Some of them, if not all, are likely to be inserted in a patch of membrane enclosed within the MS ring, but this could not be shown so far. We will refer to these proteins as to the 'export apparatus'. At the cytosolic side of the injectisome, an ATPase of the AAA^+ family (YscN) forms a hexameric ring that is activated by oligomerization (Woestyn *et al*, 1994; Pozidis *et al*, 2003; Muller *et al*, 2006; Zarivach *et al*, 2007) and resembles the flagellar ATPase FliI

*Corresponding author. Biozentrum der Universität Basel, Universität Basel, Infection Biology, Klingelbergstrasse 50-70, Basel CH 4056, Switzerland. Tel.: +41 61 267 2110; Fax: +41 61 267 2118;
E-mail: guy.cornelis@unibas.ch

Received: 12 January 2010; accepted: 13 April 2010

(Abrahams *et al*, 1994; Imada *et al*, 2007). The ATPase is associated with two proteins (YscK, L) (Jackson and Plano, 2000; Blaylock *et al*, 2006), one of them (YscL) probably exerting a control on the ATPase activity as was shown for FliH in the flagellum (Minamino and MacNab, 2000; Gonzalez-Pedrajo *et al*, 2002; McMurry *et al*, 2006). The ATPase is strikingly similar to the α and β subunits of the stator of the F_0F_1 ATP synthase (Abrahams *et al*, 1994), suggesting an evolutionary relation. This assumption is reinforced by the sequence similarity observed between $YscL_{N\text{-}term}$ and the b subunit of the F-type ATPase, and between $YscL_{C\text{-}term}$ and the δ subunit of the same ATPase (Pallen *et al*, 2006). A function of the ATPase, characterized in *S. enterica* Typhimurium SPI-1, is to detach some T3S substrates from their cytoplasmic chaperone before their export and to unfold the exported proteins in an ATP-dependent manner (Akeda and Galan, 2005). It is likely that the ATPase also directly energizes export, but the proton motive force is also involved (Wilharm *et al*, 2004; Minamino and Namba, 2008; Paul *et al*, 2008).

In the flagellum, the most proximal part of the basal body is the 45–50 nm C ring (for cytosolic) made of FliM and FliN (Driks and DeRosier, 1990; Khan *et al*, 1992; Kubori *et al*, 1997; Young *et al*, 2003; Thomas *et al*, 2006). Together with FliG, it forms the switch complex reversing the rotation of the motor, but in its absence, no filament appears, indicating that it is also involved in the export of distal constituents (Macnab, 2003). However, recent reports (Konishi *et al*, 2009; Erhardt and Hughes, 2010) showed that in C ring mutants, the export function can be partially restored by overexpression of the ATPase or the master regulator. No such C ring could be visualized so far by electron microscopy in a needle complex, but proteins of the YscQ family, which are essential components of all injectisomes, have a significant similarity to FliN and FliM. In *Pseudomonas syringae*, the orthologue of YscQ even appears as two products called $HrcQ_A$ and $HrcQ_B$, which interact with each other, and the overall fold of $HrcQ_B$ is remarkably similar to that of FliN (Fadouloglou *et al*, 2004). This suggests that injectisomes do have a C ring, although they have not been reported to rotate. YscQ and its homologues have been shown to bind the ATPase complex (Jackson and Plano, 2000) as well as substrate–chaperone complexes (Morita-Ishihara *et al*, 2006). The C ring would, therefore, form a platform at the cytoplasm/IM interface for the recruitment of other proteins. In agreement with this assumption, immunogold-labelling experiments have shown that the *Shigella* orthologue of YscQ (Spa33) localizes to a lower portion of the injectisome (Morita-Ishihara *et al*, 2006). A list of homologues in the flagellum and the various archetypal T3S systems is given in Supplementary Table 3.

The assembly of the flagellum is for the most part linear and sequential, proceeding from more proximal structures to more distal ones. The proposed scenario is that the plasma membrane ring (called the MS ring) formed by FliF assembles first, followed by periplasmic components, OM components, and finally components that lie in the cell exterior (Kubori *et al*, 1992; Macnab, 2003). The C ring (FliG, FliM, FliN) is thought to appear immediately after the MS ring, because it forms spontaneously when its components are overexpressed in the presence of FliF even in the absence of any other component (Kubori *et al*, 1997; Lux *et al*, 2000; Young *et al*, 2003).

Less is known about the assembly steps of the injectisome. The heterologous overexpression of the *S. enterica* SPI-1 MS ring components PrgH and PrgK in *Escherichia coli* leads to stable ring structures (Kimbrough and Miller, 2000). The same is true for the *Yersinia* secretin YscC together with its pilotin YscW (Koster *et al*, 1997). This suggests that the transmembrane rings might form independently. It has thus been proposed (Kimbrough and Miller, 2000) that the first step consists in the assembly of the MS ring, possibly along with the recruitment of the transmembrane proteins forming the export apparatus. In parallel, the secretin ring would form in the OM. Afterwards, the two rings would join by an unknown mechanism, allowing the assembly of the remaining machinery, which then exports the distal components, including the needle and the needle tip. The exact order of these later steps of the injectisome assembly remains largely unknown. A similar model was put forward based on the genetic analysis of the requirements for needle complex formation in *S. enterica* SPI-1 (Sukhan *et al*, 2001).

In this paper, we systematically investigate the whole assembly process of the *Yersinia* injectisome by combining four functional fluorescent hybrid proteins covering different parts of the machinery with an array of deletions. We conclude that the assembly starts from the secretin, the outermost and most stable ring, and sequentially proceeds inwards through YscD and YscJ. After completion of the membrane rings, an ATPase–C ring complex formed by YscK, YscL, YscN, and YscQ joins the machinery. All of the four participating proteins, but not the ATPase activity of YscN are required for the formation of this structure.

Results

Various substructures of the Yersinia injectisome including the C ring can be monitored using functional fluorescent fusion proteins

To visualize the injectisome and its subunits, the wild-type alleles of *yscC*, *yscD*, and *yscQ* on the virulence plasmid of *Y. enterocolitica* E40 were replaced by hybrid genes encoding the fluorescent proteins YscC–mCherry, EGFP–YscD, and EGFP–YscQ. Further, a non-polar complete deletion of *yscN* was constructed and complemented *in trans* with a plasmid encoding EGFP–YscN. The fusion proteins were expressed at near wild-type levels; no proteolytic release of the fluorophore was detected (Supplementary Figure 1).

To test the functionality of the fusion proteins, the pattern of proteins secreted into the supernatant in secretion-permissive medium (BHI-Ox) was analysed 3 h after induction of the system. YscC–mCherry, EGFP–YscN, and EGFP–YscQ were fully functional, whereas the strain expressing EGFP–YscD secreted a lower amount of effector proteins (Figure 1B). All fusion proteins allowed the formation of needles, which could be visualized by transmission electron microscopy (data not shown).

The localization of the hybrid proteins was analysed by fluorescence microscopy. Three hours after induction of synthesis of the injectisome, fluorescent spots were observed at the cell periphery for all labelled proteins (Figure 1A, three-dimensional view in Supplementary data). The formation of these spots was independent of the Ca^{2+} concentration in the medium, showing that their appearance was not directly

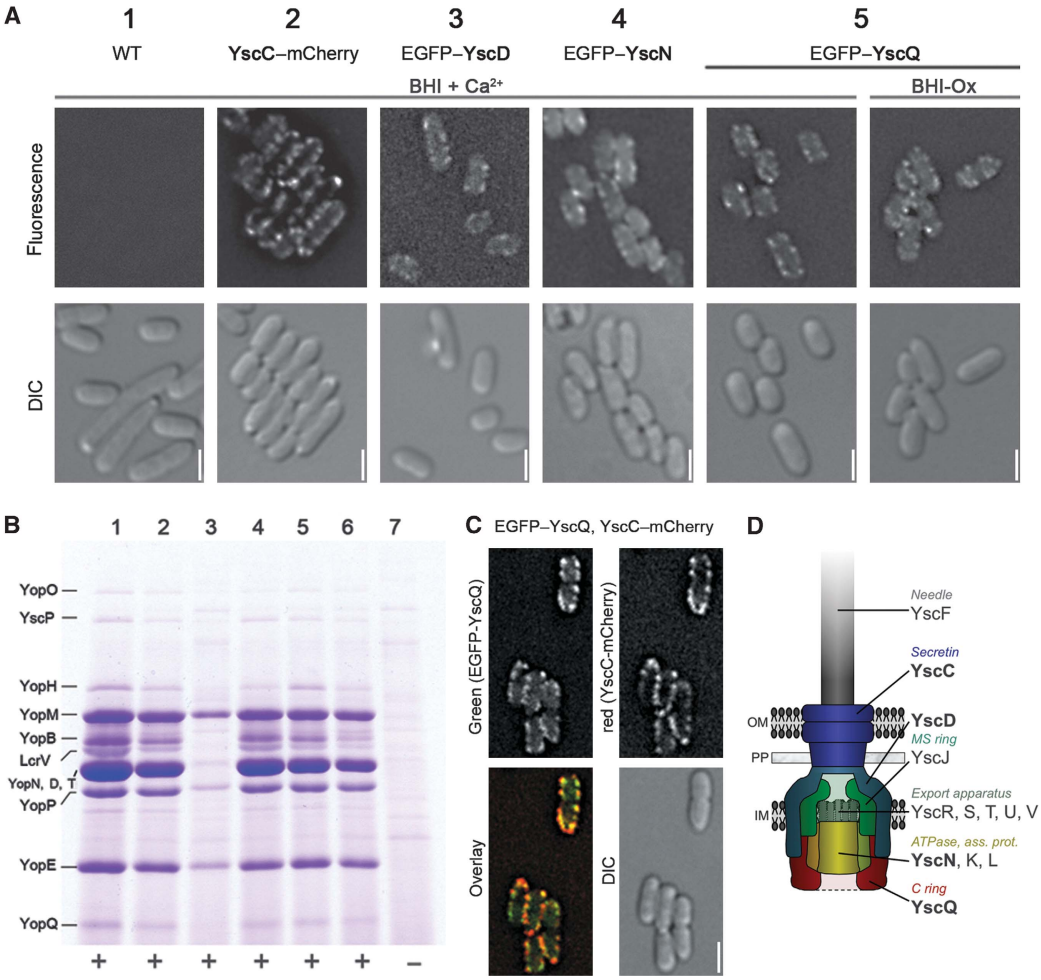

Figure 1 Fluorescently labelled Ysc proteins are functional and allow visualization of the injectisome. (**A**) Fluorescence deconvolution microscopy showing the formation of fluorescent spots at the bacterial membrane of *Y. enterocolitica* bacteria grown in secretion-non-permissive (BHI + Ca^{2+}) and secretion-permissive medium (BHI-Ox): 1—E40(pYV40) [wild type], 2—E40(pMA4005) [YscC–mCherry], 3—E40(pAD4050) [EGFP–YscD], 4—E40(pAD4136)(pAD182) [ΔYscN + pBAD-*egfp–yscN*], 5—E40(pAD4016) [EGFP–YscQ]. All fusion proteins except for EGFP–YscN are encoded under their native promoter on the pYV virulence plasmid. Upper lane: mCherry fluorescence for strain 2, EGFP fluorescence for other strains; lower lane: corresponding DIC picture. All fluorescence pictures were taken 3 h after the induction of the T3S system by temperature shift to 37°C. Scale bars: 2 μm. (**B**) Analysis of the Yop proteins secreted in secretion-permissive conditions. The tagged strains are fully functional for effector secretion, except for the strain expressing EGFP–YscD (lane 3), which shows reduced secretion. Culture supernatants were separated on a 12% SDS–PAGE gel and stained with Coomassie Brilliant Blue. Strains as listed in (**A**), 6—E40(pMAAD4006) [EGFP–YscQ, YscC–mCherry], 7—E40(pAD4051) [ΔYscD, negative control]. Bottom line: Needle formation (+/−) in the tested strains (data not shown). (**C**) Fluorescence microscopy showing the colocalization of EGFP–YscQ with YscC–mCherry in E40(pMAAD4006) bacteria. Fluorescent pictures were obtained as described in (**A**). (**D**) Model of the *Yersinia* Ysc injectisome. Fluorescently labelled proteins are shown in bold print. OM, outer membrane; PP, periplasm; IM, inner membrane.

linked to the secretion of Yop proteins by the T3S system (Figure 1A).

To ascertain that the membrane spots correspond to assembled basal bodies, we constructed a strain expressing both YscC–mCherry and EGFP–YscQ, and monitored the localization of the green fluorescence from EGFP–YscQ and the red fluorescence from YscC–mCherry. As visible in Figure 1C, the green and red spots largely colocalized, with small deviations because of chromatic aberrations of the microscope. We thus assumed that the fluorescent spots correspond to assembled basal bodies. In a minority of cells, a polarily localized YscC–mCherry spot without EGFP–YscQ equivalent could be observed in addition to the colocalizing spots. We assumed that these polar spots consist of misassembled YscC–mCherry proteins. Colocalization of spots was also observed for EGFP–YscD and EGFP–YscN with YscC–mCherry (data not shown). To test for colocalization of the needle with the basal body components, bacteria producing EGFP–YscQ were analysed by immunofluorescence with purified antibodies directed against the needle subunit. Overlays of the resulting pictures with the EGFP–YscQ fluorescence revealed that the majority of spots for YscF and YscQ colocalized (Supplementary Figure 2). A fraction of YscQ spots did not correspond to YscF spots.

Most likely, the needles of these basal bodies were detached during the immunofluorescence procedure. We conclude from all these experiments that the fluorescent spots correspond to functional injectisomes.

Assembly of the injectisome starts from the secretin ring in the OM and proceeds inwards through stepwise assembly of YscD and YscJ

As earlier work has shown that secretins can insert in the OM provided they are assisted by their pilotin (Burghout *et al*, 2004a; Guilvout *et al*, 2006), the fluorescent YscC–mCherry and its pilotin YscW were expressed *in trans* in *Y. enterocolitica* E40 (pMA8)(pRS6), in the absence of the pYV virulence plasmid encoding the T3S components. YscC–mCherry localized in membrane spots (Figure 2A), as observed before for PulD, the secretin involved in a type II secretion pathway (Buddelmeijer *et al*, 2009). These data thus confirm earlier results showing that YscC only requires its pilotin for assembly in the OM (Burghout *et al*, 2004a). In the absence of YscW, the majority of YscC–mCherry clustered in spots at the bacterial pole (Supplementary Figure 3). This phenotype was clearly distinguishable from the membrane spot formation in the presence of YscW, and confirmed the function of YscW in proper localization and oligomerization of YscC (Burghout *et al*, 2004a).

Not surprisingly, mutants lacking any of the structural ring proteins YscC, YscD, or YscJ failed to assemble the cytosolic injectisome components YscN and YscQ (Table I), showing that establishment of the membrane-spanning structure formed by YscC, YscD, and YscJ is at the beginning of injectisome formation. To test for the assembly order of these proteins, we combined the *egfp–yscD* allele on the pYV plasmid with non-polar deletions in *yscC* and *yscJ*. Although the absence of YscC clearly abolished the formation of EGFP–YscD spots at the bacterial membrane, the absence of YscJ did not affect this assembly (Figure 2B). This implies that YscC assembles first, followed by YscD, and finally YscJ.

To confirm this order of assembly, we performed co-immunoprecipitation assays using strains in which the wild-type alleles of *yscD* or *yscJ* on the virulence plasmid were replaced by *his-flag-yscD* or *yscJ-flag-his*, respectively. The affinity tagged proteins were functional for effector secretion (data not shown) and hence assumed to assemble in the same way as wild type. They were further combined

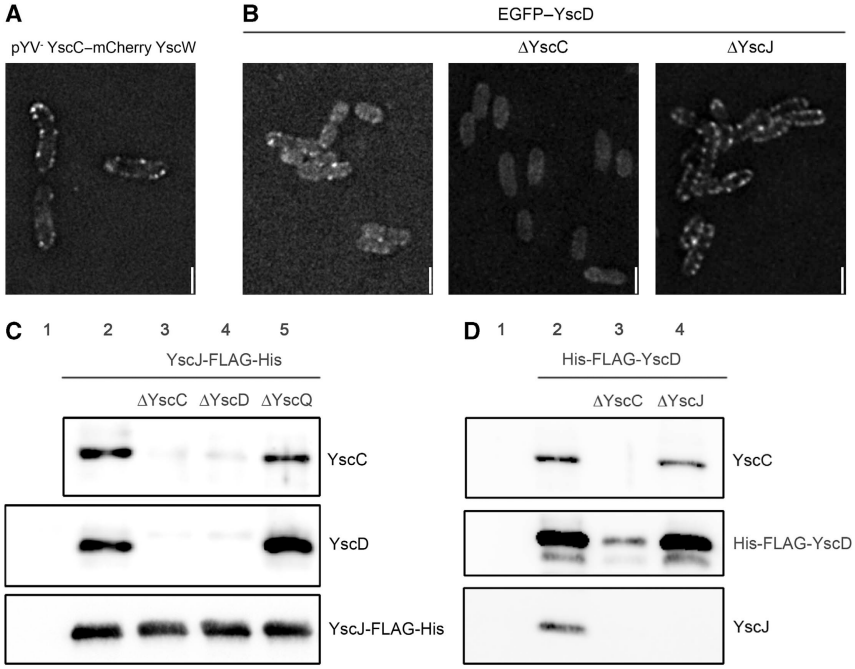

Figure 2 YscC assembly only requires its pilotin; YscD assembly requires the presence of YscC, but not of YscJ. Copurification of the three structural ring proteins suggests the stepwise assembly order YscC–YscD–YscJ. (**A**) Fluorescence microscopy showing the formation of secretin spots [YscC–mCherry] at the bacterial membrane in a strain lacking the virulence plasmid pYV, after *in trans* expression of YscC–mCherry and YscW (plasmids pMA8, pRS6) for 3 h at 37°C. Scale bars: 2 μm. (**B**) Fluorescence microscopy showing the formation of YscD spots at the bacterial membrane in strains E40(pAD4050) [EGFP–YscD], E40(pMAAD4018) [EGFP–YscD, ΔYscC], and E40(pAD4080) [EGFP–YscD, ΔYscJ]. YscD remains cytosolic in the absence of YscC, whereas it assembles in membrane spots in the absence of YscJ. (**C**) Analysis of the copurification of YscC and YscD after affinity purification of YscJ. Deletion of either YscC or YscD abolishes the copurification of the respective other protein with YscJ-FLAG-His. Bacteria were incubated for 3 h at 37°C, spheroplasted, and lysed. Proteins were purified by FLAG affinity, separated on 4–12% gradient SDS–PAGE, and analysed by immunoblot with the respective anti-YscC, -YscD, or -YscJ antibodies. All strains were ΔYadA to facilitate cell lysis: 1—E40(pLJM4029) [WT], 2—E40(pAD4054) [YscJ-FLAG-His], 3—E40(pAD4109) [YscJ-FLAG-His, ΔYscC], 4—E40(pAD4110) [YscJ-FLAG-His, ΔYscD], 5—E40(pAD4112) [YscJ-FLAG-His, ΔYscQ]. (**D**) Analysis of the copurification of YscC and YscJ after affinity purification of YscD. Whereas deletion of YscC abolishes copurification of YscJ with His-FLAG-YscD, YscJ is not required for the interaction between YscC and YscD. Samples were obtained as described for (**C**). All strains were ΔYadA to facilitate cell lysis: 1—E40(pLJM4029) [WT], 2—E40(pAD4055) [His-FLAG-YscD], 3—E40(pADMA4101) [His-FLAG-YscD, ΔYscC], 4—E40(pAD4089) [His-FLAG-YscD, ΔYscJ].

Table I Formation of fluorescent spots in various injectisome mutants

Protein missing	Family/function	Localization	YscC–mCherry fluorescence	EGFP–YscD fluorescence	EGFP–YscN fluorescence	EGFP–YscQ fluorescence
All (pYV$^-$)			+ (pMA8 + pRS6)	ND	ND	ND
YscC	Secretin	OM		− (pMAAD4018)	− (pADMA4156)	− (pADMA4151)
YscD	MS ring	IM	ND		ND	− (pAD4052)
YscJ	MS ring	IM	+ (pADMA4082)	+ (pAD4080)	− (pAD4139)	− (pADMA4082)
YscN	ATPase	Cytoplasmic, IM associated	+ (pADMA4137)	ND		− (pAD4104)
YscK	ATPase associated	Cytoplasmic, IM associated	ND	ND	− (pAD22840)	− (pAD22723)
YscL	ATPase associated	Cytoplasmic, IM associated	ND	ND	− (pAD4141)	− (pAD4039)
YscQ	C ring	Cytoplasmic, IM associated	+ (pMA4007)	+ (pAD4061)	− (pAD4142)	
YscR	Export machinery	IM	ND	ND	ND	+ (pAD4032)
YscS	Export machinery	IM	ND	ND	ND	+ (pAD4034)
YscT	Export machinery	IM	ND	ND	ND	+ (pAD4036)
YscU	Export machinery[a]	IM	ND	ND	ND	+ (pAD4026)
YscV(LcrD)	Export machinery	IM	+ (pMA4011)	ND	ND	+ (pAD4038)
YscRSTUV	Export machinery	IM	ND	ND	+ (pAD4143)	+ (pAD4108)
YscF	Needle subunit	Extracellular	+ (pMA4015)	ND	+ (pAD4157)	+ (pAD4020)
LcrV	Needle tip	Extracellular	ND	ND	ND	+ (pAD4042)
YscH	Unknown	Exported	ND	ND	ND	+ (pAD22769)
YscI	Unknown[b]	Exported	ND	ND	ND	+ (pAD4022)
YscO	Unknown	Exported	ND	ND	ND	+ (pAD4024)
YscX	Unknown	Exported	ND	ND	ND	+ (pAD4027)
YscY	Chaperone of YscX	Cytoplasmic	ND	ND	ND	+ (pAD4040)
YopN	Ca^{2+} plug	Cytoplasmic, IM associated	ND	ND	ND	+ (pAD4043)
LcrG	Ca^{2+} plug	Cytoplasmic, IM associated	ND	ND	ND	+ (pAD4041)

The formation of fluorescent spots was checked for YscC–mCherry, EGFP–YscD, EGFP–YscN, and EGFP–YscQ in combination with deletions of different proteins. +: Spot formation at the bacterial membrane; −: diffuse cytosolic fluorescence. The virulence plasmids of the corresponding strains are given in brackets (see Supplementary Table I for strain details). ND: not determined.
[a]Substrate specificity switch.
[b]Proposed inner rod.

with non-polar deletions in *yscC*, *yscD*, or *yscJ*. In each of the strains, the adhesin YadA was removed to facilitate cell lysis. Synthesis of the injectisome in these strains was induced under secretion-non-permissive conditions. Mild crosslinking was performed, spheroplasts were created, and the bacteria were lysed by the addition of detergent (see Material and methods). Afterwards, a one-step affinity purification was performed, and the (co-)purification of YscC, YscD, and YscJ was tested. YscJ-FLAG-His copurified YscC and YscD from complete injectisomes, and removal of YscQ, a protein thought to act further downstream in the assembly process, did not affect this copurification. In contrast, removal of YscC prevented copurification of YscD with YscJ-FLAG-His, and removal of YscD prevented copurification of YscC (Figure 2C). Likewise, His-FLAG-YscD copurified YscC and YscJ from complete injectisomes. However, although removal of YscC prevented copurification of YscJ with His-FLAG-YscD, removal of YscJ still allowed the copurification of YscC (Figure 2D). The amount of purified His-FLAG-YscD was reduced in the absence of YscC, most likely as a consequence of decreased cellular YscD levels, either because of its mislocalization in the absence of YscC or because of a lower expression level. Taken together, these data indicate (i) that the insertion of the secretin ring in the OM is required for the subsequent association of YscD and YscJ and (ii) that YscD makes the link between YscC and YscJ. Hence, the OM ring is the first ring of the injectisome to be assembled. This assembly step is followed by the attachment of YscD, which then allows the completion of the MS ring by YscJ.

The C ring only assembles in the presence of the membrane rings, YscN, YscK, and YscL

To determine at which stage the C ring forms during the assembly process, we combined the *egfp–yscQ* allele with an array of deletions in most injectisome genes (Table I; Supplementary Table 1 for details of strains). Deletion of any of the membrane ring proteins (YscC, YscD, or YscJ) completely abolished the formation of membrane spots and led to an increased diffuse cytoplasmic fluorescence (Figure 3). This indicates that the C ring forms after the YscCDJ ring structure. Removal of the ATPase YscN or any of its two interacting proteins YscK and YscL (Jackson and Plano, 2000; Blaylock *et al*, 2006) also fully prevented C ring formation (Figure 3), indicating that assembly of the C ring additionally requires YscN as well as YscK and YscL.

Removal of individual proteins YscR, S, T, U, or V from the export apparatus as well as a complete deletion of all these proteins did not completely abolish the formation of the C ring. However, in the absence of YscR, YscS, or YscV, the number of spots was reduced, indicating that these proteins are either beneficial (but not absolutely required) for C ring formation, or have a stabilizing effect on fully assembled injectisomes.

As expected from the fact that YscF, YscI, YscO, YscX, and YopN are substrate proteins exported by the injectisome

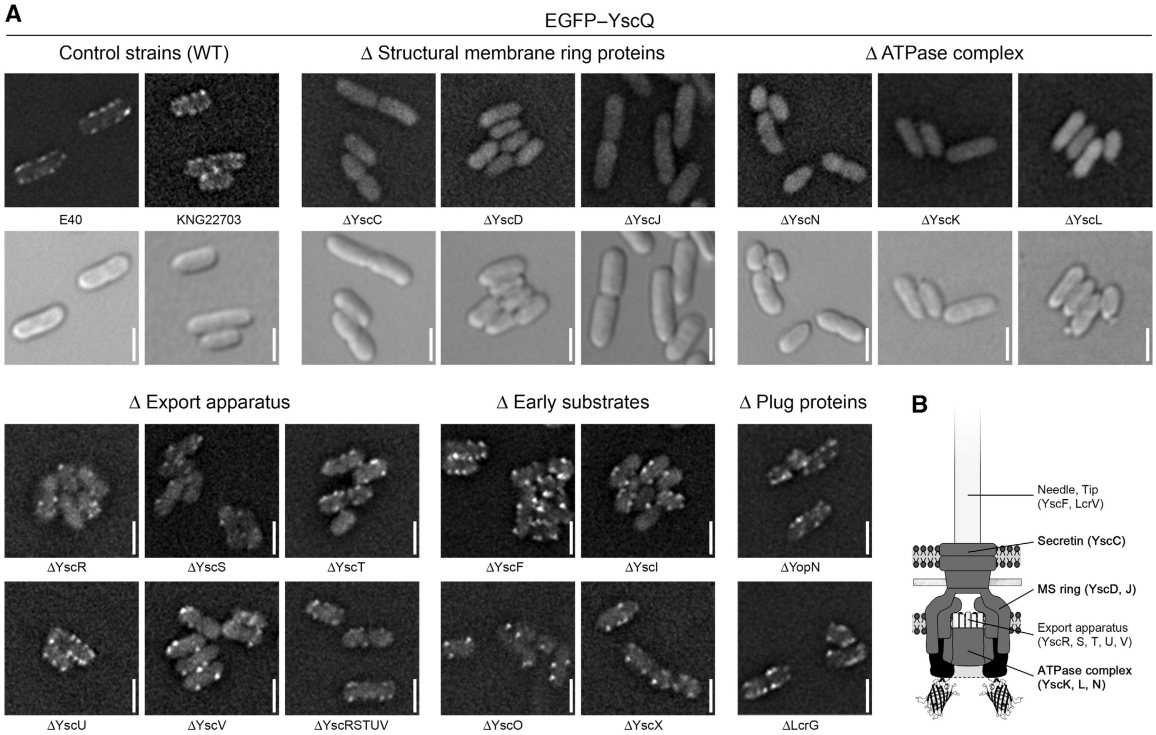

Figure 3 C ring formation requires both transmembrane rings and the ATPase complex, but not the export apparatus or any secreted substrate. (**A**) Fluorescence microscopy pictures of bacteria expressing EGFP–YscQ combined with deletions of different genes. Micrographs were taken 3 h after induction of the T3S system. (For the control strains and the strains with deletions in the proteins required for C ring formation—upper lane: EGFP fluorescence, lower lane: corresponding DIC picture). Scale bars: 2 μm. (**B**) Schematic representation of the injectisome showing the components required (bold, dark) and not required (normal, light) for C ring formation. For information about the used strains, refer to Table I.

itself, their absence also did not prevent the formation of the C ring. Likewise, deletion of LcrG, a regulatory protein (Nilles *et al*, 1997; Torruellas *et al*, 2005), had no effect on assembly of the C ring (Figure 3; see Table I for additional strains).

ATPase assembly not only requires the presence of the YscCDJ platform, but also needs YscK, YscL, and YscQ

Finally, assembly of the ATPase YscN was tested. As replacement of the wild-type allele on the virulence plasmid by a gene encoding a fluorescent fusion protein decreased the expression of downstream genes in the *virB* operon, whereas a complete deletion of *yscN* was non-polar (Figure 1B), *egfp–yscN* was cloned in a pBAD vector and used to complement *in trans* double deletions in *yscN* and several other genes. Induction of synthesis of EGFP–YscN with 0.05% arabinose led to YscN protein levels similar to the native level (Supplementary Figure 1), and to effector secretion at wild-type levels (data not shown). As shown in Figure 4, YscN assembly required the presence of YscC (secretin), YscJ (MS ring), YscK and YscL (two proteins known to interact with the ATPase), and YscQ (the C ring). In contrast, even the complete deletion of the IM export proteins YscR, S, T, U, V still allowed formation of YscN spots, albeit again in a reduced number (Figure 4).

These data suggest that the cytosolic components of the injectisome form a single large ATPase–C ring complex, requiring all of its components YscK, L, N, Q to assemble.

In agreement with the essential function of YscQ for the ATPase assembly, we did not observe any needle formation in strains that lack YscQ, but overexpress YscN, in contrast to recent results obtained with the flagellum (Konishi *et al*, 2009) (data not shown).

ATPase activity of YscN is not required for the assembly of the ATPase–C ring complex at the injectisome

To determine whether assembly of the C ring requires YscN for its ATPase activity or as a structural component, a deletion of *yscN* in an *egfp–yscQ* background was examined. As expected, the resulting strain secreted neither Yops nor the ruler and needle subunits. Secretion could be complemented *in trans* by a wild-type *yscN* allele, but not by an *yscN* allele encoding $YscN_{K175E}$ altered in the Walker box (Figure 5B and C). Interestingly, however, although $YscN_{K175E}$ was not functional, it did restore the formation of the C ring spots (Figure 5A), implying that the YscN requirement for the formation of the ATPase–C ring complex is exclusively structural.

After assembly of the ATPase–C ring complex, needle formation and effector secretion take place rapidly

The kinetics of C ring formation in a strain expressing EGFP–YscQ was followed in a time-course experiment. Pictures were taken every 20 min up to 2 h after induction of the *ysc-yop* regulon (Cornelis *et al*, 1989) in a Ca^{2+}-depleted medium. Weak diffuse cytoplasmic fluorescence could be observed 20 and 40 min after the temperature shift, suggest-

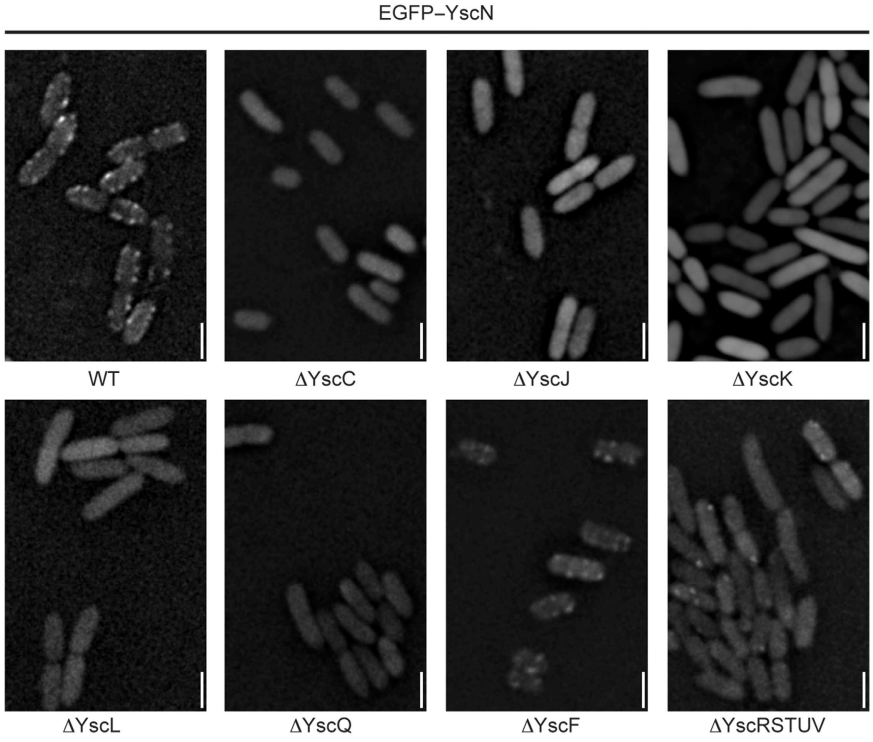

Figure 4 The assembly of the ATPase requires both transmembrane rings, YscK, YscL, and YscQ, but not the export apparatus. Fluorescence microscopy pictures of YscN null mutants complemented with EGFP–YscN combined with deletions of different genes. Wild-type protein levels were established by EGFP–YscN induction with 0.05% arabinose. Micrographs were taken 3 h after induction of EGFP–YscN and the T3S system. Scale bars: 2 μm. For information about the used strains, refer to Table I.

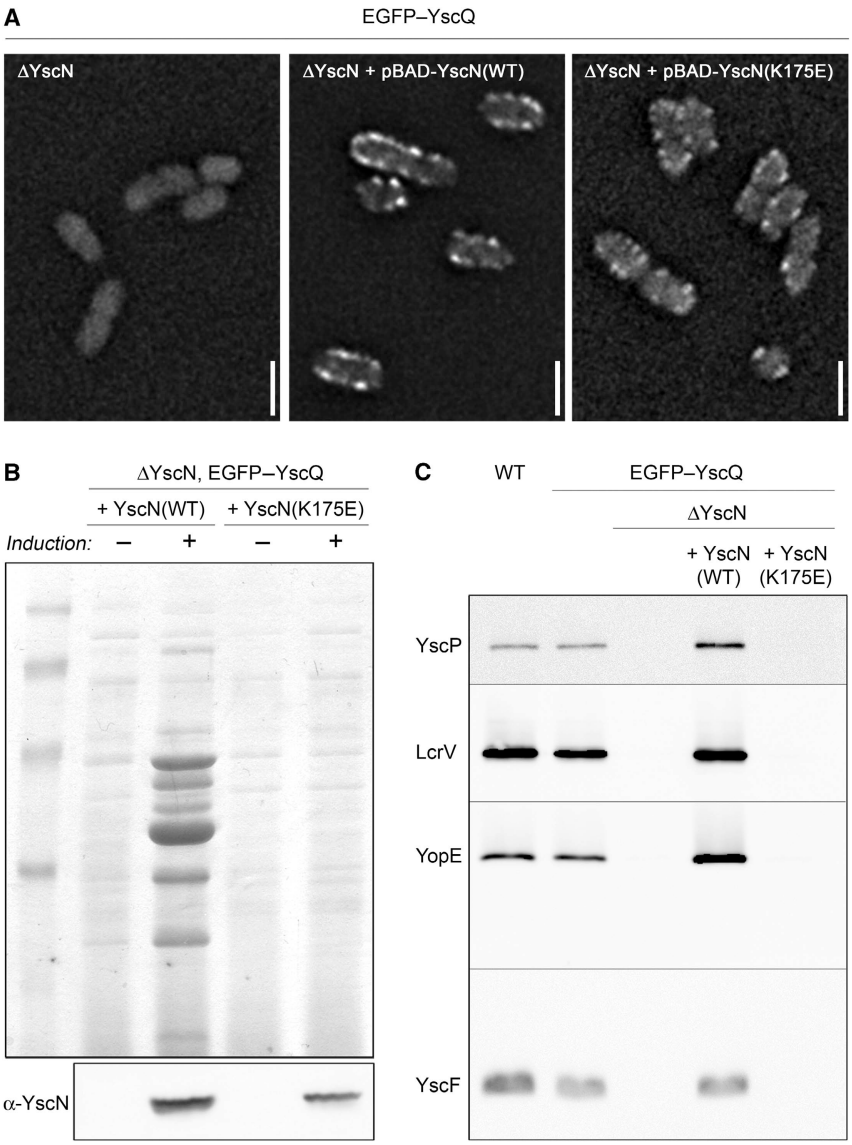

Figure 5 The structure, but not the ATPase activity of YscN, is required for the formation of the C ring. (**A**) Fluorescence microscopy showing the formation of C ring spots in E40(pAD4104) [EGFP–YscQ, ΔYscN], complemented with plasmids encoding wild-type YscN or the catalytically inactive YscN(K175E), 3 h after induction of the type III secretion system. Scale bars: 2 μm. (**B**) Upper part: Analysis of Yop protein secretion in strain E40(pAD4104) complemented with wild type, or catalytically inactive YscN. Expression of YscN was either not induced (−) or induced with 0.05% arabinose (+). Culture supernatants were separated on a 12% SDS–PAGE gel and stained with Coomassie Brilliant Blue. Lower part: Expression of YscN in the corresponding strains. Cell pellets were separated on a 12% SDS–PAGE gel and analysed by immunoblot with anti-YscN antibodies. (**C**) Export of different classes of substrates in strains expressing EGFP–YscQ, and the different YscN variants. Culture supernatants were separated on a 15% SDS–PAGE gel and analysed by immunoblot with the respective antibodies.

ing that synthesis of YscQ was turned on directly after the shift, and that EGFP folds rapidly in the *Yersinia* cytosol (Figure 6A). The rapid synthesis of YscQ was also confirmed by immunoblotting (data not shown). The first membrane spots could, however, only be observed 60 min after induction. Although the fluorescence intensity of single spots seemed to increase over time, the number of spots stayed roughly constant up to 3 h after induction (Figure 6A). Interestingly, the timeframe of appearance of the C ring was approximately the same as the timeframe of appearance of the needles (Figure 6B) and secretion of the effector proteins (Figure 6C), suggesting that needle formation and effector secretion occur within a short time after establishment of the ATPase–C ring complex. A model of injectisome assembly that incorporates the above mentioned results is depicted in Figure 7.

Discussion

The assembly of the T3S injectisome is a complex process that engages >20 different proteins, and results in the

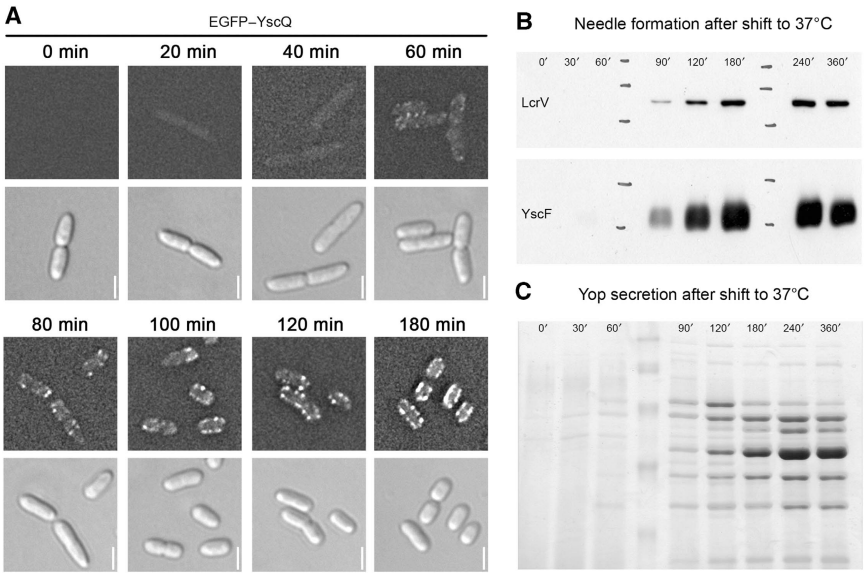

Figure 6 Formation of the C ring occurs about 60 min after induction of the T3S system. It directly precedes needle formation and effector secretion. (**A**) Fluorescence microscopy showing the formation of C ring spots [EGFP–YscQ] in strain E40(pAD4016) at various time points after induction of the synthesis of the T3S system by temperature shift to 37°C (upper lane: EGFP fluorescence; lower lane: corresponding DIC picture). Scale bars: 2 μm. (**B**) Time course of needle formation in wild-type strain E40(pYV40). Needle formation was monitored by SDS–PAGE analysis of purified needles. The needle pellet was separated on a 15% gel and analysed by immunoblot with anti-LcrV and anti-YscF antibodies, respectively. (**C**) Time course of Yop protein secretion by wild-type strain E40(pYV40). Culture supernatants were separated on a 12% SDS–PAGE gel and stained with Coomassie Brilliant Blue. All time-course experiments were performed in secretion-permissive conditions (Ca^{2+}-depleted medium).

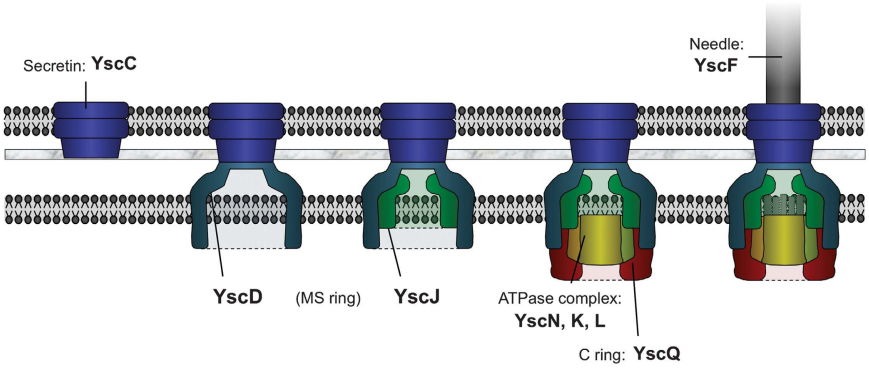

Figure 7 Model of assembly of the *Yersinia* injectisome. Formation of the injectisome is initiated by formation of the secretin ring in the outer membrane. Next, YscD attaches to YscC, which allows the subsequent completion of the MS ring by attachment of YscJ. After the formation of the membrane ring structures, the ATPase–C ring complex, consisting of YscN, K, L, and Q assembles at the cytoplasmic side of the injectisome. The exact time point of the integration of the IM proteins YscR, S, T, U, and V is unclear. Afterwards, the needle consisting of YscF and LcrV can be assembled. Bold font denotes protein names, normal font denotes functional subunits. The global structure of YscC, D, J is derived from Spreter *et al* (2009).

formation of a nanomachine spanning both bacterial membranes and protruding outside the bacterium. So far, little is known about this process. On the basis of the observation that heterologously overexpressed *S. enterica* MS ring components PrgH and PrgK form large rings in the absence of any other T3S component, a model was proposed (Kimbrough and Miller, 2002) in which the IM ring assembles first, and then fuses with the secretin ring in the OM. This model suggests the same general assembly scheme as the one that has been proposed for the flagellum (Kubori *et al*, 1997; Macnab, 2003), but does not explain how the two membrane rings find each other. The subsequent steps of assembly could not be examined so far.

To gain better insight into the assembly process and the functional relations between the proteins, we constructed strains in which a number of injectisome constituents were fused to fluorescent proteins. To minimize artefacts because of non-native expression levels or timing of the fusion proteins, we replaced the wild-type allele on the pYV virulence plasmid by the hybrid allele in the case of *yscC*, *yscD*, and *yscQ*. The hybrid *yscN* was plasmid borne, but it was expressed at wild-type level.

All recombinant injectisomes were functional, and in all cases, fluorescent spots appeared at the bacterial membrane, distributed all over the bacterial body. Colocalization of the fluorophores confirmed that the fluorescent spots correspond to injectisomes. The brightness of the spots likely results from the multimeric nature of the tagged proteins, although at this stage, one cannot conclude that each spot corresponds to only one injectisome. A fluorescence quantification based on external standards, presently in progress, will address this question.

We observed that the membrane ring-forming proteins YscC, YscD, and YscJ are required for assembly of any cytosolic structure. Importantly, by monitoring the formation of YscC–mCherry and EGFP–YscD spots, we observed that YscC assembles independently of YscD and YscJ and that YscD assembles independently of YscJ, but not of YscC. Co-immunoprecipitation assays confirmed that YscJ requires YscD to become attached to YscC. All this implies that the assembly of the injectisome is initiated by formation of the secretin ring in the OM and proceeds inwards through stepwise assembly of YscD and YscJ. These data contradict the earlier report that PrgH and PrgK, the *Salmonella* homologues of YscD and YscJ, can form a ring alone (Kimbrough and Miller, 2000). The discrepancy might result from the fact that the earlier study was based on heterologously overexpressed proteins, whereas this study is based on functional proteins produced in their natural environment at native expression levels. These data are also at odd with the report indicating that MxiD and MxiJ, the *Shigella* homologues of YscC and YscJ, interact even in the absence of the connector (Schuch and Maurelli, 2001). However, this interaction was observed in the absence of the pilot protein. In this case, the majority of secretin proteins are mislocalized to the IM (Koster *et al*, 1997), which might lead to non-native interaction with MxiJ. Interestingly, it was shown recently that the assembly of two ring-forming IM components of the *Vibrio cholerae* type II secretion complex also depends on the presence of the OM secretin (Lybarger *et al*, 2009), suggesting conservation or convergent evolution of the formation process in these two prokaryotic export systems. Taken together, our results show that the order of assembly of the OM and IM rings differs between the injectisome and the flagellum. We do not see any obvious reason for this, but this observation indicates that the two nanomachines differ more than is often thought. The flagellum is indeed significantly more complex than the injectisome because it rotates, which implies not only a motor but also bushings in the peptidoglycan and the OM. The P and L rings, having this function, are precisely replaced by a very stable secretin ring in the injectisome. This basic structural difference might explain the different order of assembly of the two nanomachines.

The outside-in assembly order consistently shown by co-immunprecipitation and fluorescence microscopy further implies that YscD is the connector between the two membrane rings, which is coherent with recent crystal structure and modelling data (Spreter *et al*, 2009). Our biochemical data allow to assess the recent models to integrate the crystal structures of the membrane ring proteins into the overall shape generated by electron microscopy averaging of purified injectisomes (Hodgkinson *et al*, 2009; Spreter *et al*, 2009). The electron density between the membranes would be generated by YscD. This in turn places YscJ in the IM, as proposed by manual fits (Moraes *et al*, 2008; Hodgkinson *et al*, 2009; Spreter *et al*, 2009), but not by the best automated fit (Hodgkinson *et al*, 2009).

After assembly of the OM and IM membrane rings, cytosolic components can assemble onto the structure. The observation that the proposed C ring component YscQ assembles in membrane spots colocalizing with the other components shows that the C ring is an integral component of the injectisome, confirming an assumption so far mainly based on immunogold-labelling experiments (Morita-Ishihara *et al*, 2006). Our data indicate that a large cytosolic complex consisting of the ATPase YscN, the two interacting proteins YscK and YscL, and the C ring component YscQ is formed, requiring all of its components, but not the ATPase activity of YscN for assembly. This differs again from the situation in the flagellum. There, FliM, FliN, and FliG (together forming the C ring) appear in significant amount in the membrane fraction in the presence of FliF (MS ring), but in the absence of FliI (ATPase) or FliH (homologue to YscL). This suggests that the flagellar C ring forms in the absence of the ATPase complex (Kubori *et al*, 1997), in agreement with the observation that it forms on overexpression of FliM, FliN, and FliG together with FliF (Lux *et al*, 2000; Young *et al*, 2003). Although the heterologous overexpression of the proteins in these studies might account for the different observations, these results can also be the consequence of functional differences between the two nanomachines. As the constraint of rotation and spatial separation of the C ring and ATPase does not exist for the injectisome, the apparatus could be optimized for secretion. A tighter contact between the ATPase complex and the C ring might be a consequence of this optimization. The fact that we could not overcome the requirement of YscQ for secretion by overexpression of the ATPase is consistent with the essential function of YscQ for assembly of the complete ATPase–C ring complex.

Our results are also in perfect agreement with earlier results showing interactions between YscK, YscL, YscN, and YscQ (Jackson and Plano, 2000). However, the hypothesis that YscQ recruits the ATPase should be revised: YscK, L, N, and Q would rather assemble in one step. The proposed function of YscL as a negative regulator of ATPase activity (Blaylock *et al*, 2006) as well as its direct interaction with YscN and YscQ (Jackson and Plano, 2000) is consistent with the presence of YscL in this complex. Less is known about the function of YscK. As it interacts with YscQ, but not with YscN and weakly at the most with YscL (Jackson and Plano, 2000; Blaylock *et al*, 2006), it might act at the interface of the ATPase–C ring complex.

Formation and assembly of the ATPase–C ring complex did not depend on any of the five proteins forming the export apparatus, even though the number of membrane spots was reduced when YscR, YscS, YscV, or the five proteins YscRSTUV were missing. This implies that a YscKLNQ complex docks onto the IM ring rather than onto the export apparatus, which agrees with the observations made with the flagellum (Kubori *et al*, 1997). As currently, little is known about stoichiometry, localization, and function of the export apparatus, its function in the assembly process remains unclear.

In conclusion, this work shows that the assembly of the injectisome starts with the formation of the stable secretin ring in the OM, and proceeds inwards through discrete attachment steps of YscD and YscJ at the IM. Afterwards,

the components of the cytosolic ATPase–C ring complex assemble at the cytosolic side of the injectisome in one step, which allows the subsequent fast steps leading to needle formation and effector secretion.

Materials and methods

Bacterial strains, plasmids, and genetic constructions

Y. enterocolitica strains and plasmids are listed in Supplementary Table 1.

E. coli Top10, used for plasmid purification and cloning, and *E. coli* Sm10 λ pir, used for conjugation, were routinely grown on LB agar plates and in LB broth. Ampicillin was used at a concentration of 200 μg/ml to select for expression vectors. Streptomycin was used at a concentration of 100 μg/ml to select for suicide vectors. Plasmids were generated using either Phusion polymerase (Finnzymes, Espoo, Finland) or Vent DNA polymerase (New England Biolabs, Frankfurt, Germany). The oligonucleotides used for genetic constructions are listed in Supplementary Table 2. Mutators for modification or deletion of genes in the pYV plasmids were constructed by overlapping PCR using purified pYV40 plasmid as template, leading to 200–250 bp of flanking sequences on both sides of the deleted or modified part of the respective gene. As an exception, pKEM5 was constructed by introduction of the deletion through religation of the 5′ phoshorylated internal oligonucleotides. For the mutator strains introducing EGFP, a precursor mutator vector was created as described above. Subsequently, the EGFP gene was inserted in frame from plasmid pEGFP-C1 into the digested precursor vectors. The respective regions containing the flanking sequences were subcloned into the pKNG101 suicide vector. For pMA12, insert 2 was created by overlapping PCR using oligos 5017 and 5087 to amplify mCherry from vector pRVCHYC-5 (Thanbichler *et al*, 2007), and oligos 5088 and 5068 to amplify the downstream flanking region from the pYV plasmid. Afterwards, ligation of *Sal*I/*Xho*I digested insert 1, containing the upstream flanking region, *Xho*I/*Xba*I digested insert 2, and *Sal*I/*Xba*I digested pKNG101 suicide vector lead to the mutator pMA12. All constructs were confirmed by sequencing using a 3100-Avant genetic analyser (Applied Biosystems, Rotkreuz, Switzerland). The allelic exchange was selected by plating diploid bacteria on sucrose (Kaniga *et al*, 1991). pAD166 expressing $YscN_{K175E}$ was generated by overlapping PCR using internal primers encoding for the modified protein sequence, and selected by colony PCR and sequencing. For pAD182 expressing EGFP–YscN, a precursor vector was generated and EGFP was introduced from pEGFP-C1, as described above.

Y. enterocolitica cultures for secretion and microscopy analysis

Induction of the *yop* regulon was performed by shifting the culture to 37°C, either in BHI-Ox (secretion-permissive conditions) or in BHI + 5 mM $CaCl_2$ (secretion-non-permissive conditions) (Cornelis *et al*, 1987). Expression of the inducible YscN constructs was induced by adding 0.05% L-arabinose to the culture just before the shift to 37°C. The carbon source was glycerol (4 mg/ml) when expressing genes from the pBAD promoter, and glucose (4 mg/ml) in the other cases.

Yop secretion

Total cell and supernatant fractions were separated by centrifugation at 20 800 *g* for 10 min at 4°C. The cell pellet was taken as total cell fraction. Proteins in the supernatant were precipitated with trichloroacetic acid 10% (w/v) final for 1 h at 4°C.

Secreted proteins were analysed by SDS–PAGE; in each case, proteins secreted by 3×10^8 bacteria were loaded per lane. Total secreted proteins were analysed by Coomassie staining of 12% SDS–PAGE gels. Detection of specific secreted proteins by immunoblotting was performed using 15% SDS–PAGE gels. For detection of proteins in total cells, 2×10^8 bacteria were loaded per lane, if not stated otherwise, and proteins were separated on 15% SDS–PAGE gels before detection by immunoblotting.

Immunoblotting was carried out using rabbit polyclonal antibodies against LcrV (MIPA220; 1:2000), YscF (MIPA223; 1:1000), YscN (MIPA189; 1:1000), YscP (MIPA57; 1:3000), or YopE (MIPA73; 1:1000). Detection was performed with secondary antibodies directed against rabbit antibodies and conjugated to horseradish peroxidase (1:5000; Dako), before development with ECL chemiluminescent substrate (Pierce).

Needle purification

Needles were purified from cultures incubated under secretion-permissive conditions. At the given time points, 48 ml bacteria were removed from the 500 ml culture, harvested by centrifugation (5 min at 4000 *g*) and resuspended in 1 ml 20 mM Tris–HCl, pH 7.5. Needle detachment was increased by repeated pipetting through a 1 ml pipet tip. Cells were pelleted by centrifugation (5 min at 4000 *g*), and the supernatant containing the needles was passed through a 0.45 μm mesh filter (cellulose acetate membrane) and then centrifuged for 60 min at 20 800 *g*. The resulting pellet was resuspended in 20 μl Laemmli buffer, 15 μl of which were analysed by SDS–PAGE followed by immunoblotting (Mueller *et al*, 2005).

Fluorescence microscopy

For fluorescence imaging, cells were placed on a microscope slide layered with a pad of 2% agarose dissolved in water or PBS. A Deltavision Spectris optical sectioning microscope (Applied Precision, Issaquah, WA) equipped with an UPlanSApo 100 × /1.40 oil objective (Olympus, Tokyo, Japan) and a coolSNAP HQ CCD camera (Photometrics, Tucson, AZ) was used to take differential interference contrast (DIC) and fluorescence photomicrographs. To visualize GFP and mCherry fluorescence, GFP filter sets (Ex 490/20 nm, Em 525/30 nm) and mRFP filter sets (Ex 560/40 nm, EM 632/60 nm), respectively, were used. DIC frames were taken with 0.3 s and fluorescence frames with 1.0 s exposure time. Per image, a Z-stack containing 20 frames per wavelength with a spacing of 150 nm was acquired. The stacks were deconvoluted using softWoRx v3.3.6 with standard settings (Applied Precision, WA). The DIC frame at the centre of the bacterium and the corresponding fluorescence frame were selected and further processed with ImageJ software.

Co-immunoprecipitation of YscC, YscD, and YscJ

Y. enterocolitica cultures were grown in secretion-non-permissive conditions to an OD_{600} of 1.5–2.2. Protein complexes were then stabilized by crosslinking with 0.25% formaldehyde for 15 min at 37°C. Cells were harvested by centrifugation (15 min at 1500 *g*, 25°) and resuspended in 1/5 volume of PBS. After a second crosslinking step (0.4% formaldehyde, 15 min, 25°C) and harvesting as before, spheroplast generation and lysis was performed as described by Kubori *et al* (1997) and Blocker *et al* (2001). In short, cells were resuspended in 1/5 original volume of ice-cold spheroplasting buffer (0.75 M sucrose, 50 mM Tris, pH adjusted with HCl to 7.8, 0.6 mg/ml lysozyme, 6 mM EDTA), and incubated at 25°C up to 90 min, until complete spheroplast formation could be observed. Cells were lysed by addition of 1% Triton X-100 and subsequent incubation at 4°C for 15 min. After addition of 15 mM $MgCl_2$, unlysed cells were removed by centrifugation (20 min at 6000 *g*, 4°C); 300 μl of anti-FLAG M2 affinity gel (Sigma-Aldrich, Buchs, Switzerland) were added to the supernatant, and the proteins were purified in batch according to the manufacturer's protocol. The elution fractions were recentrifuged to completely remove resin, and separated on 12% SDS–PAGE gels or 4–12% gradient SDS–PAGE gels (Serva, Heidelberg, Germany). Immunoblotting was carried out using rabbit polyclonal antibodies against YscC (MIPA250, 1:1000), YscD (MIPA232, 1:1000), and YscJ (MIPA66, 1:5000), as described above.

Supplementary data

Supplementary data are available at *The EMBO Journal* Online (http://www.embojournal.org).

Acknowledgements

We thank K Maylandt and I Stainier for providing strains pKEM5, pKEM4001, pSI51, and pSI4006. This work was supported by the Swiss National Science Foundation (grant 310000-113333/1) to GC.

Conflict of interest

The authors declare that they have no conflict of interest.

References

Abrahams JP, Leslie AG, Lutter R, Walker JE (1994) Structure at 2.8 A resolution of F1-ATPase from bovine heart mitochondria. *Nature* **370:** 621–628

Akeda Y, Galan JE (2005) Chaperone release and unfolding of substrates in type III secretion. *Nature* **437:** 911–915

Alfano JR, Collmer A (2004) Type III secretion system effector proteins: double agents in bacterial disease and plant defense. *Annu Rev Phytopathol* **42:** 385–414

Blaylock B, Riordan KE, Missiakas DM, Schneewind O (2006) Characterization of the Yersinia enterocolitica type III secretion ATPase YscN and its regulator, YscL. *J Bacteriol* **188:** 3525–3534

Blocker A, Gounon P, Larquet E, Niebuhr K, Cabiaux V, Parsot C, Sansonetti P (1999) The tripartite type III secreton of Shigella flexneri inserts IpaB and IpaC into host membranes. *J Cell Biol* **147:** 683–693

Blocker A, Jouihri N, Larquet E, Gounon P, Ebel F, Parsot C, Sansonetti P, Allaoui A (2001) Structure and composition of the Shigella flexneri 'needle complex', a part of its type III secreton. *Mol Microbiol* **39:** 652–663

Buddelmeijer N, Krehenbrink M, Pecorari F, Pugsley AP (2009) Type II secretion system secretin PulD localizes in clusters in the Escherichia coli outer membrane. *J Bacteriol* **191:** 161–168

Burghout P, Beckers F, de Wit E, van Boxtel R, Cornelis GR, Tommassen J, Koster M (2004a) Role of the pilot protein YscW in the biogenesis of the YscC secretin in Yersinia enterocolitica. *J Bacteriol* **186:** 5366–5375

Burghout P, van Boxtel R, Van Gelder P, Ringler P, Muller SA, Tommassen J, Koster M (2004b) Structure and electrophysiological properties of the YscC secretin from the type III secretion system of Yersinia enterocolitica. *J Bacteriol* **186:** 4645–4654

Cordes FS, Komoriya K, Larquet E, Yang S, Egelman EH, Blocker A, Lea SM (2003) Helical structure of the needle of the type III secretion system of Shigella flexneri. *J Biol Chem* **278:** 17103–17107

Cornelis G, Vanootegem JC, Sluiters C (1987) Transcription of the yop regulon from Y. enterocolitica requires trans acting pYV and chromosomal genes. *Microb Pathog* **2:** 367–379

Cornelis GR (2006) The type III secretion injectisome. *Nat Rev Microbiol* **4:** 811–825

Cornelis GR, Biot T, Lambert de Rouvroit C, Michiels T, Mulder B, Sluiters C, Sory MP, Van Bouchaute M, Vanooteghem JC (1989) The Yersinia yop regulon. *Mol Microbiol* **3:** 1455–1459

Cornelis GR, Van Gijsegem F (2000) Assembly and function of type III secretory systems. *Annu Rev Microbiol* **54:** 735–774

Cornelis GR, Wolf-Watz H (1997) The Yersinia Yop virulon: a bacterial system for subverting eukaryotic cells. *Mol Microbiol* **23:** 861–867

Crepin VF, Prasannan S, Shaw RK, Wilson RK, Creasey E, Abe CM, Knutton S, Frankel G, Matthews S (2005) Structural and functional studies of the enteropathogenic Escherichia coli type III needle complex protein EscJ. *Mol Microbiol* **55:** 1658–1670

Daniell SJ, Takahashi N, Wilson R, Friedberg D, Rosenshine I, Booy FP, Shaw RK, Knutton S, Frankel G, Aizawa S (2001) The filamentous type III secretion translocon of enteropathogenic Escherichia coli. *Cell Microbiol* **3:** 865–871

Deane JE, Roversi P, Cordes FS, Johnson S, Kenjale R, Daniell S, Booy F, Picking WD, Picking WL, Blocker AJ, Lea SM (2006) Molecular model of a type III secretion system needle: implications for host-cell sensing. *Proc Natl Acad Sci USA* **103:** 12529–12533

Driks A, DeRosier DJ (1990) Additional structures associated with bacterial flagellar basal body. *J Mol Biol* **211:** 669–672

Erhardt M, Hughes KT (2010) C-ring requirement in flagellar type III secretion is bypassed by FlhDC upregulation. *Mol Microbiol* **75:** 376–393

Fadouloglou VE, Tampakaki AP, Glykos NM, Bastaki MN, Hadden JM, Phillips SE, Panopoulos NJ, Kokkinidis M (2004) Structure of HrcQB-C, a conserved component of the bacterial type III secretion systems. *Proc Natl Acad Sci USA* **101:** 70–75

Galan JE, Collmer A (1999) Type III secretion machines: bacterial devices for protein delivery into host cells. *Science* **284:** 1322–1328

Gonzalez-Pedrajo B, Fraser GM, Minamino T, Macnab RM (2002) Molecular dissection of Salmonella FliH, a regulator of the ATPase FliI and the type III flagellar protein export pathway. *Mol Microbiol* **45:** 967–982

Grant SR, Fisher EJ, Chang JH, Mole BM, Dangl JL (2006) Subterfuge and manipulation: type III effector proteins of phytopathogenic bacteria. *Annu Rev Microbiol* **60:** 425–449

Guilvout I, Chami M, Engel A, Pugsley AP, Bayan N (2006) Bacterial outer membrane secretin PulD assembles and inserts into the inner membrane in the absence of its pilotin. *EMBO J* **25:** 5241–5249

Hodgkinson JL, Horsley A, Stabat D, Simon M, Johnson S, da Fonseca PC, Morris EP, Wall JS, Lea SM, Blocker AJ (2009) Three-dimensional reconstruction of the Shigella T3SS transmembrane regions reveals 12-fold symmetry and novel features throughout. *Nat Struct Mol Biol* **16:** 477–485

Imada K, Minamino T, Tahara A, Namba K (2007) Structural similarity between the flagellar type III ATPase FliI and F1-ATPase subunits. *Proc Natl Acad Sci USA* **104:** 485–490

Jackson MW, Plano GV (2000) Interactions between type III secretion apparatus components from Yersinia pestis detected using the yeast two-hybrid system. *FEMS Microbiol Lett* **186:** 85–90

Jin Q, He SY (2001) Role of the Hrp pilus in type III protein secretion in Pseudomonas syringae. *Science* **294:** 2556–2558

Kaniga K, Delor I, Cornelis GR (1991) A wide-host-range suicide vector for improving reverse genetics in gram-negative bacteria: inactivation of the blaA gene of Yersinia enterocolitica. *Gene* **109:** 137–141

Khan IH, Reese TS, Khan S (1992) The cytoplasmic component of the bacterial flagellar motor. *Proc Natl Acad Sci USA* **89:** 5956–5960

Kimbrough TG, Miller SI (2000) Contribution of Salmonella typhimurium type III secretion components to needle complex formation. *Proc Natl Acad Sci USA* **97:** 11008–11013

Kimbrough TG, Miller SI (2002) Assembly of the type III secretion needle complex of Salmonella typhimurium. *Microbes Infect/ Institut Pasteur* **4:** 75–82

Konishi M, Kanbe M, McMurry JL, Aizawa S (2009) Flagellar formation in C-ring-defective mutants by overproduction of FliI, the ATPase specific for flagellar type III secretion. *J Bacteriol* **191:** 6186–6191

Koster M, Bitter W, de Cock H, Allaoui A, Cornelis GR, Tommassen J (1997) The outer membrane component, YscC, of the Yop secretion machinery of Yersinia enterocolitica forms a ring-shaped multimeric complex. *Mol Microbiol* **26:** 789–797

Kubori T, Matsushima Y, Nakamura D, Uralil J, Lara-Tejero M, Sukhan A, Galan JE, Aizawa SI (1998) Supramolecular structure of the Salmonella typhimurium type III protein secretion system. *Science* **280:** 602–605

Kubori T, Shimamoto N, Yamaguchi S, Namba K, Aizawa S (1992) Morphological pathway of flagellar assembly in Salmonella typhimurium. *J Mol Biol* **226:** 433–446

Kubori T, Sukhan A, Aizawa SI, Galan JE (2000) Molecular characterization and assembly of the needle complex of the Salmonella typhimurium type III protein secretion system. *Proc Natl Acad Sci USA* **97:** 10225–10230

Kubori T, Yamaguchi S, Aizawa S (1997) Assembly of the switch complex onto the MS ring complex of Salmonella typhimurium does not require any other flagellar proteins. *J Bacteriol* **179:** 813–817

Lux R, Kar N, Khan S (2000) Overproduced Salmonella typhimurium flagellar motor switch complexes. *J Mol Biol* **298:** 577–583

Lybarger SR, Johnson TL, Gray MD, Sikora AE, Sandkvist M (2009) Docking and assembly of the type II secretion complex of Vibrio cholerae. *J Bacteriol* **191:** 3149–3161

Macnab RM (2003) How bacteria assemble flagella. *Annu Rev Microbiol* **57:** 77–100

Marlovits TC, Kubori T, Sukhan A, Thomas DR, Galan JE, Unger VM (2004) Structural insights into the assembly of the type III secretion needle complex. *Science* **306:** 1040–1042

McMurry JL, Murphy JW, Gonzalez-Pedrajo B (2006) The FliN-FliH interaction mediates localization of flagellar export ATPase FliI to the C ring complex. *Biochemistry* **45:** 11790–11798

Minamino T, MacNab RM (2000) FliH, a soluble component of the type III flagellar export apparatus of Salmonella, forms a complex with FliI and inhibits its ATPase activity. *Mol Microbiol* **37:** 1494–1503

Minamino T, Namba K (2008) Distinct roles of the FliI ATPase and proton motive force in bacterial flagellar protein export. *Nature* **451:** 485–488

Moraes TF, Spreter T, Strynadka NC (2008) Piecing together the type III injectisome of bacterial pathogens. *Curr Opin Struct Biol* **18:** 258–266

Morita-Ishihara T, Ogawa M, Sagara H, Yoshida M, Katayama E, Sasakawa C (2006) Shigella Spa33 is an essential C-ring component of type III secretion machinery. *J Biol Chem* **281:** 599–607

Mota LJ, Cornelis GR (2005) The bacterial injection kit: type III secretion systems. *Ann Med* **37:** 234–249

Mueller CA, Broz P, Muller SA, Ringler P, Erne-Brand F, Sorg I, Kuhn M, Engel A, Cornelis GR (2005) The V-antigen of Yersinia forms a distinct structure at the tip of injectisome needles. *Science* **310:** 674–676

Muller SA, Pozidis C, Stone R, Meesters C, Chami M, Engel A, Economou A, Stahlberg H (2006) Double hexameric ring assembly of the type III protein translocase ATPase HrcN. *Mol Microbiol* **61:** 119–125

Nilles ML, Williams AW, Skrzypek E, Straley SC (1997) Yersinia pestis LcrV forms a stable complex with LcrG and may have a secretion-related regulatory role in the low-Ca2 + response. *J Bacteriol* **179:** 1307–1316

Pallen MJ, Bailey CM, Beatson SA (2006) Evolutionary links between FliH/YscL-like proteins from bacterial type III secretion systems and second-stalk components of the FoF1 and vacuolar ATPases. *Protein Sci* **15:** 935–941

Paul K, Erhardt M, Hirano T, Blair DF, Hughes KT (2008) Energy source of flagellar type III secretion. *Nature* **451:** 489–492

Pozidis C, Chalkiadaki A, Gomez-Serrano A, Stahlberg H, Brown I, Tampakaki AP, Lustig A, Sianidis G, Politou AS, Engel A, Panopoulos NJ, Mansfield J, Pugsley AP, Karamanou S, Economou A (2003) Type III protein translocase: HrcN is a peripheral ATPase that is activated by oligomerization. *J Biol Chem* **278:** 25816–25824

Sani M, Allaoui A, Fusetti F, Oostergetel GT, Keegstra W, Boekema EJ (2007) Structural organization of the needle complex of the type III secretion apparatus of Shigella flexneri. *Micron* **38:** 291–301

Schraidt O, Lefebre MD, Brunner MJ, Schmied WH, Schmidt A, Radics J, Mechtler K, Galan JE, Marlovits TC (2010) Topology and organization of the Salmonella typhimurium type III secretion needle complex components. *PLoS Pathog* **6:** e1000824

Schuch R, Maurelli AT (2001) MxiM and MxiJ, base elements of the Mxi-Spa type III secretion system of Shigella, interact with and stabilize the MxiD secretin in the cell envelope. *J Bacteriol* **183:** 6991–6998

Sekiya K, Ohishi M, Ogino T, Tamano K, Sasakawa C, Abe A (2001) Supermolecular structure of the enteropathogenic Escherichia coli type III secretion system and its direct interaction with the EspA-sheath- like structure. *Proc Natl Acad Sci USA* **98:** 11638–11643

Silva-Herzog E, Ferracci F, Jackson MW, Joseph SS, Plano GV (2008) Membrane localization and topology of the Yersinia pestis YscJ lipoprotein. *Microbiology (Reading, England)* **154:** 593–607

Sorg I, Wagner S, Amstutz M, Muller SA, Broz P, Lussi Y, Engel A, Cornelis GR (2007) YscU recognizes translocators as export substrates of the Yersinia injectisome. *EMBO J* **26:** 3015–3024

Spreter T, Yip CK, Sanowar S, Andre I, Kimbrough TG, Vuckovic M, Pfuetzner RA, Deng W, Yu AC, Finlay BB, Baker D, Miller SI, Strynadka NC (2009) A conserved structural motif mediates formation of the periplasmic rings in the type III secretion system. *Nat Struct Mol Biol* **16:** 468–476

Sukhan A, Kubori T, Wilson J, Galan JE (2001) Genetic analysis of assembly of the Salmonella enterica serovar Typhimurium type III secretion-associated needle complex. *J Bacteriol* **183:** 1159–1167

Tamano K, Aizawa S, Katayama E, Nonaka T, Imajoh-Ohmi S, Kuwae A, Nagai S, Sasakawa C (2000) Supramolecular structure of the Shigella type III secretion machinery: the needle part is changeable in length and essential for delivery of effectors. *EMBO J* **19:** 3876–3887

Thanbichler M, Iniesta AA, Shapiro L (2007) A comprehensive set of plasmids for vanillate- and xylose-inducible gene expression in Caulobacter crescentus. *Nucleic Acids Res* **35:** e137

Thomas DR, Francis NR, Xu C, DeRosier DJ (2006) The three-dimensional structure of the flagellar rotor from a clockwise-locked mutant of Salmonella enterica serovar Typhimurium. *J Bacteriol* **188:** 7039–7048

Torruellas J, Jackson MW, Pennock JW, Plano GV (2005) The Yersinia pestis type III secretion needle plays a role in the regulation of Yop secretion. *Mol Microbiol* **57:** 1719–1733

Van Gijsegem F, Gough C, Zischek C, Niqueux E, Arlat M, Genin S, Barberis P, German S, Castello P, Boucher C (1995) The hrp gene locus of Pseudomonas solanacearum, which controls the production of a type III secretion system, encodes eight proteins related to components of the bacterial flagellar biogenesis complex. *Mol Microbiol* **15:** 1095–1114

Wilharm G, Lehmann V, Krauss K, Lehnert B, Richter S, Ruckdeschel K, Heesemann J, Trulzsch K (2004) Yersinia enterocolitica type III secretion depends on the proton motive force but not on the flagellar motor components MotA and MotB. *Infect Immun* **72:** 4004–4009

Woestyn S, Allaoui A, Wattiau P, Cornelis GR (1994) YscN, the putative energizer of the Yersinia Yop secretion machinery. *J Bacteriol* **176:** 1561–1569

Yip CK, Kimbrough TG, Felise HB, Vuckovic M, Thomas NA, Pfuetzner RA, Frey EA, Finlay BB, Miller SI, Strynadka NC (2005) Structural characterization of the molecular platform for type III secretion system assembly. *Nature* **435:** 702–707

Young HS, Dang H, Lai Y, DeRosier DJ, Khan S (2003) Variable symmetry in Salmonella typhimurium flagellar motors. *Biophys J* **84:** 571–577

Zarivach R, Vuckovic M, Deng W, Finlay BB, Strynadka NC (2007) Structural analysis of a prototypical ATPase from the type III secretion system. *Nat Struct Mol Biol* **14:** 131–137

SUPPLEMENTARY FIGURE 1

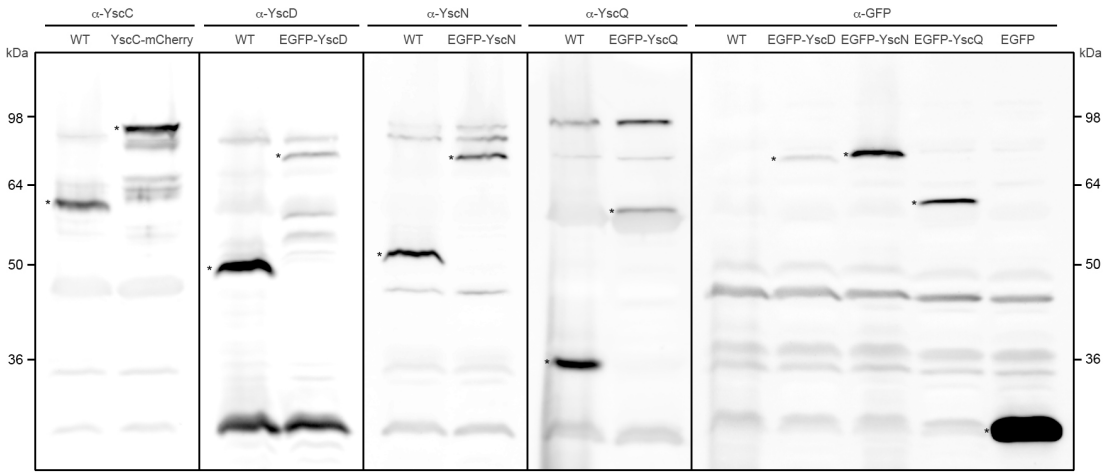

Stability of the fluorescent fusion proteins

Total cells incubated for 3 hours at 37° in non-secretion-permissive conditions were separated on a 12% SDS-PAGE gel and subsequently analyzed by immunoblot with the specific antibodies, and with a anti-GFP antibody (polyclonal rabbit, Torrey Pines Biolabs, Houston, TX, USA). WT: E40(pYV40); YscC-mCherry: E40(pMA4005); EGFP-YscD: E40(pAD4050); EGFP-YscN (ΔYscN + pBAD-EGFP-YscN): E40(pAD4136)(pAD182); EGFP-YscQ: E40(pAD4016); EGFP (pBAD-EGFP): E40(pYV40)(pISO101). All fusion proteins except for EGFP-YscN are encoded under their native promoter on the pYV virulence plasmid (see materials and methods for details).

The theoretical expected molecular weight for the wild-type and fluorescent fusion protein, respectively, are: YscC: 67.2 kDa / 97.1 kDa; YscD: 46.8 kDa / 75.9 kDa; YscN: 47.8 kDa / 77.5 kDa; YscQ: 34.4 kDa / 62.8 kDa; EGFP: 26.9 kDa. The corresponding bands are marked by asterisks.

YscC-mCherry could not be detected by the GFP antibody.

SUPPLEMENTARY FIGURE 2

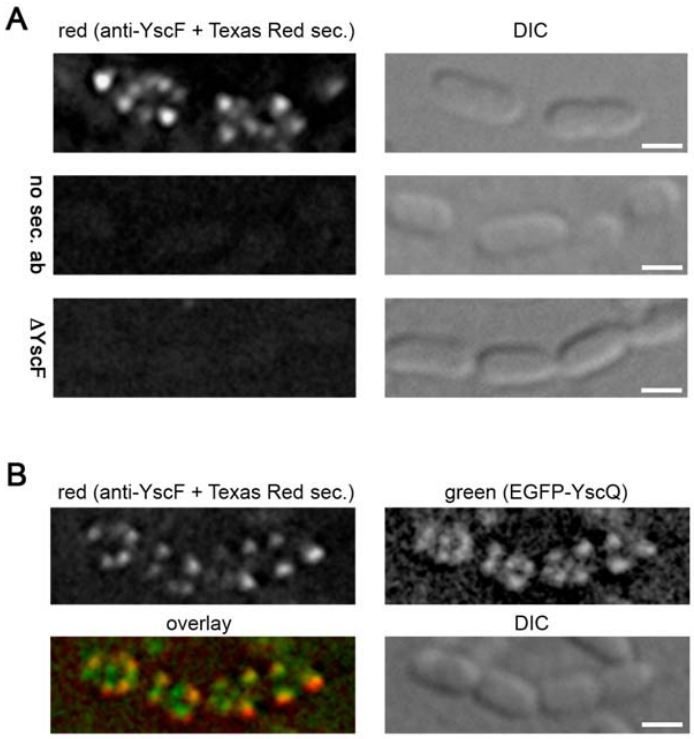

Colocalization of the needle subunit YscF with the C ring component YscQ.

A: Immunofluorescence staining of the needle component YscF. First row: E40(pAD4016) bacteria [EGFP-YscQ]; second row: E40(pAD4016) bacteria, no secondary antibody; third row: E40(pAD4020) bacteria [EGFP-YscQ, ΔYscF].

B: Fluorescence deconvolution microscopy showing the co-localization of EGFP-YscQ with YscF, visualized by immunofluorescence, in E40(pAD4016) bacteria. Sharpness and intensity of the EGFP-YscQ foci are decreased due to the immunofluorescence treatment.

All strains were incubated in secretion-non-permissive medium (BHI + Ca^{2+}). Scale bars: 2 μm.

Materials and Methods for supplementary figure 2

Immunofluorescence

Three hours after the induction of the T3S system by temperature shift to 37°, bacteria were attached to poly-D-lysine coated cover slips and fixed with 4% para-formaldehyde for 15 min at 25°. Subsequent steps were performed at 4°: Cells were blocked with 2% BSA in PBS for 60 min, incubated with primary antibody for 90 min, and subsequently incubated for 60 min either with secondary antibody, or with 2% BSA in PBS, where indicated (no sec. ab). Microscopy slides were covered with cover slips using Vectashield mounting medium and subsequently analyzed. The primary polyclonal rabbit anti-YscF antibody (MIPA 80) was first affinity-purified on YscF from purified needles (Mueller et al., 2005) from 900 ml culture, and subsequently preabsorbed with bacteria lacking YscF. The remaining solution was used undiluted with 2% BSA in PBS. The secondary antibody (Texas Red coupled swine anti-rabbit, Southern Biotech) was diluted 1:150 in 2% BSA in PBS. Further image analysis was performed as described in the corresponding section of materials and methods, Texas Red fluorescence was visualized using the mRFP filter set.

Reference for supplementary figure 2:

Mueller CA, Broz P, Muller SA, Ringler P, Erne-Brand F, Sorg I, Kuhn M, Engel A, Cornelis GR (2005) The V-antigen of Yersinia forms a distinct structure at the tip of injectisome needles. *Science* **310:** 674-676

SUPPLEMENTARY FIGURE 3

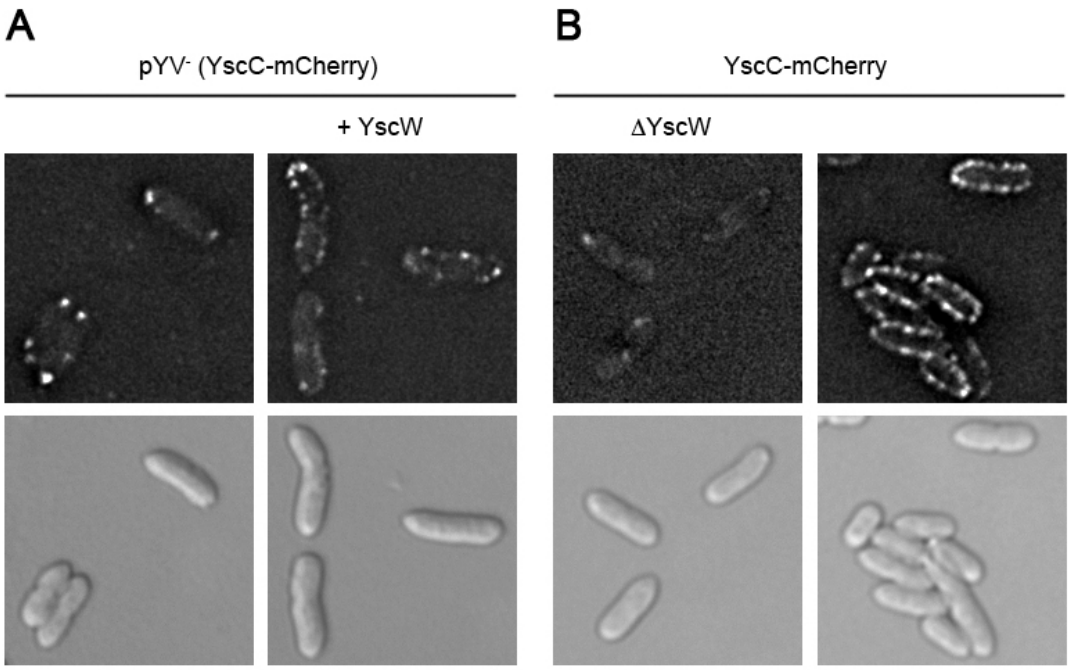

YscC-mCherry aggregates in polar spots in the absence of the pilotin YscW.

Fluorescence deconvolution microscopy showing the formation of fluorescent YscC-mCherry spots at the bacterial membrane of *Y. enterocolitica* incubated in secretion-non-permissive medium (BHI + Ca^{2+}).

A: pYV^- bacteria expressing either only YscC-mCherry from expression vector pMA8 (left side) or YscC-mCherry together with YscW from expression vectors pMA8 and pRS6 (right side). Synthesis of YscC-mCherry was induced by the addition of 0.05% arabinose, while YscW was constitutively expressed.

B: Bacteria expressing the full T3S machinery with YscC-mCherry either in the absence of YscW (W227(pADMA22784), left side) or in its presence (E40(MAAD4006), right side).

Upper lane: mCherry fluorescence; lower lane: corresponding DIC picture.

Supplementary Table 1 – List of used bacterial strains

Plasmids	Relevant characteristics	References
pYV		
pAA207	pYV227 *yscH::aphA-3* (does not encode YscH)	(Allaoui et al, 1995b)
pAA210	pYV227 *yscK::aphA-3* (does not encode YscK)	(Allaoui et al, 1995b)
pAD4016	pYV40 *egfp-yscQ* (pYV40 mutated with pAD118)	this work
pAD4020	pYV40 *egfp-yscQ* $yscF_{\Delta 1-74}$ (pISO4006 mutated with pAD118)	this work
pAD4022	pYV40 *egfp-yscQ ΔyscI* (pKEM4001 mutated with pAD118)	this work
pAD4024	pYV40 *egfp-yscQ* $yscO_{\Delta 4-149}$ (pISO4008 mutated with pAD118)	this work
pAD4026	pYV40 *egfp-yscQ ΔyscU* (pLY4001 mutated with pAD118)	this work
pAD4027	pYV40 *egfp-yscQ* $yscX_{\Delta 42-75}$ (pIM405 mutated with pAD118)	this work
pAD4032	pYV40 *egfp-yscQ* $yscR_{\Delta 2-207}$ (pAD4016 mutated with pAD128)	this work
pAD4034	pYV40 *egfp-yscQ ΔyscS* (pAD4016 mutated with pAD130)	this work
pAD4036	pYV40 *egfp-yscQ* $yscT_{\Delta 2-250}$ (pAD4016 mutated with pAD132)	this work
pAD4037	pYV40 *egfp-yscQ* $yscV_{\Delta 5-650}$ (pYV40 mutated with pAD134)	this work
pAD4038	pYV40 *egfp-yscQ* $yscV_{\Delta 5-650}$ (pAD4016 mutated with pAD134)	this work
pAD4039	pYV40 *egfp-yscQ ΔyscL* (pSI4006 mutated with pAD118)	this work
pAD4040	pYV40 *egfp-yscQ* $yscY_{\Delta 21-51}$ (pIM406 mutated with pAD118)	this work
pAD4041	pYV40 *egfp-yscQ* $lcrG_{\Delta 8-57}$ (pMRS4043 mutated with pAD118)	this work
pAD4042	pYV40 *egfp-yscQ* $lcrV_{\Delta 2-324}$ (pMRS4071 mutated with pAD118)	this work
pAD4043	pYV40 *egfp-yscQ* $yopN_{\Delta 5}$ (pIM41 mutated with pAD118)	this work
pAD4049	pYV40 his_6*-flag-yscD* (pYV40 mutated with pAD138)	this work
pAD4050	pYV40 *egfp-yscD* (pYV40 mutated with pAD140)	this work
pAD4051	pYV40 $yscD_{\Delta 2-404}$ (pYV40 mutated with pAD164)	this work
pAD4052	pYV40 *egfp-yscQ* $yscD_{\Delta 2-404}$ (pAD4016 mutated with pAD164)	this work
pAD4054	pYV40 *yscJ-flag-*his_6 *yadA::pLJM31* (pAD40085 mutated with pLJM31)	this work
pAD4055	pYV40 his_6*-flag-yscD yadA::pLJM31* (pAD4049 mutated with pLJM31)	this work
pAD4061	pYV40 *egfp-yscD* $yscQ_{\Delta 2-295}$ (pISOA4015 mutated with pAD140)	this work
pAD4078	pYV40 Δ*yscJ* (pYV40 mutated with pAD158)	this work
pAD4080	pYV40 *egfp-yscD* Δ*yscJ* (pAD4050 mutated with pAD158)	this work
pAD4082	pYV40 *egfp-yscQ* Δ*yscJ* (pAD4016 mutated with pAD158)	this work

pAD4088	pYV40 *his$_8$-flag-yscD ΔyscJ* (pAD4078 mutated with pAD138)	this work
pAD4089	pYV40 *his$_8$-flag-yscD ΔyscJ yadA::pLJM31* (pAD4088 mutated with pLJM31)	this work
pAD4091	pYV40 *yscJ-flag-his$_8$ yscC$_{Δ2-598}$* (pAD40085 mutated with pMA26)	this work
pAD4092	pYV40 *yscJ-flag-his$_8$ yscD$_{Δ2-404}$* (pAD40085 mutated with pAD164)	this work
pAD4104	pYV40 *egfp-yscQ yscN$_{Δ2-427}$* (pAD4016 mutated with pAD168)	this work
pAD4106	pYV40 *yscJ-flag-his$_8$ yscQ$_{Δ2-295}$* (pAD40085 mutated with pISOA131)	this work
pAD4107	pYV40 *ΔyscRSTU yscVΔ$_{5-680}$* (pYV40 mutated with pAD170)	this work
pAD4108	pYV40 *egfp-yscQ ΔyscRSTU yscVΔ$_{5-680}$* (pAD4038 mutated with pAD170)	this work
pAD4109	pYV40 *yscJ-flag-his$_8$ yscC$_{Δ2-598}$ yadA::pLJM31* (pAD4091 mutated with pLJM31)	this work
pAD4110	pYV40 *yscJ-flag-his$_8$ yscD$_{Δ2-404}$ yadA::pLJM31* (pAD4092 mutated with pLJM31)	this work
pAD4111	pYV40 *yscJ-flag-his$_8$ yscQ$_{Δ2-295}$ yadA::pLJM31* (pAD4106 mutated with pLJM31)	this work
pAD4136	pYV40 *yscN$_{Δ2-427}$* (pYV40 mutated with pAD168)	this work
pAD4139	pYV40 *yscN$_{Δ2-427}$ ΔyscJ* (pAD4078 mutated with pAD168)	this work
pAD4141	pYV40 *yscN$_{Δ2-427}$ ΔyscL* (pSI4006 mutated with pAD168)	this work
pAD4142	pYV40 *yscN$_{Δ2-427}$ yscQΔ$_{2-295}$* (pISOA4015 mutated with pAD168)	this work
pAD4143	pYV40 *yscN$_{Δ2-427}$ ΔyscRSTU yscVΔ$_{5-680}$* (pAD4107 mutated with pAD168)	this work
pAD4157	pYV40 *yscF$_{Δ1-74}$ yscN$_{Δ2-427}$* (pISO4006 mutated with pAD168)	this work
pAD22723	pYV227 *egfp-yscQ ΔyscK* (pAA210 mutated with pAD118)	this work
pAD22729	pYV227 *egfp-yscQ* (pYV227 mutated with pAD118)	this work
pAD22769	pYV227 *egfp-yscQ ΔyscH* (pAA207 mutated with pAD118)	this work
pAD22840	pYV227 *yscN$_{Δ2-427}$ ΔyscK* (pAA210 mutated with pAD168)	this work
pAD40082	pYV40 *yscJ-his$_8$* (pYV40 mutated with pAD104)	this work
pAD40085	pYV40 *yscJ-flag-his$_8$* (pYV40 mutated with pAD110)	this work
pADMA4099	pYV40 *his$_8$-flag-yscD yscC$_{Δ2-598}$* (pYV40 mutated with pMA27)	this work
pADMA4101	pYV40 *his$_8$-flag-yscD yscC$_{Δ2-598}$ yadA::pLJM31* (pADMA4099 mutated with pLJM31)	this work
pADMA4137	pYV40 *yscC-mCherry yscN$_{Δ2-427}$* (pMA4005 mutated with pAD168)	this work
pADMA4151	pYV40 *egfp-yscQ yscC$_{Δ2-598}$* (pAD4016 mutated with pMA26)	this work
pADMA4156	pYV40 *yscC$_{Δ2-598}$ yscN$_{Δ2-427}$* (pMA4005 mutated with pAD168)	this work
pADMA22784	pYV227 *egfp-yscQ yscC-mCherry yscW::aphA-3* (pMA22708 mutated with pAD118)	this work
pIM405	pYV40 *yscX$_{Δ42-75}$*	(Iriarte & Cornelis, 1999)
pIM406	pYV40 *yscY$_{Δ21-45}$*	(Iriarte & Cornelis, 1999)
pIM41	pYV40 *yopN$_{45}$* (does not encode YopN)	(Boland et al, 1996)
pISO4006	pYV40 *yscF$_{Δ1-74}$* (pYV40 mutated with pISO85)	this work

pISO4008	pYV40 *yscO*$_{\Delta 4\text{-}149}$ (pYV40 mutated with pISO110)	this work
pISOA4015	pYV40 *yscQ*$_{\Delta 2\text{-}295}$ (pYV40 mutated with pISO131)	this work
pKEM4001	pYV40 Δ*yscI* (pYV40 mutated with pKEM5)	this work
pLJM4029	pYV40 *yadA::pLJM31* (does not encode YadA)	(Mota et al, 2005)
pLY4001	pYV40 *ΔyscU*	(Sorg et al, 2007)
pMA22708	pYV227 *yscC-mCherry yscW::aphA-3* (pRS227 mutated with pMA12)	this work
pMA4005	pYV40 *yscC-mCherry* (pYV40 mutated with pMA12)	this work
pMA4007	pYV40 *yscC-mCherry yscQ*$_{\Delta 2\text{-}295}$ (pISO4015 mutated with pMA12)	this work
pMA4011	pYV40 *yscC-mCherry yscV*$_{\Delta 5\text{-}680}$ (pAD4037 mutated with pMA12)	this work
pMA4015	pYV40 *yscC-mCherry yscF*$_{\Delta 1\text{-}74}$ (pISO4006 mutated with pMA12)	this work
pMAAD4006	pYV40 *egfp-yscQ yscC-mCherry* (pAD4016 mutated with pMA12)	this work
pMAAD4018	pYV40 *yscC*$_{\Delta 2\text{-}598}$ *egfp-yscD* (pYV40 mutated with pMA28)	this work
pMRS4043	pYV40 *lcrG*$_{\Delta 8\text{-}57}$	(Sarker et al, 1998b)
pMRS4071	pYV40 *lcrV*$_{\Delta 1\text{-}324}$	(Sarker et al, 1998a)
pRS227	pYV227 *yscW::aphA-3* (does not encode YscW)	(Allaoui et al, 1995a)
pSI4006	pYV40 Δ*yscL* (pYV40 mutated with pSI51)	this work
pYV227	wild-type pYV plasmid of *Y.enterocolitica* W22703	(Cornelis & Colson, 1975)
pYV40	wild-type pYV plasmid of *Y.enterocolitica* E40	(Sory et al, 1995)
Suicide vectors and mutators		
pAD104	pKNG101 *yscJ-his*$_8^+$ (*his*$_8$ cloned in-frame at the C-terminus of *yscJ*)	this work
pAD110	pKNG101 *yscJ-flag-his*$_8^+$ (*flag-his*$_8$ cloned in-frame at the C-terminus of *yscJ*)	this work
pAD118	pKNG101 *egfp-yscQ*$^+$ (*egfp* cloned in-frame at the N-terminus of *yscQ*)	this work
pAD128	pKNG101 *yscR*$_{\Delta 2\text{-}207}^+$	this work
pAD130	pKNG101 *ΔyscS*$^+$	this work
pAD132	pKNG101 *yscT*$_{\Delta 2\text{-}250}^+$	this work
pAD134	pKNG101 *yscV*$_{\Delta 5\text{-}680}^+$	this work
pAD138	pKNG101 *his*$_8$*-flag-yscD*$^+$ (*his*$_8$*-flag* cloned in-frame at the N-terminus of *yscD*)	this work
pAD140	pKNG101 *egfp-yscD*$^+$ (*egfp* cloned in-frame at the N-terminus of *yscD*)	this work
pAD158	pKNG101 *ΔyscJ*$^+$	this work
pAD164	pKNG101 *yscD*$_{\Delta 2\text{-}404}^+$	this work
pAD168	pKNG101 *yscN*$_{\Delta 2\text{-}427}^+$	this work
pAD170	pKNG101 *ΔyscRSTU*$^+$	this work
pISO85	pKNG101 *yscF*$_{\Delta 1\text{-}74}^+$	this work
pISO110	pKNG101 *yscO*$_{\Delta 4\text{-}149}^+$	this work
pISOA131	pKNG101 *yscQ*$_{\Delta 2\text{-}295}^+$	this work
pKEM5	pKNG101 *ΔyscI*$^+$	this work
pKNG101	*ori*$_{R6K}$ *sacBR*$^+$ *oriT*$_{RK2}$ *strAB*$^+$ (suicide vector)	(Kaniga et al, 1991)
pLJM31	pKNG101 *yadA*	(Mota et al, 2005)
pMA12	pKNG101 *yscC-mCherry*$^+$ (*mCherry* cloned in-frame at the C-terminus of *yscC*)	this work
pMA26	pKNG101 *yscC*$_{\Delta 2\text{-}598}^+$	this work
pMA27	pKNG101 *yscC*$_{\Delta 2\text{-}598}^+$ *his*$_8$*-flag-yscD*$^+$	this work
pMA28	pKNG101 *yscC*$_{\Delta 2\text{-}598}^+$ *egfp-yscD*$^+$	this work
pSI51	pKNG101 *ΔyscL*$^+$	this work
Clones and vectors		
pAD165	pBAD::*yscN*$_{WT}$ (complete *yscN* gene)	this work
pAD166	pBAD::*yscN*$_{K175E}$ (complete *yscN* gene with Lys to Glu mutation in pos. 175)	this work
pAD182	pBAD::*egfp-yscN*$_{WT}$ (complete *yscN* gene with N-terminal *egfp*)	this work
pBAD-his/B	pBR322-derived expression vector	Invitrogen
pEGFP-C1	contains *egfp* gene	BD Biosciences Clontech
pISO101	pBAD::*egfp*	this work
pISOA129	pBAD::*his*$_6$*-yscQ* (complete *yscQ* gene with N-terminal *his*$_6$)	this work
pMA8	pBAD::*yscC-mCherry* (complete *yscC* gene with C-terminal *mCherry*)	this work
pRVCHYN-5	contains *mCherry* gene	(Thanbichler et al, 2007)
pRS6	contains *yscW* (*virG*)	(Allaoui et al, 1995a)

References for Supplementary Table 1:

Allaoui A, Scheen R, Lambert de Rouvroit C, Cornelis GR (1995a) VirG, a Yersinia enterocolitica lipoprotein involved in Ca2+ dependency, is related to exsB of Pseudomonas aeruginosa. *Journal of bacteriology* **177:** 4230-4237.

Allaoui A, Schulte R, Cornelis GR (1995b) Mutational analysis of the Yersinia enterocolitica virC operon: characterization of yscE, F, G, I, J, K required for Yop secretion and yscH encoding YopR. *Molecular microbiology* **18:** 343-355.

Boland A, Sory MP, Iriarte M, Kerbourch C, Wattiau P, Cornelis GR (1996) Status of YopM and YopN in the Yersinia Yop virulon: YopM of Y.enterocolitica is internalized inside the cytosol of PU5-1.8 macrophages by the YopB, D, N delivery apparatus. *The EMBO journal* **15:** 5191-5201.

Cornelis G, Colson C (1975) Restriction of DNA in Yersinia enterocolitica detected by recipient ability for a derepressed R factor from Escherichia coli. *Journal of general microbiology* **87:** 285-291

Iriarte M, Cornelis GR (1999) Identification of SycN, YscX, and YscY, three new elements of the Yersinia yop virulon. *Journal of bacteriology* **181:** 675-680.

Kaniga K, Delor I, Cornelis GR (1991) A wide-host-range suicide vector for improving reverse genetics in gram-negative bacteria: inactivation of the blaA gene of Yersinia enterocolitica. *Gene* **109:** 137-141

Koster M, Bitter W, de Cock H, Allaoui A, Cornelis GR, Tommassen J (1997) The outer membrane component, YscC, of the Yop secretion machinery of Yersinia enterocolitica forms a ring-shaped multimeric complex. *Molecular microbiology* **26:** 789-797.

Mota LJ, Journet L, Sorg I, Agrain C, Cornelis GR (2005) Bacterial injectisomes: needle length does matter. *Science* **307:** 1278

Sarker MR, Neyt C, Stainier I, Cornelis GR (1998a) The Yersinia Yop virulon: LcrV is required for extrusion of the translocators YopB and YopD. *Journal of bacteriology* **180:** 1207-1214

Sarker MR, Sory MP, Boyd AP, Iriarte M, Cornelis GR (1998b) LcrG is required for efficient translocation of Yersinia Yop effector proteins into eukaryotic cells. *Infection and immunity* **66:** 2976-2979.

Sorg I, Wagner S, Amstutz M, Muller SA, Broz P, Lussi Y, Engel A, Cornelis GR (2007) YscU recognizes translocators as export substrates of the Yersinia injectisome. *The EMBO journal* **26:** 3015-3024

Sory MP, Boland A, Lambermont I, Cornelis GR (1995) Identification of the YopE and YopH domains required for secretion and internalization into the cytosol of macrophages, using the cyaA gene fusion approach. *Proceedings of the National Academy of Sciences of the United States of America* **92:** 11998-12002.

Thanbichler M, Iniesta AA, Shapiro L (2007) A comprehensive set of plasmids for vanillate- and xylose-inducible gene expression in Caulobacter crescentus. *Nucleic acids research* **35:** e137

Supplementary Table 2 – List of used oligonucleotides

No.	Sequence	features	used for cloning of	template
4523	gatcgggccctcagtttgacacctacatacctca	ApaI site	pAD104 and pAD110, ext. fwd. primer	pYV40
4532	gtgatggtgatggtgatggtggtgaccaccgccacctttcttcctctggagccaaaaatattgagcaa gattgg		pAD104, int. rev. primer	pYV40
4533	caccaccatcaccatcaccatcactgaggttacaacgcaagaagtgatg		pAD104 and pAD110, int. fwd. primer	pYV40
4527	gatctctagaacagttcgagctgtgattgg	XbaI site	pAD104 and pAD110, ext. rev. primer	pYV40
4534	ccttgtagtcaccaccgccacctttcttcctctggagccaaaaatattgagcaagattgg		pAD110, int. fwd. primer 1	pYV40
4535	gtgatggtgatggtgatggtggtgcttatcatcgtcgtccttgtagtcaccaccgcca		pAD110, int. fwd. primer 2	pYV40
4762	gatcgggccctgaattgggggctattatg	ApaI site	pAD118, ext. fwd. primer	pYV40
4767	ctgctccaccggatccatacggcaaccggtctcattcttcagcctcccac	AgeI and BamHI sites for *egfp* insertion	pAD118, int. rev. primer	pYV40
4768	tatggatccggtggagcaggtggtgccggaggtagtttgttaaccttgccacaagc		pAD118, int. fwd. primer	pYV40
4763	gatctctagaaatggagcccctagtaagtcg	XbaI site	pAD118, ext. rev. primer	pYV40
4929	gatcgggcccgaaccaacttccggttcaag	ApaI site	pAD128 and pAD170, ext. fwd. primer	pYV40
4930	ccagcccatgcgtcatgaaatcgtaacctctgtca		pAD128, int. rev. primer	pYV40
4931	ttacgatttcatgacgcatgggctggtgatta		pAD128, int. fwd. primer	pYV40
4932	gatctctagaagcaaacagtgtgaccacca	XbaI site	pAD128, ext. rev. primer	pYV40
4933	gatcgggcccctgcgtttacggtgagtgag	ApaI site	pAD130, ext. fwd. primer	pYV40
4934	aagccacgaggcgtcaccctccgtaactaatcacc		pAD130, int. rev. primer	pYV40
4935	tacggagggtgacgcctcgtggcttggtaatg		pAD130, int. fwd. primer	pYV40
4936	gatctctagaagacataaagagccaatgaacagac	XbaI site	pAD130, ext. rev. primer	pYV40
4937	gatcgggccctggctggtgctagtcctttc	ApaI site	pAD132, ext. fwd. primer	pYV40
4938	cagtaaacttatagtcatcttatgccttgtatcttcatc		pAD132, int. rev. primer	pYV40
4939	aaggcataagatgactataagtttactgatccctgttttgg		pAD132, int. fwd. primer	pYV40
4940	gatctctagactctgctctgcgggatta	XbaI site	pAD132, ext. rev. primer	pYV40
4941	gatcgggcccgctgacgttaaatcctgagca	ApaI site	pAD134, ext. fwd. primer	pYV40
4942	agtaccggcaagtcatggggattcattatgatcttt		pAD134, int. rev. primer	pYV40
4943	tgaatccccatgacttgccggtactttcatacca		pAD134, int. fwd. primer	pYV40
4944	gatctctagaggataagcacgatccaaacc	XbaI site	pAD134, ext. rev. primer	pYV40
4858	gatcgggccctggtcaggatctacgtactggt	ApaI site	pAD138 and pAD140, ext. fwd. primer	pYV40
4861	cttatcatcgtcgtccttgtagtcgtgatggtgatggtgatggtggtgtctcacaatacgccacgctta		pAD138, int. rev. primer	pYV40
4862	gactacaaggacgacgatgataagggtggagcaggtggtgccggaggtagttgggtctgtcgttttt atca		pAD138, int. fwd. primer	pYV40
4859	gatctctagaaccctacttccagacaagtgc	XbaI site	pAD138 and pAD140, ext. rev. primer	pYV40
4863	ctgctccaccagaattcatacggcaaccggtctcacaatacgccacgctta	AgeI and EcoRI sites for *egfp* insertion	pAD140, int. rev. primer	pYV40
4864	tatgaattctggtggagcaggtggtgccggaggtagttgggtctgtcgtttttatca		pAD140, int. fwd. primer	pYV40

4528	gatcgggccctgcggcaatgtcagaagata	ApaI site	pAD158, ext. fwd. primer	pYV40
5079	ttgcgttgtaacctagttctcacccccccttc		pAD158, int. rev. primer	pYV40
5080	gggtgagaactaggttacaacgcaagaagtgatg		pAD158, int. fwd. primer	pYV40
4527	gatctctagaacagttcgagctgtgattgg	XbaI site	pAD158, ext. rev. primer	pYV40
4925	gatcgggcccgatgaaatatctaatcaaagcactacc	ApaI site	pAD164, ext. fwd. primer	pYV40
4926	cacaaattcccgtttcacaatacgccacgcttag		pAD164, int. rev. primer	pYV40
4927	tggcgtattgtgaaacgggaatttgtgatccag		pAD164, int. fwd. primer	pYV40
4928	gatctctagatcctgctacataatgaataatggcta	XbaI site	pAD164, ext. rev. primer	pYV40
5275	gactacatgttgtcactagatcagatacctcatcatattcgt	PciI site	pAD165 and pAD166, ext. fwd. primer	pYV40
5276	aagcagtgtactttcaccaccaccggcggccgcgaagat	mutated *yscN* sequence encoding GGGE175	pAD166, int. rev. primer	pYV40
5277	ggtggtggtgaaagtacactgcttgcttcgc	mutated *yscN* sequence encoding GGGE175	pAD166, int. fwd. primer	pYV40
5278	gactctcgagtatcattgggtcagcgtctc	XhoI site	pAD165 and pAD166, ext. rev. primer	pYV40
5271	gactgggcccagcggggtattgccataag	ApaI site	pAD168, ext. fwd. primer	pYV40
5272	ctcattgaaatggagcataaatccataatggttgaaat		pAD168, int. rev. primer	pYV40
5273	atggatttatgctccatttcaatgagacgctga		pAD168, int. fwd. primer	pYV40
5274	gacttctagactttacaattcagtgtggtgttttt	XbaI site	pAD168, ext. rev. primer	pYV40
5297	ttttgcctttctatcatgaaatcgtaacctctgtca		pAD170, int. rev. primer	pYV40
5298	gttacgatttcatgatagaaaggcaaaatatcgagaaaca		pAD170, int. fwd. primer	pYV40
5299	gatctctagatcctaatataagtgaacctcttgttgg	XbaI site	pAD170, ext. rev. primer	pYV40
5475	gactacatgttgctagcatcagggccctatgctctcactagatcagatacctc	PciI site, NheI and ApaI sites for *egfp* insertion	pAD182, fwd. primer	pYV40
5278	gactctcgagtatcattgggtcagcgtctc	XhoI site	pAD182, rev. primer	pYV40
3316	gatcgtcgacctcgatgacacaattaga	SalI site	pISO85, ext. fwd. primer	pYV40
3955	gccttgcattaagtctttcatttattttagacctcctgctac		pISO85, int. rev. primer	pYV40
3956	gtagcaggaggtctaaaataaatgaaagacttaatgcaaggc		pISO85, int. fwd. primer	pYV40
3317	gatcgtcgacctcgatgacacaattaga	XbaI site	pISO85, ext. rev. primer	pYV40
3313	gatcgtcgacttgtcagcaaggagcaca	SalI site	pISO110, ext. fwd. primer	pYV40
4167	cattaggcgttcctgtgatggcgtatcattgggtcag		pISO110, int. rev. primer	pYV40
4168	ctgacccaatgatacgccatcacaggaacgcctaatg		pISO110, int. fwd. primer	pYV40
4166	catgtctagacctctttcctaccgggttgaaacg	XbaI site	pISO110, ext. rev. primer	pYV40
4537	gatcgagatcttgatgagtttgttaaccttgcca	BglII site	pISOA129	pYV40
4538	gatcaagctttcatgaaatcgtaacctctg	HindIII site	pISOA129	pYV40
4539	acgcgtcgaccggctcatcccaagtaaccc	SalI site	pISO131, ext. fwd. primer	pYV40
4541	caggcgttcaattcgaaccctcattcttcagcctcccactc		pISO131, int. rev. primer	pYV40
4542	gagtgggaggctgaagaatgagggttcgaattgaacgcctg		pISO131, int. fwd. primer	pYV40
4540	ctagtctagacgtgaggctaacctcattagc	XbaI site	pISO131, ext. rev. primer	pYV40
3352	gatcgtcgaccgtttcggtcaacatcaa	SalI site	pKEM5	pYV40

3509	gaactagtgaaagttaagacttc	5' phosphorylated	pKEM5	pYV40
3510	ttatgtctccatatcaatttgatg	5' phosphorylated	pKEM5	pYV40
3353	gatctctagatctcgtgtggatagccct	XbaI site	pKEM5	pYV40
5013	gactccatggctttttccgctacattctttttttc	NcoI site	pMA8, int. fwd. primer for insert 1	pYV40
5016	cacgtctcgagtacctccggcaccgcctgcgccacccaatacgccacgcttaggtgctg	XhoI site, GGAGGAGG linker	pMA8 and pMA12, int. rev. primer for insert 1	pYV40
5017	taagatctcgagctccggagaattcg	amplifies *mCherry*	pMA8 and pMA12 fwd. primer for insert 2	pRVCHYN-5
5018	gcatggtaccttacttgtacagctcgtccatgcc	KpnI site	pMA8, int. rev. primer for insert 2	pRVCHYN-5
5066	agtcgtcgaccttgaataagttattaggtggctcc	SalI site	pMA12, insert 1	pYV40
5087	ccacgcttaggtgctgaaaccttgtacagctcgtccatgcc	amplifies *mCherry*	pMA12, int. rev. primer for insert 2	pYV40
5088	ggcatggacgagctgtacaaggtttcagcacctaagcgtggcgtattgtgagttgg		pMA12, int. fwd. primer for insert 3	pYV40
5068	agactctagaatacctttcttcatcgaccatcagc	XbaI site	pMA12, ext. rev. primer for insert 3, pMA26, pMA27, pMA28	pYV40, pAD4049, pAD4050
5235	gcatgtcgactgggctaaacgttatcctcaaactttag	SalI site	pMA26, pMA27, pMA28	pYV40, pAD4049, pAD4050
5236	ccacgcttaggtgctgaaaccatattacttaattccaccccacgc		pMA26, pMA27, pMA28	pYV40, pAD4049, pAD4050
5237	gcgtggggtggaattaagtaatatggtttcagcacctaagcgtgg		pMA26, pMA27, pMA28	pYV40, pAD4049, pAD4050

Supplementary Table 3 - Conserved homologs in the flagellum and in the injectisomes from *Yersinia* spp, *S. enterica* Typhimurium SPI-I, *Shigella* spp and plant pathogens (adapted from Cornelis, 2006)

Flagellum	Injectisomes				
	Yersinia Ysc	*S. typhimurium* SPI-1	*S. flexneri*	Plant pathogens	Function/Location/Structure
-	YscC	InvG	MxiD	HrcC	Secretin Outer membrane
FliG	YscD	PrgH	MxiG	HrcD	MS ring (low degree of conservation)
FliF	YscJ	PrgK	MxiJ	HrcJ	MS ring Lipoprotein (EscJ in EPECs)
FliI	YscN	InvC/SpaL	Spa47	HrcN	ATPase
FliN+FliM	YscQ	InvK/SpaO	Spa33	HrcQ ($HrcQ_A$ + $HrcQ_B$)	Putative C-ring
FliP	YscR	InvL/SpaP	Spa24	HrcR	Export apparatus Inner membrane protein
(FliQ)	YscS	SpaQ	Spa9	HrcS	Export apparatus Inner membrane protein
FliR	YscT	InvN/SpaR	Spa29	HrcT	Export apparatus Inner membrane protein
FlhB	YscU	SpaS	Spa40	HrcU	Export apparatus Inner membrane protein involved in substrate specificity switching
FlhA	YscV*	InvA	MxiA	HrcV	Export apparatus Inner membrane protein

*initially described as LcrD

Reference for Supplementary Table 3:

Cornelis GR (2006) The type III secretion injectisome. *Nat Rev Microbiol* **4:** 811-825

5 The Injectisome at the Bacterial Surface

5.1 Introduction

In the last decade injectisomes from *S. enterica*, *S. flexneri* and EPEC were purified and single particle electron microscopy structures were shown (Blocker et al, 2001; Kubori et al, 1998; Sekiya et al, 2001; Tamano et al, 2000). But these purified particles are merely the structural skeleton of the injectisomes and consist mainly of 5 proteins, which build up the inner and outer membrane rings, the needle and the rod. The ATPase complex and the export machinery are missing. Up to now there is neither a single particle structure of an injectisome out of the Ysc family nor an *in situ* structure of any T3S injectisome. Several *in situ* structures of flagella have been show by cryo electron tomography (cryo-ET) (Chen et al, 2011; Kudryashev et al, 2010; Murphy et al, 2006). This allowed the identification of structures missing in purified flagella, like a density in the cytosol just below the centre, which is very likely made up by the ATPase complex. Thus we decided to look at the Ysc injectisomes of *Y. enterocolitica* by cryo-ET. A major factor in getting high-resolution cryo-ET structures is the sample size. The mean distance travelled by an electron between two scattering events at a voltage of 300 kV is about 350 nm (Grimm et al, 1996; Milne & Subramaniam, 2009). This means at a sample size of about 1000 nm, which corresponds to the diameter of *Y. enterocolitica* cells, only cellular components with high local contrast can be visualized. Thus smaller cells would be a great advantage. For *E. coli* so called minicells were already reported in 1967 (Adler et al, 1967). This minicells are devoid of the chromosome due to asymmetric septum placement caused by a defect in the Min system. The Min system consists of MinC, MinD and MinE. MinD is a membrane-associated protein, supposed to make a helical structure, placing MinC, which prevents the septum initiator FtsZ from forming a stable ring. MinE causes oscillation of the MinD structure from pole to pole, by activation of the ATPase activity of MinD that releases it from the membrane (Fig. 5.1; for review see (Rothfield et al, 2005)). Thus we created a deletion of *minD*, which as expected resulted in a strain misplacing the septum, forming long cells as well as very small cells, minicells. These minicells contained injectisomes, allowing us to show the first *in situ* structure of an injectisome.

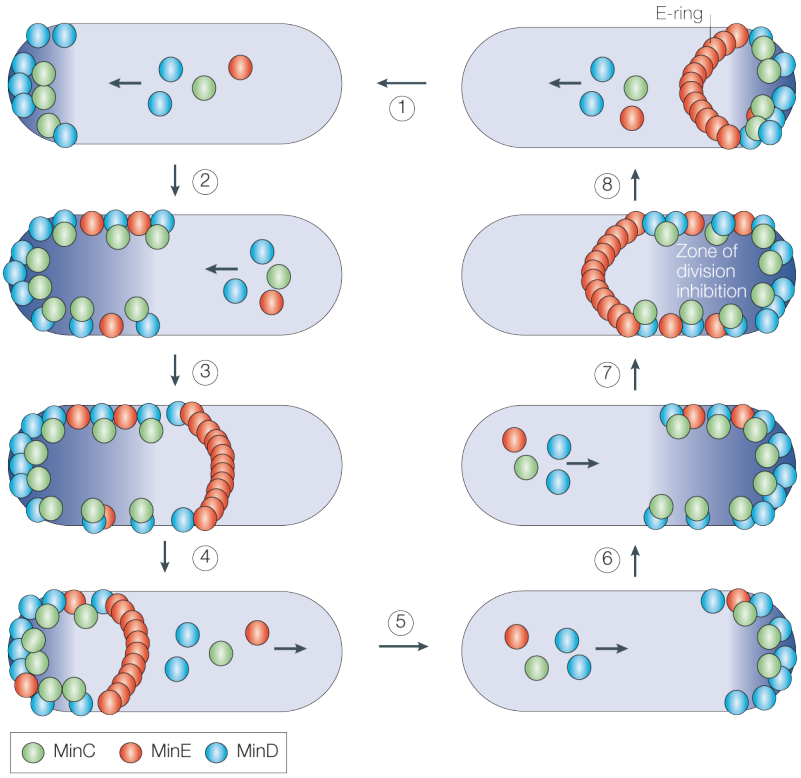

Fig. 5.1: The MinCDE oscillation cycle (Rothfield et al, 2005)

MinC and MinD assemble from the pole towards midcell (1-2 and 5-6). A MinE ring is assembled at the leading edges (3 and 7) disassembling the MinCD structure (4 and 8). Released MinC and MinD can reassemble at the opposite poles (1 and 5).

5.2 Statement of Personal Contribution

For this manuscript, I generated all the new plasmids and mutants needed, performed almost all the bacteria work, did the fluorescence microscopy (supplementary information) and helped writing.

5.3 Manuscript

In situ structure of the *Yersinia enterocolitica* injectisome

Mikhail Kudryashev[a], Marlise Amstutz[b], Daniel Castaño-Díez[a], Christopher K. E. Bleck[a], Julia Kowal[a], Guy R. Cornelis[b,1], Henning Stahlberg[a,1]

[a]Center for Cellular Imaging and NanoAnalytics (C-CINA), Biozentrum, University of Basel, WRO-1058, Mattenstrasse 26, CH-4058 Basel

[b]Focal Area Infection Biology, Biozentrum, University of Basel, Klingelbergstrasse 50/70 CH-4056 Basel / Switzerland

Total character count (main text, incl. spaces): **~22345** (without table, refs, and figure legends)
References in the main text: 69
Running title: The *Yersinia* injectisome
Subject category: Biophysics and Computational Biology/ Microbiology

ABSTRACT

Bacterial type III secretion systems (T3SS) are multi protein complexes, called injectisomes, which secrete effector proteins into eukaryotic host cells to manipulate them to their benefit. Despite the success in structural characterization of isolated injectisomes from *Shigella flexneri* and *Salmonella* Typhimurium the injectisome appearance in bacteria *in vivo* remains elusive. We present an entire *in situ* structure of the *Yersinia enterocolitica* injectisome from cryo electron tomography at a resolution of 3.7 nm and an *in situ* structure of *S. flexneri* at a resolution of 6 nm. Injectisomes *in situ* are significantly stretched compared to the isolated structures. Variational analysis of sub-tomograms suggests a significant elongation flexibility of the basal body. A structure that could be attributed to the ATPase YscN responsible for type III export was seen fully or partially assembled only in half of the particles. We further demonstrate how the injectisomes are embedded into bacterial outer membranes by structural characterization of YscC secretin reconstituted on lipid vesicles. We thus generate a hierarchical model of the injectisome assembly *in situ* and demonstrate differences between isolated macromolecular complexes and their appearance *in vivo*.

Keywords: type III secretion, bacterial pathogenesis, sub-volume averaging, needle complex

Injectisomes are complex nanomachines allowing Gram-negative bacteria to export effector proteins in one step across the two bacterial membranes and an eukaryotic cell membrane (1). The assembly involves 34 different proteins, most of them forming the structure and the others acting as ancillary components driving the assembly (1-3). Phylogenic analyses based on the most conserved proteins classify injectisomes into 7 different families (Ysc, Ssa-Esc, Inv-Mxi-Spa, Hrc1, Hrc2, Rhizobiales, and Chlamydiales) (4, 5). Parts of the *Salmonella enterica SPI-I* and the *Shigella flexneri* injectisomes, both from the same Inv-Mxi-Spa family and part of the enteropathogenic *E. coli* (EPEC) injectisome (Ssa-Esc family) could be purified as a complex cylindrical structure, resembling the flagellar basal body (2, 3, 6-9). Such purification has not been achieved for the Ysc injectisomes. Cryo electron microscopy (cryo-EM) studies revealed that injectisomes consist of two pairs of rings that span the inner (IM) and outer (OM) bacterial membranes, joined together by a narrower cylinder and terminated by a needle (10, 11). The ring that spans the OM and protrudes into the periplasm consists of a 12-14mer of a protein from the YscC family of secretins (12-14). The lower ring spanning the IM ring is made of a lipoprotein (YscJ in *Yersinia,* MxiJ in *S. flexneri,* PrgK in *S. enterica SPI-1*) proposed to form a 24-subunit ring (9, 10, 15-17) and a protein from the less-conserved YscD family (MxiG in *S. flexneri*, PrgH *in S.enterica* SPI-1*)*. The latter protein has the same general fold as the two others and, based on its structure, it was proposed to act as a connector (14), an hypothesis which was confirmed by deciphering the sequential assembly of the *Yersinia* Ysc apparatus (18). The cryo-EM analysis also allowed visualizing an internal cylinder called the rod, and a socket (19). Finally, the needle is a hollow tube assembled through helical polymerization of a small protein (20, 21). It terminates with a pentameric tip structure serving as a scaffold for the formation of a pore in the host cell membrane (7, 22-26).

Besides this structurally well-characterized needle complex, the injectisome also includes five essential integral inner membrane proteins (YscR, S, T, U, V in *Yersinia*), which are believed to form the export channel across the inner membrane. YscRST consist essentially of transmembrane helices, while YscU (FlhB in the flagellum) and YscV (FlhA in the flagellum) have a significant cytosolic

62 domain. The cytosolic domain of YscU undergoes an auto-cleavage, which has been shown to be
63 involved in the sequential switching of substrate specificity (27-31). The cytosolic domain of YscV
64 (FlhA in the flagellum) consists of four individual domains that are likely to lead to polymerization.
65 So far, the structural information concerning this basic "type-III secretion translocon" remains scarce.
66 Molecular studies have shown that transfer through this translocon requires an ATPase of the AAA^+
67 family (YscN in *Yersinia*, FliI in the flagellum), which forms a hexameric ring and is activated by
68 oligomerization (32-37). The ATPase is associated with two proteins (YscK and YscL in *Yersinia*)
69 (38, 39), one of them (YscL, FliH in the flagellum) exerting a control on the ATPase activity (40-42).
70 The ATPase is strikingly similar to the α and β subunits of the stator of the F_0F_1 ATP synthase (34,
71 36), suggesting an evolutionary relation. This assumption is reinforced by the sequence similarity
72 observed between $YscL_{N\text{-}term}$ and the b subunit of the F-type ATPase, and between $YscL_{C\text{-}term}$ and the δ
73 subunit of the same ATPase (43). Furthermore, the small FliJ protein was recently shown to have a
74 structure very similar to that of the γ subunit of the ATPase (44).

75 Finally, in the flagellum, the most proximal part of the basal body is the 40-50 nm C ring made
76 of FliM and FliN (45-50). Together with FliG, it forms the switch complex reversing the rotation of
77 the motor, but in its absence, no filament appears, indicating that it is also involved in the export of
78 distal constituents (51). No such C ring could be visualized so far by electron microscopy in a needle
79 complex, but proteins of the YscQ family, which are essential components of all injectisomes, have a
80 significant similarity to FliN and to FliM. In *Pseudomonas syringae*, the ortholog of YscQ even
81 appears as two products called $HrcQ_A$ and $HrcQ_{B,}$, which interact with each other, and the overall fold
82 of $HrcQ_B$ is remarkably similar to that of FliN (52). This suggests that injectisomes do have a C ring,
83 although they have not been reported to rotate. In agreement with this assumption, immunogold-
84 labelling experiments have shown that the *Shigella* ortholog of YscQ (Spa33) localizes to a lower
85 portion of the injectisome (53).

86 Here we use cryo electron tomography with sub-tomogram averaging to present a 3D
87 reconstruction of the bacterial secretion system *in situ*, the entire *Yersinia* and *Shigella* injectisomes at

88 a resolution of 3.7 nm and 6 nm, respectively, and we studied *in situ* variation. The structures of the
89 injectisomes *in situ* are longer and thinner than the previously available structures from isolated
90 needle complexes suggested, and we observed strong variations in basal body length and distance
91 between the membranes. Further, we visualized the cytosolic part of an injectisome, which we
92 compare to the type III export machinery of bacterial flagella.

Results and Discussion

Visualization of injectisomes in situ

We used cryo electron tomography (cryo-ET) to visualize the *Yersinia enterocolitica* injectisomes *in situ* (Fig. 1). Visual inspection showed significant heterogeneity among the individual injectisomes. Some bacteria showed two periplasmic layers surrounding the entire observed bacteria and surrounding the injectisomes. The needle length was variable with the mean length from the outer membrane to the needle tip being 65 nm, std = 11, consistent with earlier measurements (54).

Since the large diameter of *Y. enterocolitica* reduced the quality of cryo electron microscopy (cryo-EM) images, we engineered bacterial minicells devoid of genetic material (55, 56). These were much smaller and still had the injectisomes assembled as shown by fluorescence imaging of EGFP fused to the putative C-ring protein YscQ (18, 53) (Fig. 1*C*, see *SI Appendix*). Tomograms of minicells showed a higher signal to noise ratio (SNR), often revealing the lipid bilayers as two separate leaflets, or the central channel of the needle as a hollow tube (Fig. 1*C*). While *wt* bacteria showed on average 6.2 injectisomes per cell in tomograms, minicells showed on average 2.9 injectisomes (Fig. 1*E*). The largest number of injectisomes observed in one cell was 28. The true numbers per cell are likely higher, since due to the "missing wedge effect" about only half of the T3SS are observable in cryo-ET. Closely neighboring or paired injectisomes were frequently observed (Fig. 1*B, C*). Statistical analysis and computer simulations documented the tendency of injectisomes to cluster in *wt* and minicells (Fig. 1*F*, and *SI Appendix*), which may facilitate synchronized multi-injectisome secretion upon contact with the host cell.

Structure of the injectisomes

We used sub-tomogram averaging to combine data from tomograms of minicells and from focal-pair tomograms (57) of *wt* cells. The average structure with a resolution of 3.7 nm (Fig. 2*A*, Fig. S2*D*, and *SI Appendix*) allowed identification of the core structural proteins according to a recent model (11, 58) (Fig. 2*A*). The average structure of the injectisome showed a vertical distance of 33 nm

between the centers of the membranes. The largest lateral diameter in the periplasmic part close to the cytoplasmic membrane was 18 nm; the largest diameter at the outer membrane was 12 nm (Fig. 2*A*). The needle channel was resolved in the center of the structure, closer to the cytoplasmic membrane and at the outer membrane; the outer membrane was resolved as two separate layers. The average revealed a ring-like structure under the cytoplasmic membrane of an outer diameter of 21 nm (Fig. *A*, yellow), surrounding a smaller ring-like structure ~5 nm underneath the membrane and of 11 nm outer diameter and ~6 nm height (Fig. 2*A*, red). Our reconstruction did not allow detection of any rotational symmetry. We applied smooth rotational symmetrization to the injectisomes, which improves the signal to noise ratio of the reconstruction for the pixels that do not lie on the central axis.

We further generated a reconstruction of the *S. flexneri* injectisome by cryo-ET and sub-volume averaging at 6 nm resolution (Fig. 2B, Fig. S3, and *SI Appendix*). Comparing the *in situ* structures of the *Y. enterocolitica* and *S. flexneri* injectisomes with available high-resolution single particle cryo-EM reconstructions from *Shigella flexneri* (EMD-1617 (10)) and *Salmonella enterica* (EMD-1871 (11)) revealed striking differences in the dimensions: the *in situ* injectisomes are significantly longer and have smaller outer diameters (Fig. 2*B*). Such elongation has not been observed for bacterial flagellar motors, where the dimensions from *in situ* cryo-ET agree well with cryo-EM of isolated particles up to a resolution of 5-8 nm (56). We performed one-dimensional isotropic stretching of the structure of isolated *S. flexneri* injectisome to match the positions of attachment to the membranes (Fig. 2*C*) and estimated the required stretching as 44%. The *in situ* injectisome from *S. flexneri,* matched the membrane-to-membrane dimensions of *Y. enterocolitica,* suggesting the same docking positions for the injectisome components.

The outer membrane secretin YscC could be distinguished in the reconstruction (Fig. 2*A*). The structure of the corresponding InvG from the *S. enterica* complex (Fig. S4) could not be rigidly docked into the *Y. enterocolitica* map either leaving the density of $YscC_N$ unaccounted for ("Fit 1"), or $YscC_C$ only partially immersed to the outer membrane ("Fit 2"). We thus reconstituted YscC into lipid vesicles (see *SI Appendix*), performed cryo-ET and generated an average structure of the YscC

multimer at a resolution of 2.4 nm (Fig. 2*D*). The structure shows 3 main rings: one inserted into the membrane bilayer, a second ~5.5 nm below and the third most flexible ring ~12 nm below the outer membrane. Our *in situ* reconstruction of the entire injectisome shows the center of the corresponding density 17 nm below the membrane, corresponding to a ~40% stretch of YscC. Our secretin structure shows membrane insertion of YscC, although higher resolution is needed to gain mechanistic insights into YscC's anchoring into the lipid bilayer. The stretching of YscC is the similar to the stretching of the entire injectisome, suggesting the elongation to be distributed equally over all periplasmic components YscCDJ.

Elasticity of the injectisome

We further explored *in situ* variation among the individual *Y. enterocolitica* injectisomes by multivariate statistical analysis (MSA) (Fig. 3, and *SI Appendix*). Injectisomes varied most in the inter-membrane distance, ranging from 30 nm to 40 nm (MSA results from mask 2, Fig. 3*A* and *C* and Fig. S2 *E* and *F*), a value exceeding what could be attributed to stress during sample preparation. Of the two observed presumed peptidoglycan layers, the outer layer maintained a constant distance to the outer membrane, while the position of the inner layer was less well defined. Even the shortest of our MSA class averages was still longer than the isolated *Shigella* injectisome (Fig. 3*E*).

MSA analysis under the outer membrane area (mask 1 in Fig. 3 *A* and *B*) assigned 25% of the particles to a class showing higher density in the area of the periplasmic channel, 25% showed open space in the area of the periplasmic channel, 27% showed an intermediate state (Fig. 3*B*), and the remaining 23% could not be assigned to any clear structure concerning the channel. If real, these differences may represent closed/open functional states of the periplasmic channel. A similar classification was previously detected for the purified *S. enterica* needle complex with the yet unassembled needle (12). However, all *in situ* injectisome classes in our case had the assembled needle, suggesting that the closed state is a feature also existing in the assembled injectisome *in situ*.

MSA of the cytosolic export apparatus (mask 3 in Fig. 3 *A* and *D*) assigned 32% of the particles to a class showing a large ~15 nm high barrel-like structure, which we interpreted as the hexameric YscN ATPase. It was larger than in the average structure including all the particles. About half of the particles did not have this structure, the corresponding space seemed empty. The remaining 22% of the particles produced a structure between the two other classes, suggesting a partial occupancy of that location, or a faulty recognition by the MSA analysis. This speaks for a transient association and dissociation of the ATPase. This classification based on the region of the YscN ATPase (mask 3 in Fig. 3*A*) produced class averages that also showed significant differences in the secretin region outside of the mask, suggesting a correlation between the presence of the ATPase and state of the periplasmic channel region. As also the homologous HrcN from *P. syringae* (33, 34), YscN is likely a stable hexameric unit.

The MSA classification showed variable occupation of the ATPase density regions for injectisomes (Fig. 3*D*). Such transient presence might also apply for the FliI ATPase in flagella, and might have been the cause for the apparently different structures observed in flagella of different bacteria (50). Follow-up investigations employing optical super-resolution real time fluorescence microscopy, or photo bleaching, might be able to shed more light on the dynamics of the ATPase association with the injectisome.

YscQ is homologous to the C-ring protein FliN of the flagellar system(53), which also plays a role in type III protein export (59, 60). YscQ assembles to the injectisome after YscCDJ (18) and is expected to form a ring at the cytoplasmic side of the injectisome. Our reconstruction did not reveal a ring of the dimensions of C-rings of flagellar motors (~40 nm in diameter, ~17 nm high (61)). Instead, we identified a smaller cytoplasmic ring with a diameter of ~21 nm and height of ~6 nm attached to the cytoplasmic membrane of the injectisome (Fig. 2*A*, yellow). This ring may be composed of proteins with transmembrane and cytoplasmic domains, as for example cytoplasmic domain of YscD or YscV, which was recently shown to form multimers (62), or their combinations with other soluble proteins like YscQ. This may allow YscQ to recruit substrate for further export.

194 Our analysis of the injectisome structure in its cellular context revealed new insights into the
195 assembly and function of this fascinating machinery. This was made possible through developments
196 in minicell preparation, cryo electron tomography imaging, and sub-volume data analysis, in
197 combination with a statistical analysis of molecular variations of the structure *in situ*. Our analysis
198 points out potential differences between the structure of protein nanomachines *in vitro* and *in situ*.
199 Further improvements in resolution are required to bring new insights into the structure and function
200 of various bacterial secretion systems, including the *Yersinia* injectisome.

Materials and Methods

Bacterial strains, plasmids, and genetic constructions

E. coli BW19610 (63) used for cloning and *E.coli* Sm10 λ *pir*$^+$ used for conjugation were routinely grown in Luria broth (LB) or on LB agar (LA) plates at 37°C. Streptomycin was used at a concentration of 100 µg/ml to select for suicide vectors. All *Y. enterocolitica* strains are derivates of E40 (64), where for biosafety reasons six effector genes were deleted, as well as the *asd* gene. They were routinely grown at 25°C in brain heart infusion (BHI) broth containing 35 µg/mL nalidixic acid. To allow growth of *asd* mutant strains, the medium was supplemented with 50 µg/mL meso-diaminopimelic acid. *Shigella flexneri* SC560 (65) were routinely grown at 37°C in BHI containing 100 µg/ml streptomycin. Mutator plasmid pMK3 was made by amplification of the *asd* 5' region with oligos 3541/3543 and the 3' region with oligos 3542/3544. The 5' region was digested with *Sal*I/*Eco*RI and the 3' region with *Eco*RI/*Xba*I. Both fragments together were ligated into the *Sal*I/*Xba*I restriction site of pKNG101. To construct pMA87, flanking regions of about 250 bp just upstream and downstream of *minD* were amplified from purified genomic DNA from *Y. enterocolitica* E40 using oligonucleotides 6416/6417 and 6418/6419 respectively (see Table S3). The two fragments were joined by overlapping polymerase chain reaction (PCR), and the resulting fragment was cloned into the *Sal*I/*Xba*I restriction sites of suicide vector pKNG101 (66). To construct pMA6, full-length *yscC* with a stop codon was amplified from the pYVe40 plasmid using primers 5013/5014 and introduced into the *Nco*I/*Eco*RI restriction sites of pBAD/mycHisA.

Y. enterocolitica mutant generation

Mutant strains were generated by two-step allelic exchange (66). The *Y. enterocolitica* parent was mated on a plate with *E. coli* Sm10 λ *pir*$^+$ containing the corresponding mutator plasmid. To select for integration of the mutator plasmid the conjugation mix was plated on nalidixic acid and streptomycin. In a second step the streptomycin selection pressure was released during several generation times allowing the excision of the mutator plasmid. Plating on LA containing 5 % sucrose allowed selection for colonies that underwent the second recombination step and had lost the mutator

plasmid. These colonies were screened for the mutant allele by colony PCR. As an exeption yadA mutants were made by insertion of the entire mutator plasmid pLJM31 into yadA. To avoid wild type revertants by excision of the plasmid, constant streptomycin selection was applied.

Cryo-electron tomography

Bacteria culture or liposomes containing YscC were gently spun 5 min at 300 x g and resuspended in PBS with 10 nm colloidal gold particles were added. Three µL of solution was deposited on Quantifoil grids (Quantifoil Micro Tools GmbH, Jena, Germany) and were plunge frozen into liquid nitrogen-cooled liquid ethane with a FEI Vitrobot MK4. For imaging of regularly sized *Y. enterocolitica* cells we used focal pair tomography (57): two tomograms were acquired for each imaged bacteria first at an underfocus of 2 µm ("low defocus") and then at an underfocus 15 µm ("high defocus"), using the FEI batch tomography tool on an FEI Titan Krios equipped with a GIF and US1000 post-GIF CCD. The total dose used for each tomogram was kept below 10 k electrons/nm^2, aiming at an angular coverage of 120 degrees in 41 steps of 3 degrees. *Yersinia* minicells were imaged with the nominal underfocus of 6 µm with 2 degree angular step and the electron dose kept under 15 k e^-/nm^2. *S. flexneri* cells were imaged at underfocus 15 µm with 3 degree step with the electron dose kept below 20 k e^-/nm^2. Liposomes containing YscC were imaged at underfocus 2 µm with 2 degree step with the electron dose kept below 10 k e/nm^2. The pixel size was 0.74 nm for *Y. enterocolitica* and 1.05 nm for *S. flexneri,* 0.54 for YscC on lipid vesicles.

Image processing.

For detailed description please see methods in *SI Appendix*. Briefly, tomograms were reconstructed by weighted back projection using Etomo (67) and further processed with AV3 processing package (68), in combination with Dynamo (69). Prealigned particles were aligned to a common reference and iterative refinement was performed till convergence. For *Yersinia* injectisomes we used datasets derived from minicells and from focal pair tomograms of the entire cells (57). Multidimensional statistical analysis was performed by K-means clustering based on principal component analysis of voxels inside the masks specified in Fig. 3.

253 **Acknowledgement:**

254 We thank B. Anderson, R. Pantelic, K. Goldie and M. Chami for technical assistance, M. Kuhn and
255 A. Diepold for plasmid and strain contribution and K. Namba and A. Diepold for discussions. This
256 work was in part supported by the Swiss National Science Foundation (SNF 3100AOB-128659, SNF
257 Sinergia CRSII3_125110, NCCRs Struct. Biol., Nano, and TransCure), and the Swiss Initiative for
258 Systems Biology (SystemsX.ch).

259 **Author contributions:** GC and HS inspired and designed the research, MA generated minicells and
260 performed fluorescent microscopy, MK performed EM imaging and data processing, CB and JK
261 contributed to EM analysis, DCD provided essential analytical tools and expertise in data analysis. All
262 authors contributed to data interpretation and writing the manuscript.

263

264 The structures will be deposited to the EMDB upon acceptance of the manuscript.

265 The authors declare no competing financial interests.

266 [1]to whom correspondence should be addressed. Email: Guy.Cornelis@unibas.ch or
267 Henning.Stahlberg@unibas.ch

268

269

LITERATURE CITED

1. Cornelis GR (2006) The type III secretion injectisome. *Nat Rev Microbiol* 4(11):811-825.
2. Kubori T*, et al.* (1998) Supramolecular structure of the Salmonella typhimurium type III protein secretion system. *Science* 280(5363):602-605.
3. Blocker A*, et al.* (1999) The tripartite type III secreton of Shigella flexneri inserts IpaB and IpaC into host membranes. *J Cell Biol* 147(3):683-693.
4. Troisfontaines P & Cornelis GR (2005) Type III secretion: more systems than you think. *Physiology (Bethesda)* 20:326-339.
5. Pallen MJ, Beatson SA, & Bailey CM (2005) Bioinformatics, genomics and evolution of non-flagellar type-III secretion systems: a Darwinian perspective. *FEMS Microbiol Rev* 29(2):201-229.
6. Daniell SJ*, et al.* (2001) The filamentous type III secretion translocon of enteropathogenic Escherichia coli. *Cell Microbiol* 3(12):865-871.
7. Sani M*, et al.* (2007) Structural organization of the needle complex of the type III secretion apparatus of Shigella flexneri. *Micron* 38(3):291-301.
8. Sekiya K*, et al.* (2001) Supermolecular structure of the enteropathogenic Escherichia coli type III secretion system and its direct interaction with the EspA-sheath- like structure. *Proc Natl Acad Sci U S A* 98(20):11638-11643.
9. Kimbrough TG & Miller SI (2000) Contribution of Salmonella typhimurium type III secretion components to needle complex formation. *Proc Natl Acad Sci U S A* 97(20):11008-11013.
10. Hodgkinson JL*, et al.* (2009) Three-dimensional reconstruction of the Shigella T3SS transmembrane regions reveals 12-fold symmetry and novel features throughout. *Nat Struct Mol Biol* 16(5):477-485.
11. Schraidt O & Marlovits TC (2011) Three-dimensional model of Salmonella's needle complex at subnanometer resolution. *Science* 331(6021):1192-1195.
12. Marlovits TC*, et al.* (2004) Structural Insights into the Assembly of the Type III Secretion Needle Complex. *Science* 306(5698):1040-1042.
13. Burghout P*, et al.* (2004) Structure and electrophysiological properties of the YscC secretin from the type III secretion system of Yersinia enterocolitica. *J Bacteriol* 186(14):4645-4654.
14. Spreter T*, et al.* (2009) A conserved structural motif mediates formation of the periplasmic rings in the type III secretion system. *Nat Struct Mol Biol* 16(5):468-476.
15. Crepin VF*, et al.* (2005) Structural and functional studies of the enteropathogenic Escherichia coli type III needle complex protein EscJ. *Mol Microbiol* 55(6):1658-1670.
16. Yip CK*, et al.* (2005) Structural characterization of the molecular platform for type III secretion system assembly. *Nature* 435(7042):702-707.
17. Silva-Herzog E, Ferracci F, Jackson MW, Joseph SS, & Plano GV (2008) Membrane localization and topology of the Yersinia pestis YscJ lipoprotein. *Microbiology* 154(Pt 2):593-607.
18. Diepold A*, et al.* (2010) Deciphering the assembly of the Yersinia type III secretion injectisome. *Embo J* 29(11):1928-1940.

19. Marlovits TC*, et al.* (2006) Assembly of the inner rod determines needle length in the type III secretion injectisome. *Nature* 441(7093):637-640.
20. Cordes FS*, et al.* (2003) Helical structure of the needle of the type III secretion system of Shigella flexneri. *J Biol Chem* 278(19):17103-17107.
21. Deane JE*, et al.* (2006) Molecular model of a type III secretion system needle: Implications for host-cell sensing. *Proc Natl Acad Sci U S A* 103(33):12529-12533.
22. Mueller CA*, et al.* (2005) The V-antigen of Yersinia forms a distinct structure at the tip of injectisome needles. *Science* 310(5748):674-676.
23. Gebus C, Faudry E, Bohn YS, Elsen S, & Attree I (2008) Oligomerization of PcrV and LcrV, protective antigens of Pseudomonas aeruginosa and Yersinia pestis. *J Biol Chem* 283(35):23940-23949.
24. Veenendaal AK*, et al.* (2007) The type III secretion system needle tip complex mediates host cell sensing and translocon insertion. *Mol Microbiol* 63(6):1719-1730.
25. Mueller CA, Broz P, & Cornelis GR (2008) The type III secretion system tip complex and translocon. *Mol Microbiol* 68(5):1085-1095.
26. Broz P*, et al.* (2007) Function and molecular architecture of the Yersinia injectisome tip complex. *Mol Microbiol* 65(5):1311-1320.
27. Edqvist PJ*, et al.* (2003) YscP and YscU regulate substrate specificity of the Yersinia type III secretion system. *J Bacteriol* 185(7):2259-2266.
28. Sorg I*, et al.* (2007) YscU recognizes translocators as export substrates of the Yersinia injectisome. *Embo J* 26(12):3015-3024.
29. Wiesand U*, et al.* (2009) Structure of the type III secretion recognition protein YscU from Yersinia enterocolitica. *J Mol Biol* 385(3):854-866.
30. Botteaux A*, et al.* (2010) The 33 carboxyl-terminal residues of Spa40 orchestrate the multi-step assembly process of the type III secretion needle complex in Shigella flexneri. *Microbiology* 156(Pt 9):2807-2817.
31. Zarivach R*, et al.* (2008) Structural analysis of the essential self-cleaving type III secretion proteins EscU and SpaS. *Nature* 453(7191):124-127.
32. Woestyn S, Allaoui A, Wattiau P, & Cornelis GR (1994) YscN, the putative energizer of the Yersinia Yop secretion machinery. *J Bacteriol* 176(6):1561-1569.
33. Pozidis C*, et al.* (2003) Type III protein translocase: HrcN is a peripheral ATPase that is activated by oligomerization. *J Biol Chem* 278(28):25816-25824.
34. Muller SA*, et al.* (2006) Double hexameric ring assembly of the type III protein translocase ATPase HrcN. *Mol Microbiol* 61(1):119-125.
35. Zarivach R, Vuckovic M, Deng W, Finlay BB, & Strynadka NC (2007) Structural analysis of a prototypical ATPase from the type III secretion system. *Nat Struct Mol Biol* 14(2):131-137.
36. Imada K, Minamino T, Tahara A, & Namba K (2007) Structural similarity between the flagellar type III ATPase FliI and F1-ATPase subunits. *Proc Natl Acad Sci U S A* 104(2):485-490.
37. Abrahams JP, Leslie AG, Lutter R, & Walker JE (1994) Structure at 2.8 A resolution of F1-ATPase from bovine heart mitochondria. *Nature* 370(6491):621-628.

38. Jackson MW & Plano GV (2000) Interactions between type III secretion apparatus components from Yersinia pestis detected using the yeast two-hybrid system. *FEMS Microbiol Lett* 186(1):85-90.
39. Blaylock B, Riordan KE, Missiakas DM, & Schneewind O (2006) Characterization of the Yersinia enterocolitica type III secretion ATPase YscN and its regulator, YscL. *J Bacteriol* 188(10):3525-3534.
40. Minamino T & MacNab RM (2000) Interactions among components of the Salmonella flagellar export apparatus and its substrates. *Mol Microbiol* 35(5):1052-1064.
41. Gonzalez-Pedrajo B, Fraser GM, Minamino T, & Macnab RM (2002) Molecular dissection of Salmonella FliH, a regulator of the ATPase FliI and the type III flagellar protein export pathway. *Mol Microbiol* 45(4):967-982.
42. McMurry JL, Murphy JW, & Gonzalez-Pedrajo B (2006) The FliN-FliH interaction mediates localization of flagellar export ATPase FliI to the C ring complex. *Biochemistry* 45(39):11790-11798.
43. Pallen MJ, Bailey CM, & Beatson SA (2006) Evolutionary links between FliH/YscL-like proteins from bacterial type III secretion systems and second-stalk components of the FoF1 and vacuolar ATPases. *Protein Sci* 15(4):935-941.
44. Ibuki T*, et al.* (2011) Common architecture of the flagellar type III protein export apparatus and F- and V-type ATPases. *Nat Struct Mol Biol* 18(3):277-282.
45. Driks A & DeRosier DJ (1990) Additional structures associated with bacterial flagellar basal body. *J Mol Biol* 211(4):669-672.
46. Khan IH, Reese TS, & Khan S (1992) The cytoplasmic component of the bacterial flagellar motor. *Proc Natl Acad Sci U S A* 89(13):5956-5960.
47. Thomas DR, Francis NR, Xu C, & DeRosier DJ (2006) The three-dimensional structure of the flagellar rotor from a clockwise-locked mutant of Salmonella enterica serovar Typhimurium. *J Bacteriol* 188(20):7039-7048.
48. Young HS, Dang H, Lai Y, DeRosier DJ, & Khan S (2003) Variable symmetry in Salmonella typhimurium flagellar motors. *Biophys J* 84(1):571-577.
49. Kubori T, Yamaguchi S, & Aizawa S (1997) Assembly of the switch complex onto the MS ring complex of Salmonella typhimurium does not require any other flagellar proteins. *J Bacteriol* 179(3):813-817.
50. Chen S*, et al.* (2011) Structural diversity of bacterial flagellar motors. *EMBO J*.
51. Macnab RM (2003) How Bacteria Assemble Flagella. *Annu Rev Microbiol* 57:77-100.
52. Fadouloglou VE*, et al.* (2004) Structure of HrcQB-C, a conserved component of the bacterial type III secretion systems. *Proc Natl Acad Sci U S A* 101(1):70-75.
53. Morita-Ishihara T*, et al.* (2006) Shigella Spa33 is an essential C-ring component of type III secretion machinery. *J Biol Chem* 281(1):599-607.
54. Journet L, Agrain C, Broz P, & Cornelis GR (2003) The needle length of bacterial injectisomes is determined by a molecular ruler. *Science* 302(5651):1757-1760.

55. Adler HI, Fisher WD, Cohen A, & Hardigree AA (1967) MINIATURE escherichia coli CELLS DEFICIENT IN DNA. *Proc Natl Acad Sci U S A* 57(2):321-326.
56. Liu J, Chen CY, Shiomi D, Niki H, & Margolin W (2011) Visualization of bacteriophage P1 infection by cryo-electron tomography of tiny Escherichia coli. *Virology* 417(2):304-311.
57. Kudryashev M, Stahlberg, H., Castano-Diez, D. (2011) Assessing benefits of Focal pair tomography. *J Struct Biol*.
58. Worrall LJ, Lameignere E, & Strynadka NC (2011) Structural overview of the bacterial injectisome. *Curr Opinion Microbiol* 14(1):3-8.
59. Gonzalez-Pedrajo B, Minamino T, Kihara M, & Namba K (2006) Interactions between C ring proteins and export apparatus components: a possible mechanism for facilitating type III protein export. *Mol Microbiol* 60(4):984-998.
60. Paul K & Blair DF (2006) Organization of FliN subunits in the flagellar motor of Escherichia coli. *J Bact* 188(7):2502-2511.
61. Chen C, Chen YH, & Lin WW (1999) Involvement of p38 mitogen-activated protein kinase in lipopolysaccharide-induced iNOS and COX-2 expression in J774 macrophages. *Immunology* 97(1):124-129.
62. Diepold A, Wiesand U, & Cornelis GR (2011) The assembly of the export apparatus (YscR,S,T,U,V) of the Yersinia type III secretion apparatus occurs independently of other structural components and involves the formation of an YscV oligomer. *Mol Microbiol* 82(2):502-514.
63. Howitt RL, Beever RE, Pearson MN, & Forster RL (2006) Genome characterization of a flexuous rod-shaped mycovirus, Botrytis virus X, reveals high amino acid identity to genes from plant 'potex-like' viruses. *Arch Virol* 151(3):563-579.
64. Sory MP, Boland A, Lambermont I, & Cornelis GR (1995) Identification of the YopE and YopH domains required for secretion and internalization into the cytosol of macrophages, using the cyaA gene fusion approach. *Proc Natl Acad Sci U S A* 92(26):11998-12002.
65. Sansonetti PJ (1991) Genetic and molecular basis of epithelial cell invasion by Shigella species. *Rev Infect Dis* 13 Suppl 4:S285-292.
66. Kaniga K, Delor I, & Cornelis GR (1991) A wide-host-range suicide vector for improving reverse genetics in gram-negative bacteria: inactivation of the blaA gene of Yersinia enterocolitica. *Gene* 109(1):137-141.
67. Kremer JR, Mastronarde DN, & McIntosh JR (1996) Computer visualization of three-dimensional image data using IMOD. *J Struct Biol* 116(1):71-76.
68. Puthothu B, Krueger M, Forster J, & Heinzmann A (2006) Association between severe respiratory syncytial virus infection and IL13/IL4 haplotypes. *J Infect Dis* 193(3):438-441.
69. Castano-Diez D, Kudryashev, M., Arheit, M., Stahlberg, H (2011) Dynamo: A flexible, user-friendly development tool for subtomogram averaging of cryo-EM data in High Performance Computing environments *Submitted*.

453 **Figures and figure legends:**

454

455 **Fig. 1**. Visualization of *Y. enterocolitica* injectisomes *in situ*. (*A*) left: cryo-EM image (left) with a 20
456 nm thick slice through a tomogram showing an injectisome (black arrowhead, right); Right: volume
457 rendering of the same bacteria showing the cytoplasmic (yellow) and outer (blue) membranes and
458 injectisomes (red). Scale bar: 300 nm. (*B*) Differences between the injectisomes. Left to right: regular;
459 tilted, with dim basal body, denser peptidoglycan, larger periplasmic space and paired injectisomes.
460 Box size: 200 nm. (*C*) A 22 nm thick section through a tomogram showing two periplasmic layers
461 (white arrowheads). Inset: adjacent injectisomes traversed by two periplasmic layers. Scale bar: 100
462 nm. (*D*) The distribution of measured needle lengths. (*E*) Distributions of the numbers of needles
463 observed per regular cell (blue) and minicell (red). (*F*) Distributions of distances between each pair of
464 needles within every tomogram. Blue: regular cells, red: minicells, black: simulated distances for
465 randomly distributed needles.

466
467
468 **Fig. 2.** Components of the injectisome *in situ* structure. *(A)* A slice through the average structure of
469 the injectisome and a model with indicated components. OM - outer membrane, PL - peptidoglycan
470 layers, CM - cytoplasmic membrane. *(B)* Comparison of the *Y. enterocolitica* and *S. flexneri in situ*
471 injectisomes with high-resolution single particle structures of *S. flexneri* (EM Data Bank entry EMD
472 1871) and *S. enterica* (EMD 1617). Blue and purple bars indicate the outer (OM) and cytoplasmic
473 (CM) membranes. *(C)* Overlay of the in situ and stretched in vitro structures of the *S. flexneri*
474 injectisome. *(D)* Average structure of liposome-reconstituted YscC, and a comparison of matching
475 densities in the *Y. enterocolitica* injectisome. Scale bars: 10 nm.

476

Fig. 3. Variations within the different components of the *Y. enterocolitica* injectisome. *(A)* Average structure with the three masks used for analysis, Scale bar: 10 nm. *(B)* Class averages according to the mask 1, showing a "closed", "open", and "intermediate" state of the periplasmic gate. *(C)* Elongational flexibility of the injectisomes from regular cells resulting from classification within the mask 2. Top: 8 different class averages, 14% of non-assignable particles were excluded. Bottom: height of 3 recognizable features over center of the cytoplasmic membrane for the different classes: outer membrane, dense spot on YscC and YscC-YscD junction. *(D)* Class averages of the export apparatus area derived from classification within mask 3. Note the correlation between the presence of the export apparatus and the gate conformation. *(E)* Comparison of the shortest class average 8 from *(C)* to the isolated *S. flexneri* injectisome (EMD 1871).

Fig. 1

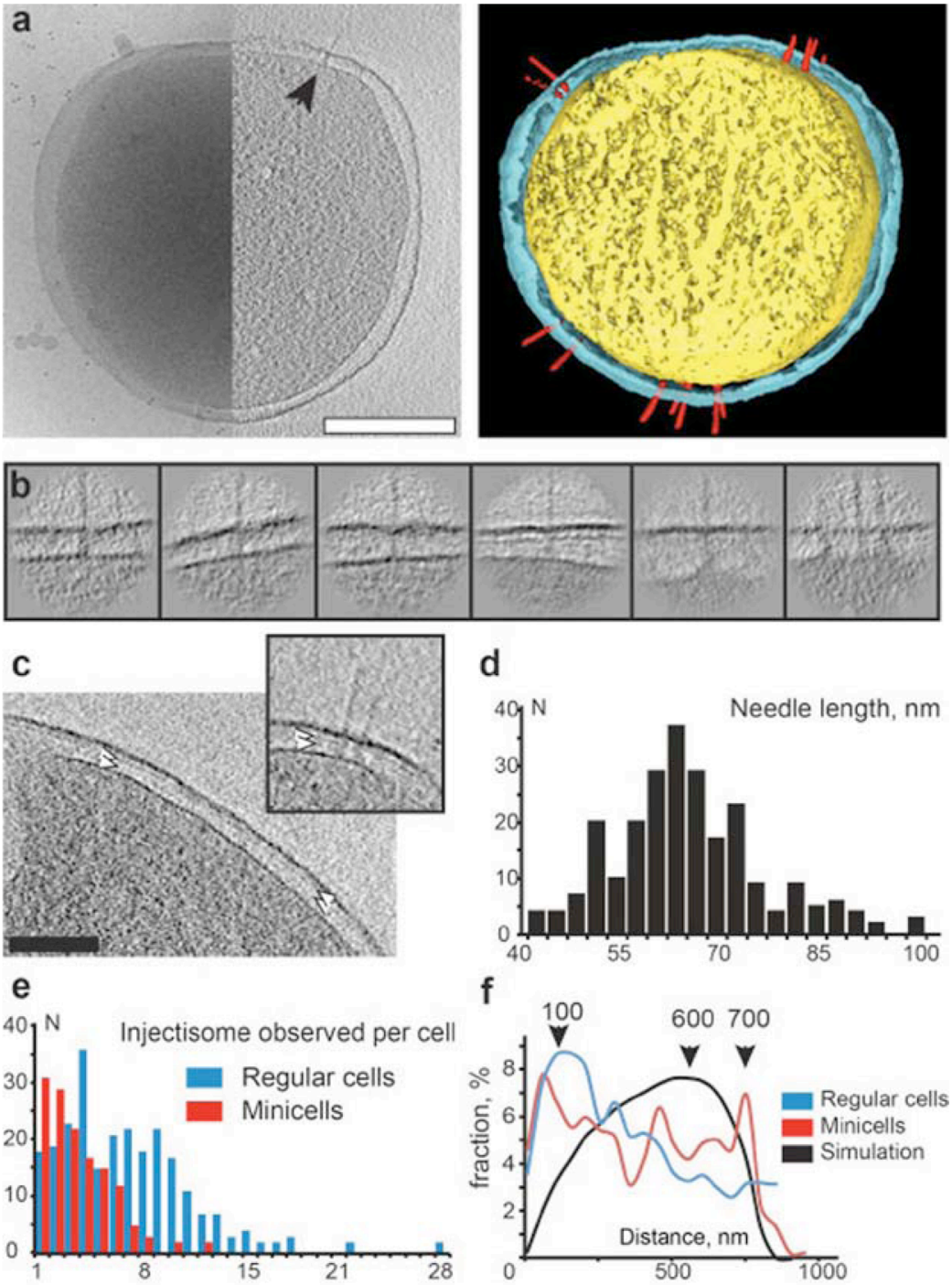
a
b
c
d
N
Needle length, nm
40
30
20
10
0
40
55
70
85
100
e
N
Injectisome observed per cell
Regular cells
Minicells
40
30
20
10
0
1
8
15
21
28
f
100
600
700
fraction, %
8
6
4
2
0
Regular cells
Minicells
Simulation
Distance, nm
0
500
1000

Fig. 2

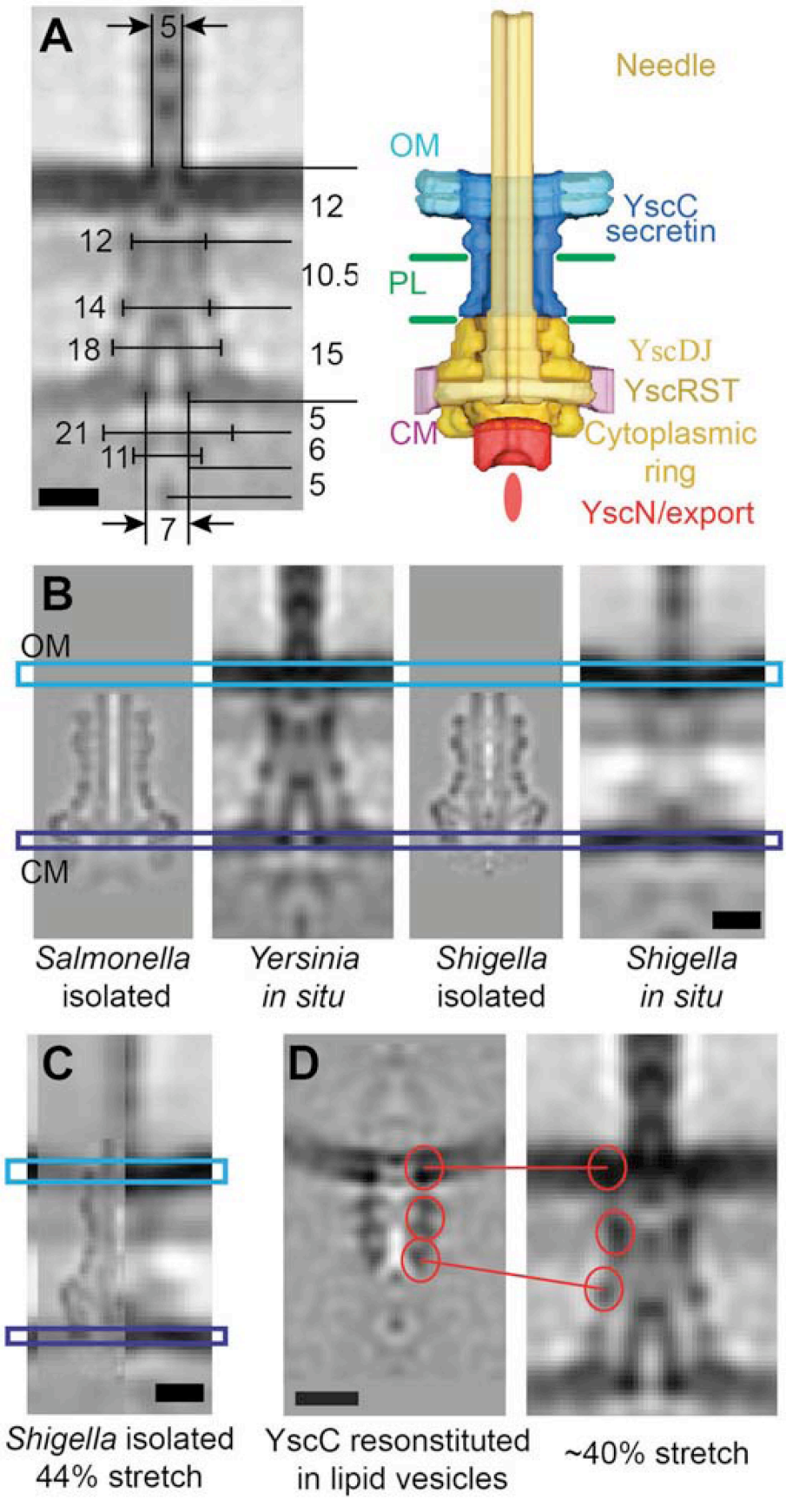
A
5
12
12
10.5
14
18
15
5
21
6
11
5
7
Needle
OM
YscC
secretin
PL
YscDJ
YscRST
CM
Cytoplasmic
ring
YscN/export
B
OM
CM
Salmonella
isolated
Yersinia
in situ
Shigella
isolated
Shigella
in situ
C
D
Shigella isolated
44% stretch
YscC resonstituted
in lipid vesicles
~40% stretch

Fig. 3

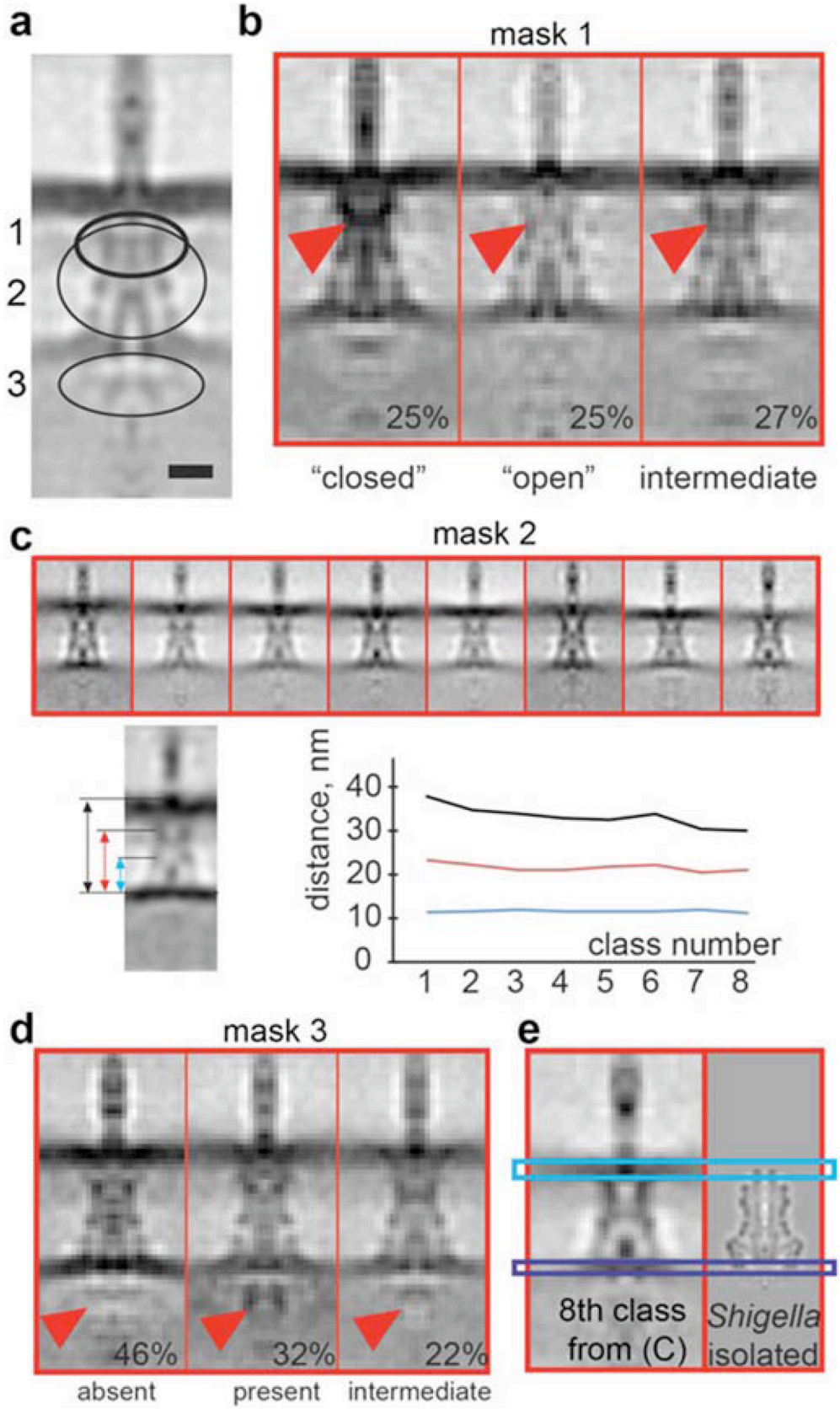
a
b
mask 1
1
2
3
25%
25%
27%
"closed"
"open"
intermediate
c
mask 2
distance, nm
40
30
20
10
0
class number
1 2 3 4 5 6 7 8
d
mask 3
46%
32%
22%
absent
present
intermediate
e
8th class from (C)
Shigella isolated

In situ structure of the *Yersinia enterocolitica* injectisome

Mikhail Kudryashev, Marlise Amstutz, Daniel Castaño-Díez, Christopher K. E. Bleck, Julia Kowal, Guy R. Cornelis, Henning Stahlberg

Supplementary Information

Fig. S1*. Y. enterocolitica* minicells.

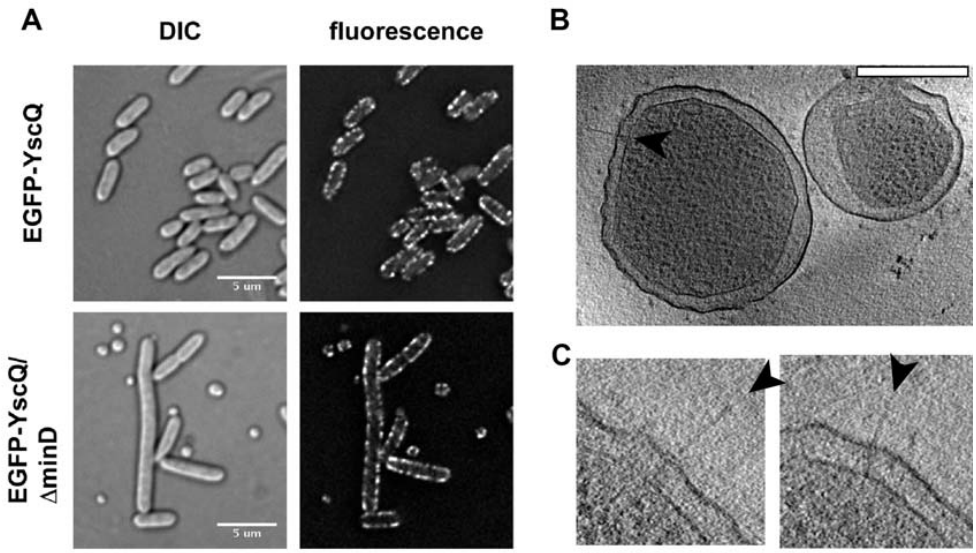

(A) Differential interference contrast (DIC) (left) and fluorescence (right) imaging of regular (top) and *minD* mutant *Y. enterocolitica* cells (bottom). Minicells appear together with extra-long bacteria. EGFP is coupled to YscQ. (scale bar 5 μm)

(B) A 22 nm thick slice through a tomogram of two minicells showing an injectisome (black arrowhead).

(C) Injectisomes from minicells showing outer membrane as resolved bilayer and the middle channel resolved as a tube.

Fig. S2. Structural flexibility of the injectisome.

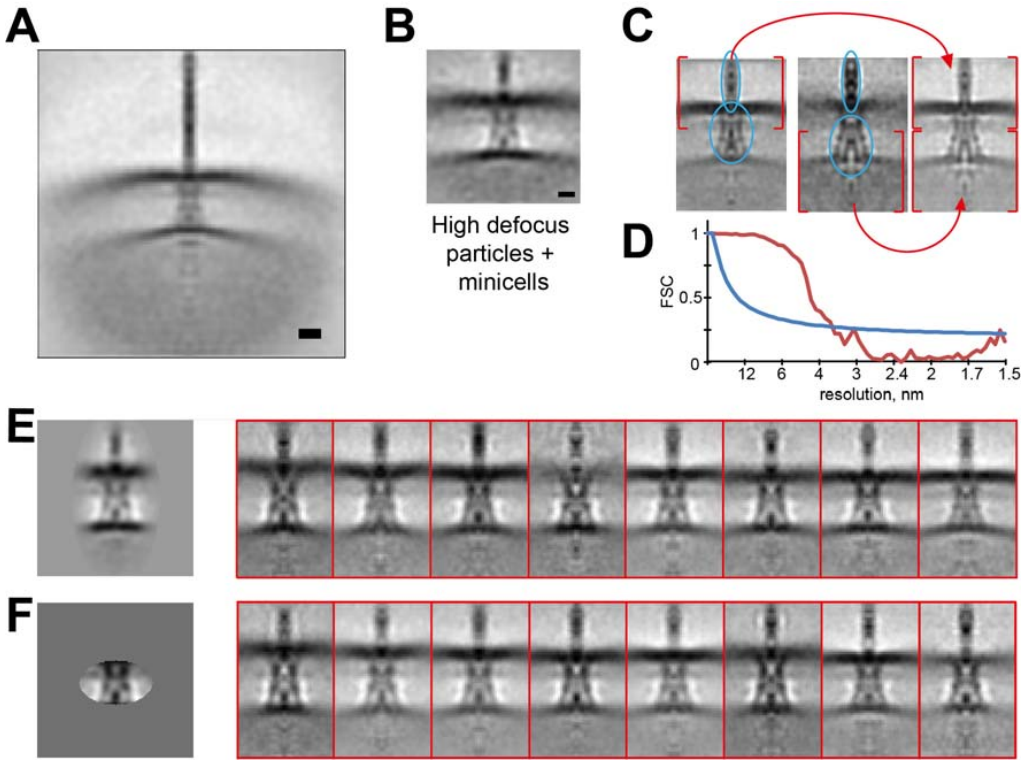

(A) Initial alignment of the injectisomes to the common origin with the reduced pixel size, Scale bar: 20 nm.

(B) Consecutive alignment of high-defocus and minicell particles according to the cytoplasmic membrane at a resolution of ~6 nm. Scale bar: 10 nm.

(C) Composite average produced by merging two independent alignments including the outer membrane (left) and cytoplasmic membrane (middle) of selected low-defocus and minicell particles together.

(D) Fourier Shell Correlation (FSC) plot between half-populations of aligned particles, averaged between two of the alignments for the two masks from (C) (red line), indicating a resolution of 3.7 nm; blue: 1 bit information threshold.

(E) Left: average structure of the injectisome from (B) with an applied wide mask for K-means classification; right: class averages.

(F) Left: average structure of the injectisome from (B) with an applied tight mask for K-means classification; right: class averages.

Fig. S3. Visualization of injectisomes in *Shigella flexneri* with cryo electron tomography.

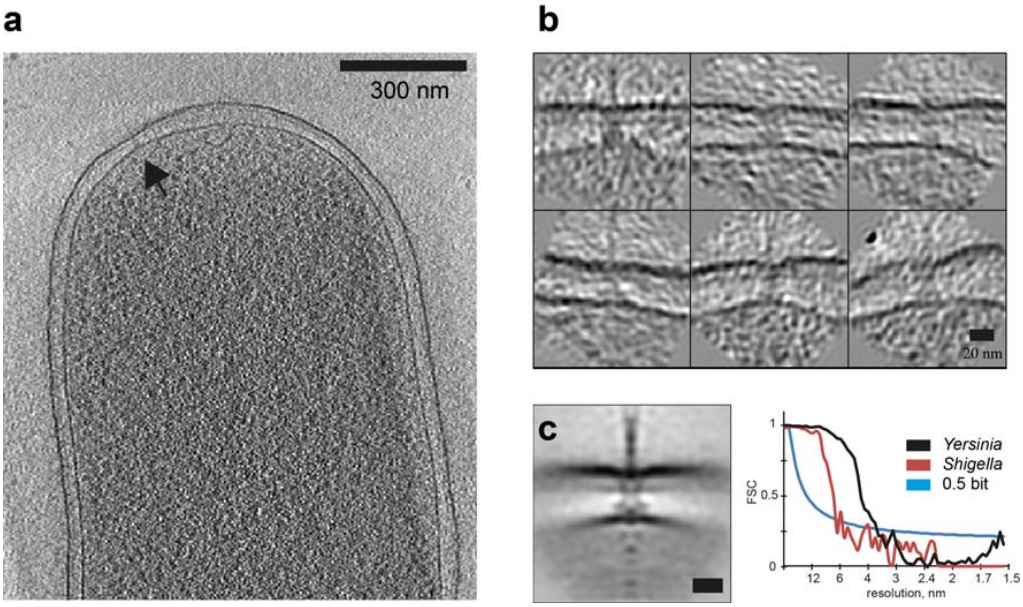

(A) A 30 nm thick section through a tomogram of an *S. flexneri* cell. Arrows point to the basal bodies of the injectisomes. Scale bar: 300 nm;

(B) Typical views in the *S. flexneri* injectisomes oriented vertically. Scale bar: 20 nm.

(C) Left: average structure of the *S. flexneri* injectisome *in situ*. Scale bar: 20 nm; Right: comparison of Fourier Shell Correlations for *S. flexneri* (red) and *Y. enterocolitica* (black); Blue line: 0.5 bit information threshold. Resolution of *S. flexneri* is 6 nm, *Y. enterocolitica* is 3.7 nm.

Fig. S4. Docking of InvG into the reconstruction

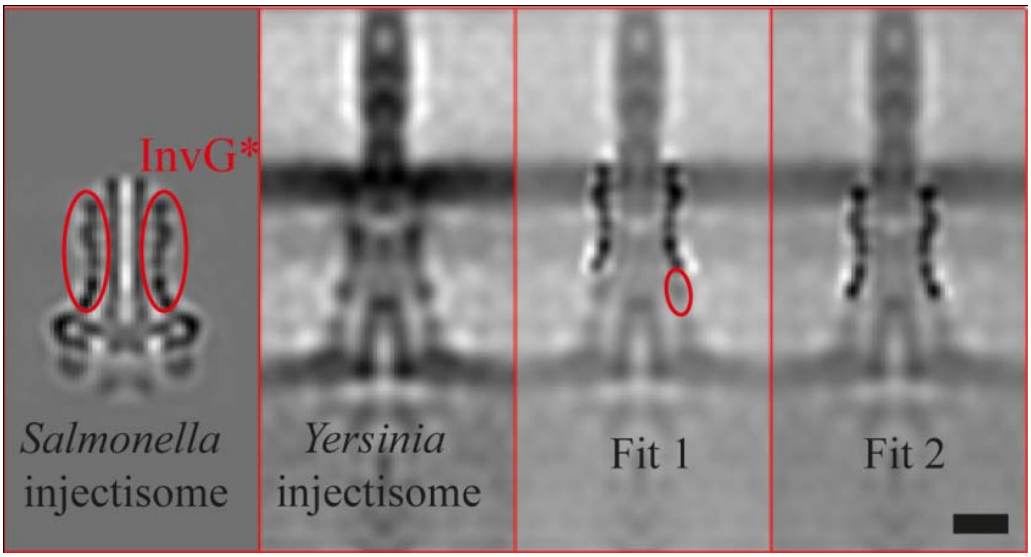

Two possible models for docking of the InvG structure (1) into the determined density map of the *Y. enterocolitica* injectisome. Scale bar: 10 nm.

Table S1 – *Y. enterocolitica* mutant strains

Mutant strain	Relevant characteristics	Parent	Mutator Plasmid	References
IML421	*yopH*$_{\Delta 1\text{-}352}$, *yopO*$_{\Delta 65\text{-}55}$, *yopP*$_{238}$, *yopE*$_{21}$, *yopM*$_{23}$, *yopT*$_{135}$ *(ΔyopHOPEMT)*			(2)
IML421asd	*ΔyopHOPEMT asd*$_{\Delta 292\text{-}610}$ [1)] (biosafety level 1 strain requiring mDAP[2)] for growth)	IML421	pMK3	this work
AD4085	*ΔyopHOPEMT asd*$_{\Delta 292\text{-}610}$ *egfp-yscQ*$^{+}$	IML421asd	pAD118	this work
AD4086	*ΔyopHOPEMT asd*$_{\Delta 292\text{-}610}$ *egfp-yscQ*$^{+}$ *yadA*$_{686\text{-}956}$	AD4085	pLJM31	this work
MA4039	*ΔyopHOPEMT asd*$_{\Delta 292\text{-}610}$ *egfp-yscQ*$^{+}$ *minD*	AD4085	pMA87	this work
MA4053	*ΔyopHOPEMT asd*$_{\Delta 292\text{-}610}$ *minD*	IML421asd	pMA87	this work
MA4055	*ΔyopHOPEMT asd*$_{\Delta 292\text{-}610}$ *egfp-yscQ*$^{+}$ *minD yadA*$_{686\text{-}956}$	MA4039	pLJM31	this work
MA4056	*ΔyopHOPEMT asd*$_{\Delta 292\text{-}610}$ *minD yadA*$_{686\text{-}956}$	MA4053	pLJM31	this work

[1)] asd = aspartate-β-semialdehyde Dehydrogenase
[2)] mDAP = meso-diaminopimelic acid

Table S2 – Mutator plasmids

Plasmid	Relevant characteristics	References
pKNG101	oriR6K, mobRK2, Sm^{R}, sacB (sucrose sensitivity)	(3)
pMK3	pKNG101 *asd*$_{\Delta 292\text{-}610}$	this work
pMA87	pKNG101 *minD*	this work
pAD118	pKNG101 *egfp-yscQ*$^{+}$	(4)
pLJM31	pKNG101 *yadA*$_{686\text{-}956}$ [3)]	(5)
pRS6	pACYC184 *cat*::*yscW*	(6)
pBAD/mycHisA	pBR322 origin, araBAD promoter, Amp^{R}	Invitrogen
pMA6	pBAD *yscC*	this work

[3)] Note: this vector inserts itself into the middle of *yadA* and therefore disrupts *yadA*.

Table S3 – List of used oligonucleotides

No.	Sequence	features	cloning of	template
3541	GATCGTCGACATGGTCGGCTCAGTA[4)]	SalI restriction site	pMK3	genomicDNA E40
3542	GATCTCTAGATTCGCAGCATACGGC[4)]	XbaI restriction site	pMK3	genomicDNA E40
3543	CAGTGAATTCCGGCGTCAATCCAATA[4)]	EcoRI restriction site	pMK3	genomicDNA E40
3544	GACTGAATTCGTGACTGCGGCCACT[4)]	EcoRI restriction site	pMK3	genomicDNA E40
6416	CATGGTCGACATTGCCGACGGCAATATTC[4)]	SalI restriction site	pMA87	genomicDNA E40
6417	AAAGTCTAACAAAGCCATGGTGAAATGGATTCCTTGTCAAAAG	overlap to 6418	pMA87	genomicDNA E40
6418	CTTTTGACAAGGAATCCATTTCACCATGGCTTTGTTAGACTTT	overlap to 6417	pMA87	genomicDNA E40
6419	CATGTCTAGACCGGTAATGTCACGTTAAG[4)]	XbaI restriction site	pMA87	genomicDNA E40
5013	GACTCCATGGCTTTTCCGCTACATTCTTTTTTC[4)]	NcoI restriction site	pMA6	pYVe40
5014	CTGAATTCACAATACGCCACGCTTAGGTGC[4)]	EcoRI restriction site	pMA6	pYVe40

[4)] Restriction sites are underlined

Supplemental Materials and Methods

Y. enterocolitica *cultures for type-III secretion and microscopy analysis*

Cultures were inoculated at an optical density (OD_{600}) of 0.1 in BHI-Ox media supplemented with glycerol (4 mg/mL) and $MgCl_2$ (20 mM). After 2 h of growth at 25°C, induction of the *yop* regulon was performed by shifting the culture to 37° (7). After 4 h of incubation at 37°C, cultures were used for further analysis.

Fluorescence microscopy

For fluorescence imaging, about 2 µL of bacterial culture were placed on a microscope slide layered with a pad of 2% agarose in PBS. A Deltavision Spectris optical sectioning microscope (Applied Precision, Issaquah, WA, USA) equipped with an UPlanSApo 100x/1.40 oil objective (Olympus, Tokyo, Japan) and a coolSNAP HQ CCD camera (Photometrics, Tucson, AZ, USA) was used to take differential interference contrast (DIC) and fluorescence photomicrographs. GFP filter sets (Ex 490/20 nm, Em 525/30 nm) were used for GPF visualization. DIC frames were taken with 0.1 s and fluorescence frames with 1.0 s exposure time. Per image, a Z-stack containing 20 frames per wavelength with a spacing of 150 nm was acquired. The stacks were deconvolved using softWoRx v3.3.6 with standard settings (Applied Precision, WA). A representative DIC frame and the corresponding fluorescence frame were selected and further processed with the ImageJ software.

YscC purification and reconstitution on liposomes

The pYV–cured *Y. enterocolitica* strain carrying plasmids pMA6 and pRS6 (6) containing the yscC and yscW genes, respectively, was grown in brain heart infusion (BHI) broth. To induce expression of yscC, bacteria were inoculated at OD600=0.1 in BHI broth supplemented with glycerol (4 mg/mL), $MgCl_2$ (20 mM), sodium oxalate (20 mM) (BHI-OX), ampicillin (100 mg/ml), nalidixic acid (25 µg/ml), and tetracycline (10 µg/ml). The culture was grown for 2 h at room temperature, induced with 0.05% arabinose and grown for 6 h at 37°C. The entire YscC purification was performed on ice. Bacterial cells were washed with 0.9% NaCl, resuspended in 50 mM Tris-HCl pH

8.5 and 1 mM EDTA and disrupted using a sonicator. The membrane fraction was isolated by ultracentrifugation for 1 h at 150,000 x g (4°C), and membrane proteins were solubilized in buffer containing 2% DDM (n-dodecyl-β-D-maltopyranoside, Anatrace), 50 mM Tris-HCl pH 7.8, 250 mM NaCl, 5 mM EDTA and protease inhibitor (complete protease inhibitor, Roche) for 1.5 hour at room temperature. Insoluble material was removed by ultracentrifugation for 1 h at 150,000 x g (4°C). After the addition of sucrose to a final concentration of 15% (wt/wt), the extracted membrane proteins were layered on top of a 20–40% (wt/wt) sucrose gradient in gradient buffer (0.04% DDM, 50 mM Tris-HCl pH 7.8, 250 mM NaCl, 5 mM EDTA, protease inhibitor) and centrifuged at 38000 rpm in an SW41 rotor (Beckman) for 30 h. Fractions containing YscC were dialyzed against chromatography buffer (0.04% DDM, 10 mM Tris-HCl pH 7.8, 100 mM NaCl, 0.1 mM EDTA) and loaded on MonoQ 5/50 GL ion exchange column (GE Healthcare). YscC was eluted at 400–500 mM NaCl. The pure YscC oligomer was separated from YscC oligomer dimers and small contaminants by gel filtration using a Superose 6 10/300 GL column (GE Healthcare). Fractions containing YscC were stored at -20°C for electron microscopy.

To reconstitute YscC into liposomes, the purified secretin (0.2 mg/ml) was mixed with DDM-solubilized *E. coli* polar lipids at 5:1 lipid-to-protein ratio and vigorously mixed overnight with Bio-Beads (Bio-Rad) at room temperature.

Image processing procedures.

High defocus tomographs from focal pairs and tomograms of minicells were aligned by gold marker fiducials using Etomo (8) and reconstructed by weighted back projection using custom written Matlab scripts.

Central positions and directions of needles were manually determined for 421 injectisomes from the tomograms of minicells and for 1490 injectisomes from tomograms of regular sized cells acquired as focal pairs. Injectisomes were extracted to volumes of 128x128x128 voxels. Low-defocus (high resolution) particles were generated by a combination of global high- and low-defocus tilt series alignment, followed by refinement of patches of micrographs around the injectisomes ("local feature

118 refinement" method described in more details in Ref. (9)). From 1490 particles, 520 were selected for
119 high-resolution processing based on having good correlation of high- and low-defocus injectisome
120 volumes to each other. In addition, some tomograms of particles that did not contain projections of the
121 injectisomes in all low-defocus tilt series images were also discarded.

122 An initial average structure was produced as a sum of all injectisomes with the volumes rotated
123 such that the needles were pointing into the same (vertical) direction. Next, multiple rounds of
124 alignment with restricted angular rotation ranges were performed on high-defocus particles and on
125 minicell dataset particles, considering only voxels within a mask on the needle and the outer
126 membrane area with a pixel size 1.48 nm (Fig. S2*A*). The information about the missing wedge was
127 used to constrain correlation during alignment of particles to the average, and appropriate Fourier
128 component weighting was performed during generating the average at the end of each iteration. Next,
129 two independent alignments were calculated with two different soft masks: one containing the outer
130 membrane and the needle structures, and another one containing the cytoplasmic membrane and the
131 needle structure (Fig. S2*C*). During alignment we imposed 19-fold axial symmetry to the reference at
132 the start of each iteration, while we applied 12-fold rotational symmetry to the final structures. The
133 two resulting structures were aligned against each other by cross correlation maximization. Cropping
134 them together approximately in mid-height between the two membranes produced a merged structure.
135 The resulting volume was limited to 3.7 nm resolution, which was determined from Fourier Shell
136 Correlation (FSC) using the 1-bit criterion (10) (Fig. S2*D*). For this we made an average FSC inside
137 the two used alignment masks. The processing was done by AV3 processing package for Matlab (11),
138 in-house written scripts, and our Dynamo software tool for user-friendly sub-tomogram averaging
139 (http://www.dynamo-em.org) (12).

140 For the initial alignment of YscC we manually clicked into the membrane part and inside the
141 liposome in order to establish the initial orientation of the molecule for 282 particles. We used a
142 featureless plane with a ball as an initial reference for the alignment, after which the half of particles
143 with higher correlation coefficient contributed to the reference for next iteration.

For classification we used principal component analysis with K-means clustering. First aligned particles were generated with imposed 12 fold symmetry and equalized missing wedge. Only the particles that had correlation coefficient to the average over the mean value of the dataset were considered. Next, Eigenimages were calculated only taking into account voxels inside specified masks. Based on the Eigenimage weights, K-means classifications were calculated for different numbers of classes. The mask used for the overall variability analysis in Fig. S2*E* was soft, while all the other masks had hard edges.

Volume rendered visualizations were produced semi-automatically with Amira (http://www.amira.com). The reconstruction of the *Y. enterocolitica* injectisome will be deposited to the EMD upon acceptance of the manuscript.

MSA analysis of sub-volumes

Multivariate statistical analysis (MSA) was performed on injectisome sub-volumes within elliptical, Gaussian masked, areas. The largest mask, mask 3 in Fig. 3, revealed a strong variation in the inter-membrane distance, as described in the main text. While our reconstruction made from all injectisomes did not reveal the outer second periplasmic density layer, our MSA data showed in the majority of sub-volume class averages that outer second periplasmic layer at different positions, suggesting that its height also varies among the individual injectisomes with respect to the cytoplasmic membrane. The inner (bottom) periplasmic layer was less well visible in the class averages, suggesting a less defined contact between it and the basal body.

Docking of InvG into Y. enterocolitica YscC densities

Docking was done manually. Based on InvG docking, two possible locations for YscC were found, that place YscC either fully into the outer membrane, or solely adjacent to the inner surface of the outer membrane, as described in the manuscript. A possible third docking position as an intermediate between these two positions would place only the outer ring of the YscC secretin into the OM.

Distance distribution simulation

For the graph in Fig. 1*E* we simulated distances between randomly distributed injectisomes on the surface of a hypothetical bacteria. Using the number of injectisomes derived per minicell, we randomly generated position on a sphere with a radius of 250 nm for every hypothetical minicell, simulating two angles with radial angles in the range of 0º to 360º, and azimuthal angles in the range of -60º to 60º to simulate the lower detection probability at the top and bottom of minicells due to the missing wedge problem. Regular Euclidean distances between the injectisomes were measured from these generated positions. The simulation was performed 1000 times and the average values are presented.

Literature used in the Supplemental Online Materials:

1. Hodgkinson JL*, et al.* (2009) Three-dimensional reconstruction of the Shigella T3SS transmembrane regions reveals 12-fold symmetry and novel features throughout. *Nat Struct Mol Biol* 16(5):477-485.
2. Iriarte M & Cornelis GR (1998) YopT, a new Yersinia Yop effector protein, affects the cytoskeleton of host cells. *Mol Microbiol* 29(3):915-929.
3. Kaniga K, Delor I, & Cornelis GR (1991) A wide-host-range suicide vector for improving reverse genetics in gram-negative bacteria: inactivation of the blaA gene of Yersinia enterocolitica. *Gene* 109(1):137-141.
4. Diepold A*, et al.* (2010) Deciphering the assembly of the Yersinia type III secretion injectisome. *EMBO J* 29(11):1928-1940.
5. Mota LJ, Journet L, Sorg I, Agrain C, & Cornelis GR (2005) Bacterial injectisomes: needle length does matter. *Science* 307(5713):1278.
6. Allaoui A, Scheen R, Lambert de Rouvroit C, & Cornelis GR (1995) VirG, a Yersinia enterocolitica lipoprotein involved in Ca2+ dependency, is related to exsB of Pseudomonas aeruginosa. *J Bacteriol* 177(15):4230-4237.
7. Cornelis G, Vanootegem JC, & Sluiters C (1987) Transcription of the yop regulon from Y. enterocolitica requires trans acting pYV and chromosomal genes. *Microb Pathog* 2(5):367-379.
8. Kremer JR, Mastronarde DN, & McIntosh JR (1996) Computer visualization of three-dimensional image data using IMOD. *J Struct Biol* 116(1):71-76.
9. Kudryashev M, Stahlberg H, & Castano-Diez D (2011) Assessing the benefits of focal pair cryo-electron tomography. *J Struct Biol*.
10. van Heel M & Schatz M (2005) Fourier shell correlation threshold criteria. *J Struct Biol* 151(3):250-262.
11. Forster F, Medalia O, Zauberman N, Baumeister W, & Fass D (2005) Retrovirus envelope protein complex structure in situ studied by cryo-electron tomography. *Proc Natl Acad Sci U S A* 102(13):4729-4734.

12. Castano-Diez D, Kudryashev, M., Arheit, M., Stahlberg, H (2011) Dynamo: A flexible, user-friendly development tool for subtomogram averaging of cryo-EM data in High Performance Computing environments *Submitted*.

5.4 Supplementary Result: Number and Distribution of Injectisomes by Fluorescence Microscopy

It is difficult to count the total number of injectisomes per cell by cryo-ET. Due to the "missing wedge effect" and the fact that not the entire bacterium fits in the field of view at this magnification, injectisomes may not be seen. Also it is difficult to identify the basal bodies if the needle is missing. Unfortunately the needle seems to break of very easily (Journet et al, 2003). All handling before plunge freezing the bacteria for cryo-ET is done with special care, but centrifugation of the bacteria to get a denser suspension is not avoidable. Therefore the in average 6.2 injectisomes counted per cell is an underestimation of the real number of injectisomes per cell. Thus in a different approach to count the number of injectisomes per cell we counted the number of fluorescent foci made by EGFP-YscQ and YscC-mCherry (Fig. 5.2). In average we counted 15 fluorescent foci per cell (both for EGFP-YscQ and YscC-mCherry). It has to be noted, that the resolution of around 250 nm from the fluorescence micrographs is not high enough to resolve the single injectisomes. Considering the data from cryo-ET showing the tendency for injectisomes to be close to each other, but without any sign of big clusters of more than 3 injectisomes, we can assume that the average number of injectisome (in our setting) is maximally 2 or 3 times the number of counted fluorescent foci.

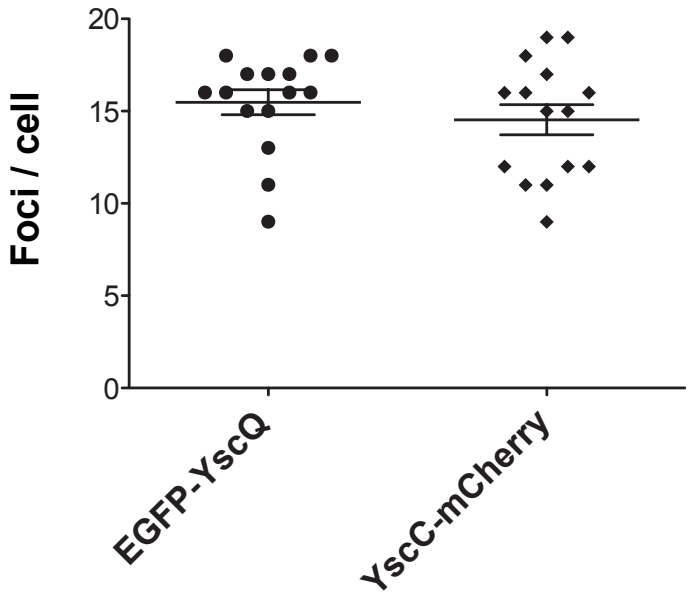

Fig. 5.2: Injectisomes per bacterium

Fluorescent foci, made by EGFP-YscQ (•) and YscC-mCherry (◆) in the same cell, were counted manually. Average with error bars is indicated.

6 Role of Genomic Factors in Assembly and Arrangement

6.1 Abstract

In addition to the two bacterial membranes the nascent injectisome needs to pass the peptidoglycan layer. The loci encoding for EPEC/EHEC, *Shigella* and *Salmonella* T3SS encode as well for a lytic transglycosylase, which is able to degrade the peptidoglycan, probably assisting the injectisome to incorporate into the peptidoglycan layer. No such enzyme has been found on the pYV for the *Yersinia* Ysc system. Here we investigated, the involvement of different chromosomal encoded lytic transglycosylases in the assembly of the injectisomes. Secondly we explored the distribution of the injectisomes in the bacteria. Therefore we compared injectisome localization with different cytoskeletal elements. As well we considered membrane composition for a driving force in injectisome arrangement. Unfortunately, the staining of the inner membrane of Gram-negative bacteria is a challenge. We conclude that the injectisome distribution is not random, but further investigation will be needed to decipher the underlying cause for this distribution.

6.2 Introduction

6.2.1 The Peptidoglycan of Gram-negative Bacteria

The peptidoglycan, also called murein, is a cell wall made out of sugar chains cross-linked via peptides to form a meshwork circumventing the entire bacterium. This peptidoglycan sacculus maintains the bacterial shape and protects it from osmotic challenges. The peptidoglycan layer of Gram-negative bacteria, which is placed between the inner and outer membrane, is rather thin, about 6 nm (*E. coli*) (Matias et al, 2003). The sugar chains are made up of alternating β-1,4-linked N-acetylglucosamine (GlcNac) and N-acetylmuramic acid (MurNac). Peptides can vary slightly, but the most common is L-Ala-D-Glu-mDAP-D-Ala-D-Ala, with L-Ala attached to MurNac.

The peptidoglycan synthesis can very roughly be divided in 3 steps (Fig. 6.1). First the precursor synthesis in the cytosplasm, second flipping at the inner membrane and third polymerization in the periplasm. In the cytoplasm fructose-6-phosphate is used as substrate to form uridine-diphosphate-GlcNac (UDP-GlcNac), of which a part is used to build UDP-MurNac. The pentapeptide stem is assembled directly on UDP-MurNac (for a detailed review see (Barreteau et al, 2008)). Uridine-monophosphate is released, when UDP-MurNac-pentapeptide is transferred to undecaprenyl phosphate at the inner leaflet of the inner membrane, building lipid I. Then lipid II is made by the transfer of the GlcNac moiety from UDP-GlcNac to lipid I. Lipid II is flipped over into the periplasm (for a detailed review see (Bouhss et al, 2008)). In the periplasm the GlcNac-MurNac-pentapeptide subunits are polymerized to long chains by a glycosyltransferase. A transpeptidase cross-links the different strains over the peptides to build a stable meshwork. This meshwork has only very few gaps and tears. Thus globular proteins larger than about 50 kDa cannot just freely diffuse trough the peptidoglycan layer (Demchick & Koch, 1996)

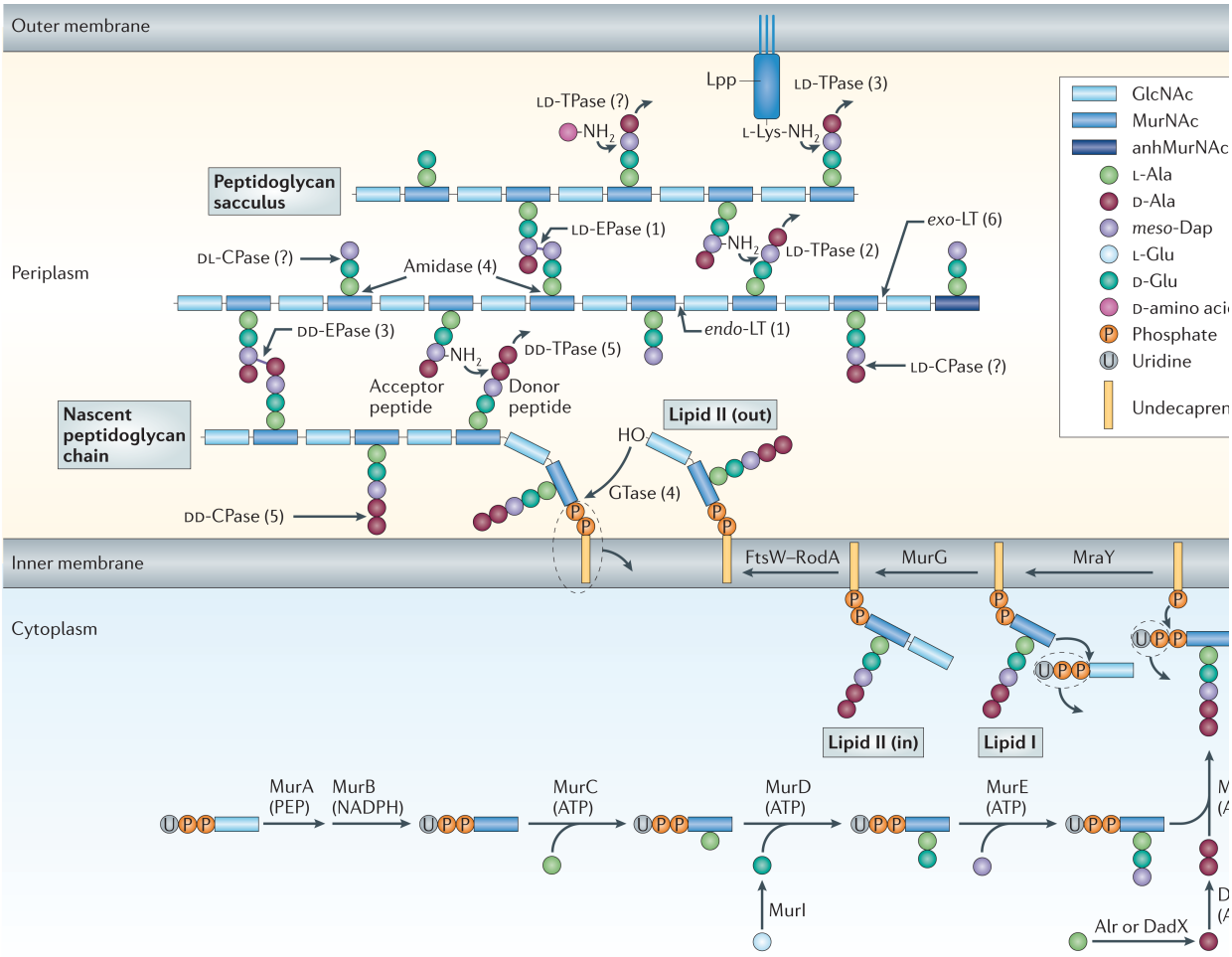

Fig. 6.1: Schematic illustration of peptidoglycan synthesis (Typas et al, 2012)

GlcNac, MurNac pentapeptides are synthesized in the cytoplasm. A linkage to the transport lipid (undecaprenyl phosphate) at the inner membrane allows flipping into the periplasm. A glycosyltransferase (GTase) catalyses polymerization of a nascent peptidoglycan chain, followed by attachment of the new chain to the sacculus by a transpeptidase (TPase). Peptides are trimmed by carboxypeptidases (CPases), and crosslinks are cleaved by endopeptidases (EPases). Peptides on glycan chains can be removed by amidases. Lytic transglycosylases (LTs) cleave in the glycan chain to form 1,6-anhydro-N-acetylmuramic acid (anhMurNAc) residues. Attachment to the major outer-membrane lipoprotein (Lpp) is promoted through TPases. Alr, Ala racemase, catabolic; DdlA, D-Ala–D-Ala ligase A; GlcNAc, N-acetylglucosamine; meso-Dap, meso-diaminopimelic acid; MraY, UDP-MurNAc-pentapeptide phosphotransferase; MurA, UDP-GlcNAc enolpyruvyl transferase; MurB, UDP-MurNAc dehydrogenase; MurC, UDP-MurNAc–L-Ala ligase; MurD, UDP-MurNAc-L-Ala-D-Glu ligase; MurE, UDP- MurNAc-L-Ala-D-Glu–meso-Dap ligase; MurF, UDP-MurNAc-tripeptide–D-alanyl-D-Ala ligase; MurG, UDP-GlcNAc-undecaprenoyl-pyrophosphoryl-MurNAc-pentapeptide transferase; MurI, Glu racemase; PEP, phosphoenolpyruvate.

6.2.2 The Bacterial Cytoskeleton

In earlier days the general believe was that bacteria, unlike eukaryotic cells, don't contain a cytoskeleton. Bacterial structures were thought to be randomly arranged and stochastically distributed to daughter cells. In the last decade this view has drastically changed, as the bacterial cytoskeleton was discovered and its understanding has progressed significantly. A landmark discovery was the description of the actin-like filaments made by MreB, which is found in almost all rod shaped bacteria, while it is absent in cocci (Daniel & Errington, 2003). Although MreB and actin share a low amino acid sequence identity, they have a highly similar three-dimensional fold. Like each member of the actin family MreB contains two main domains with two subdomains each. The interdomain cleft accommodates a nucleotide-binding site. Purified MreB forms filaments after addition of ATP or GTP (van den Ent et al, 2001). A helical distribution around the entire cell could be demonstrated by GFP fusions to MreB (Jones et al, 2001). Addition of S-(3,4-dichlorobenzyl)isothiourea called A22 leads to rapid delocalization of GFP-MreB, which then leads to rounding up of the cells (Gitai et al, 2005). The same operon as *mreB* encodes *mreC* and *mreD*. In *E. coli* MreB, MreC and MreD form a membrane bound complex (Kruse et al, 2005). In contrast to this in *C. crescentus* fluorescent fusion to MreB and MreC resulted in two independent spiral structures (Dye et al, 2005). Very interestingly the peptidoglycan synthesizing machinery, which can be stained with a fluorescent vancomycin derivate, shows a very similar arrangement as MreB (Daniel & Errington, 2003). Furthermore the helical arrangement of the transpeptidase penicillin-binding protein 2 (PBP2) is dependent on MreB (Figge et al, 2004) and MreC (Divakaruni et al, 2005). This leads to the conclusion that MreB is important for the positioning of the peptidoglycan synthesizing machinery (Fig. 6.2) (Divakaruni et al, 2007).

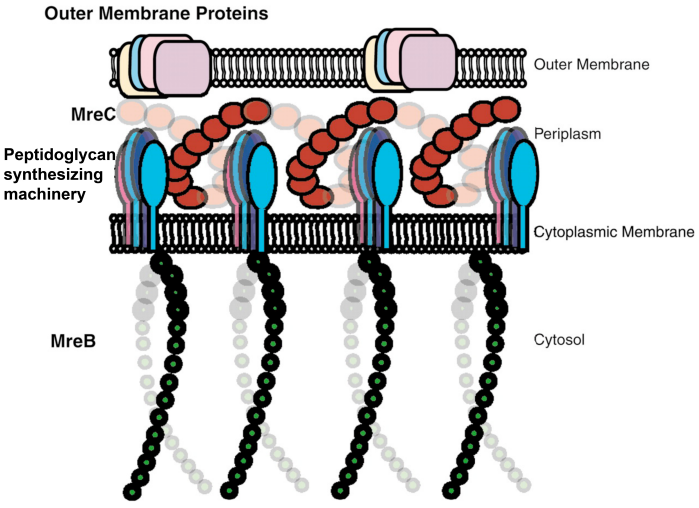

Fig. 6.2: Schematic illustration showing interplay between cytoskeletal elements and the peptidoglycan synthesizing machinery (Divakaruni et al, 2005)

MreB (green) is proposed to organize the peptidoglycan synthesizing machinery (multi coloured), which is anchored in the inner membrane. MreC (red) is suggested to organize outer membrane proteins (multi coloured) by linking them through some intermediary proteins to the MreB cytoskeleton.

Another bacterial cytoskeletal element is made by proteins of the MinD/ParA family. It does not have a homologue in eukaryotic cells. MinD is involved in septum placement (see as well chapter 5), while ParA is engaged in DNA segregation. Purified MinD of *Pyrococcus furiosus* has been shown to form filaments in presence of ATP (Suefuji et al, 2002), similar to MreB. Bundling of MinD filaments was obtained by addition of MinE, which as well induced the ATPase activity of MinD and the disassembly of the filaments. Thus MinE is responsible for the steady state of MinD filaments (Suefuji et al, 2002). At its C-terminus MinD contains a membrane-targeting sequence, which upon interaction with phospholipid bilayers undergoes structural changes into an amphipathic helix (Szeto et al, 2002). In *E. coli*, fluorescent fusions to MinD show helical structures winding around the bacterial membrane similar to MreB. But MinD seems to have in average a higher packing density of the helical loops (Shih et al, 2003).

6.2.3 Special Lipid Patches in Bacteria

Lipid rafts are membrane patches with special lipid composition that were identified in eukaryotic cells. They are enriched in sterols and sphingolipids. Some proteins have been described as lipid raft markers. The most prominent one is Flotillin, also referred to as Reggie (Langhorst et al, 2005). Flotillin homologues have been found in prokaryotes. In *B. subtilis* and *S. aureus* the Flotillin homologues were recently shown to cluster in lipid patches, which are proposed to be bacterial lipid rafts (López & Kolter, 2010). Independent of this study, it was demonstrated that membrane staining of *B. subtilis* with a compound staining anionic phospholipids, FM 4-64, shows a spiral pattern. Furthermore these membrane spirals colocalize with GFP-MinD (Barák et al, 2008).

6.2.4 Muramidases in Type Three Secretion Systems

Several macromolecular machines span the inner and outer membrane of Gram-negative bacteria and cross as well the peptidoglycan layer (Fig. 6.3). Very often the loci encoding such systems also contain an orf coding for a muramidase; e.g. *pilT* for type IV pili, *virB1* for type IV secretion systems (Koraimann, 2003). In the flagellar system the peptidoglycan-hydrolyzing activity of FlgJ has been shown to be essential. An *flgJ* mutant loses its ability to swarm on semi-solid agar plates (Nambu et al, 1999). Also most of the T3SS contain a lytic transglycosylase (LT). However IpgF in *S. flexneri* and IagB in *S. enterica* seem to be dispensable for T3S (Allaoui et al, 1993; Sukhan et al, 2001). But it in zymogram assays their peptidoglycan degrading capacity has been demonstrated (Zahrl et al, 2005). The deletion of EtgA, in EHEC and EPEC, leads to substantially reduced secretion (García-Gómez et al, 2011; Yu et al, 2010). Despite extensive BLAST searches on the pYV plasmid, which otherwise contains all the genes necessary for the T3SS, no muramidase gene could be identified for the *Y. enterocolitica* Ysc T3SS. This absence of a muramidase on the pYV is very intriguing. How

can the injectisome pass the peptidoglycan? Why is the activity of IpgF and IagB maintained although they do not seem to be necessary in laboratory conditions?

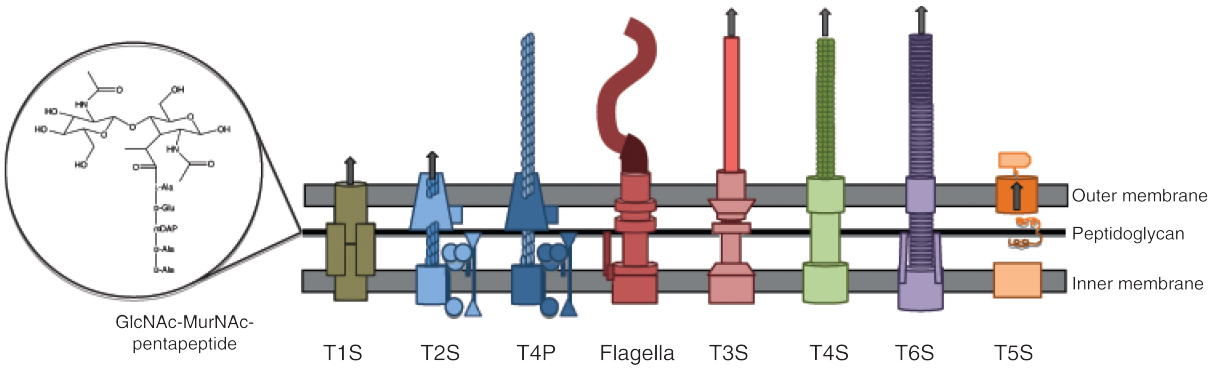

Dedicated Peptidoglycan-degrading enzyme	?	?	Yes	Yes	Yes	Yes	?	?
Activity			LT	Muramidase LT Peptidase	LT	LT		
Peptidoglycan-binding protein	?	Yes	Yes	Yes	Yes	?	Yes	?

Fig. 6.3: Many structures spanning the inner and outer membrane have dedicated peptidoglycan-degrading enzymes (Scheurwater & Burrows)

Schematic illustration of type 1 to 6 secretion systems, the type 4 pili (T4P) and flagella. Dedicated peptidoglycan-degrading enzymes, muramidases or lytic transglycosylases (LT), are found in T3SS, T4SS, T4P and flagella.

6.3 Results

6.3.1 Construction of a Restriction Mutant of *Y. enterocolitica* 8081

In order to investigate chromosomal encoded functions necessary for the assembly of the *Yersinia* Ysc T3SS we decided to turn to the sequenced wild type strain *Y. enterocolitica* 8081 (serotype 0:8) (Portnoy et al, 1981) (NC_008800.1). However, this strain contains an efficient restriction system, including *Yersinia* endonuclease I (*Yen*I), which is an isoschizomer of the commercially available *Pst*I and cuts the CTGCA/G sequence (Miyahara et al, 1988). To facilitate the introduction of plasmids in this strain we started by knocking out *yen*I. Therefore a *Pst*I restriction site free suicide plasmid, containing homologous to the regions flanking *yen*I, was constructed. This plasmid was readily introduced into the *Y. enterocolitica* 8081 strain, and after two step homologues recombination a *yen*I mutant strain, MA8040, was obtained. The loss of the restriction enzyme was verified by transformation with a plasmid containing the *Pst*I motif. While no plasmid containing colonies could be obtained with the wt strain, there was no significant difference in obtained colonies using a plasmid with and or without *Pst*I sequence after transformation into strain MA8040 (data not shown).

6.3.2 Role of Endogenous Muramidases

To study the role of the endogenous muramidases in the assembly of the Ysc machinery we first performed BLAST searches with the sequences of IpgF and IagB against the genome of *Y. enterocolitica* 8081 (data not shown), in both cases the two best hits were a hypothetical protein YE3411 (E-value $<10^{-26}$) and not very surprisingly YsaH (E-value $<10^{-23}$). YsaH is the homologue of IpgF/IagB in the second T3SS, called Ysa system, which is chromosomally encoded, in the 8081 strain but missing in the E40 strain. Hence we ignored this second hit. To check if YE3411 is implicated in injectisome assembly, we constructed a fusion protein with mCherry, in a strain encoding as well EGFP-YscQ, thus producing GFP labelled injectisomes. To this end, an integrative plasmid, containing the mCherry sequence was introduced into the genome directly after the last amino acid, but before the stop codon, of YE3411. The plasmid was left inside, which should not disturb, as the mRNA of YE3411 is monocistronic. After induction of the synthesis of T3S apparatus, fluorescence micrographs were taken. No obvious change in injectisome arrangement, neither in distribution nor in amount, could be observed. YE3411-mCherry was localized all around the cell membrane, with some brighter foci at the cell poles (Fig. 6.4). Additional to YE3411 we used the same approach to assess all annotated membrane bound lytic transglycosylases in the *Y. enterocolitica* 8081 genome. None of these mutations had a direct influence on injectisome formation. MltA- and MltB-mCherry showed

fluorescent foci close to the membranes, but they did not colocalize with EGFP foci of the injectisomes. MltC-mCherry resulted in fluorescence around the bacteria membrane with some brighter spots, often seen at the forming septa. The expression conditions of MltD- and MltF-mCherry appeared to be different from the expression conditions of the injectisomes. Thus no or almost no fluorescence was seen for these constructs. For MltF some odd looking bacteria were observed. These bacteria were very rare, but they showed fluorescence foci for MltF-mCherry (Fig. 6.4).

In an alternative approach YE3411, the soluble lytic transglycosylase, *slt*, or the flagellar muramidase gene, *flgJ*, were deleted and the injectisome formation was evaluated via EGFP-YscQ foci formation. None of these mutations altered the injectisome arrangement (Fig. 6.5A). As described in Nambu et al. (Nambu et al, 1999), an *flgJ* mutant was unable to swarm on semi-solid agar (Fig. 6.5B).

There was no evidence that one of the tested muramidases could be piercing the hole into the peptidoglycan for the injectisome to pass. A different possible scenario is that the injectisomes are inserted directly in the nascent peptidoglycan. To test this hypothesis we tried to make a mutant encoding for a PBP2-mCherry hybrid protein. Unfortunately this construct seemed to be lethal and in spite of intense trials no mutant was obtained.

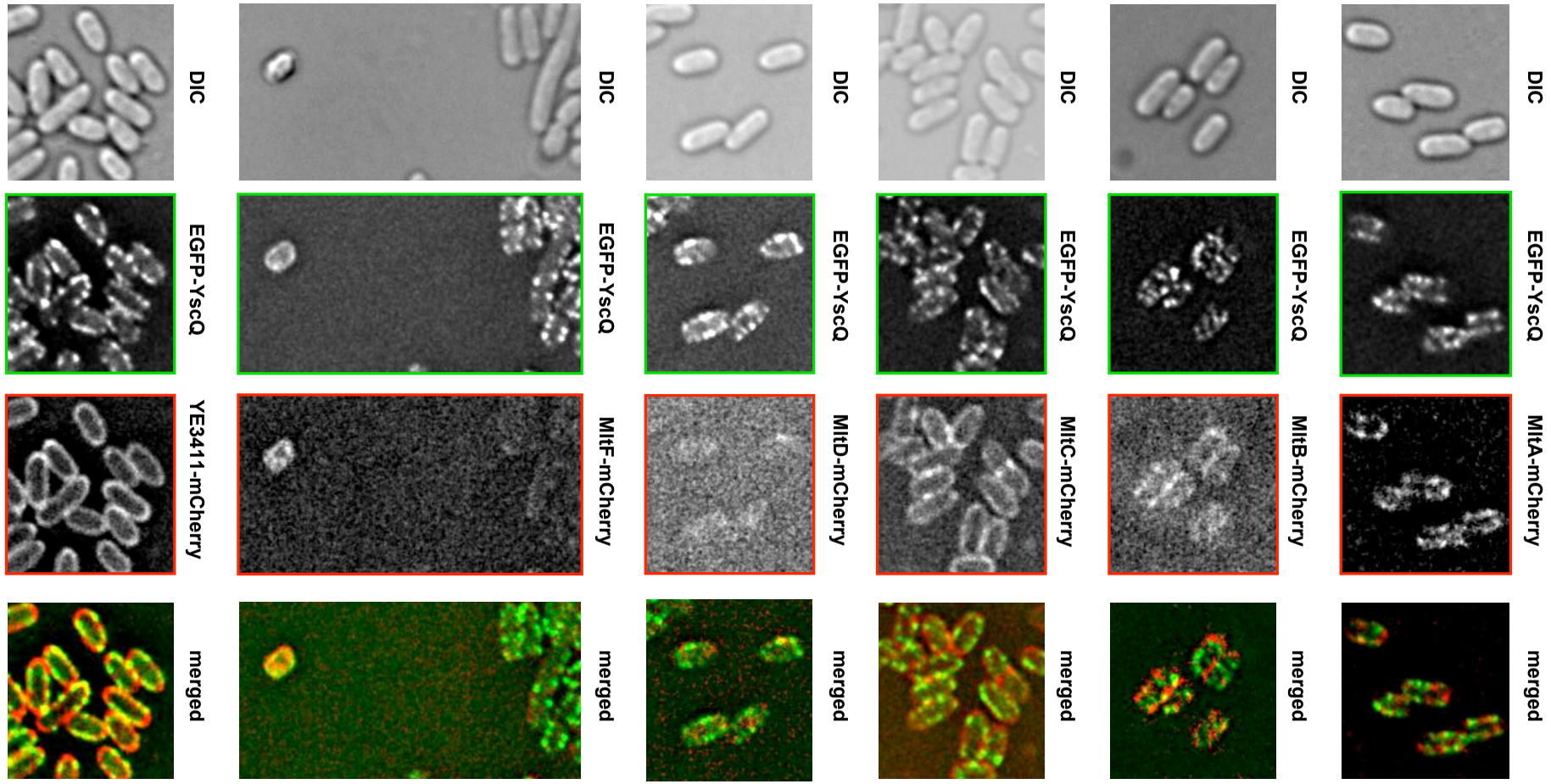

Fig. 6.4: Colocalization of the injectisome with different muramidases

Each row contains a set of representative images, taken in the same frame with different illumination, of one strain. In the left column are DIC pictures, 2nd column pictures taken in the GFP channel, 3rd column RFP channel and last column is a merge of the GFP image with its corresponding RFP image. All strains contain EGFP-YscQ and a muramidase fused to mCherry; from top to bottom: MltA-mCherry; MltB-mCherry; MltC-mCherry; MltD-mCherry; MltF-mCherry and YE3411-mCherry.

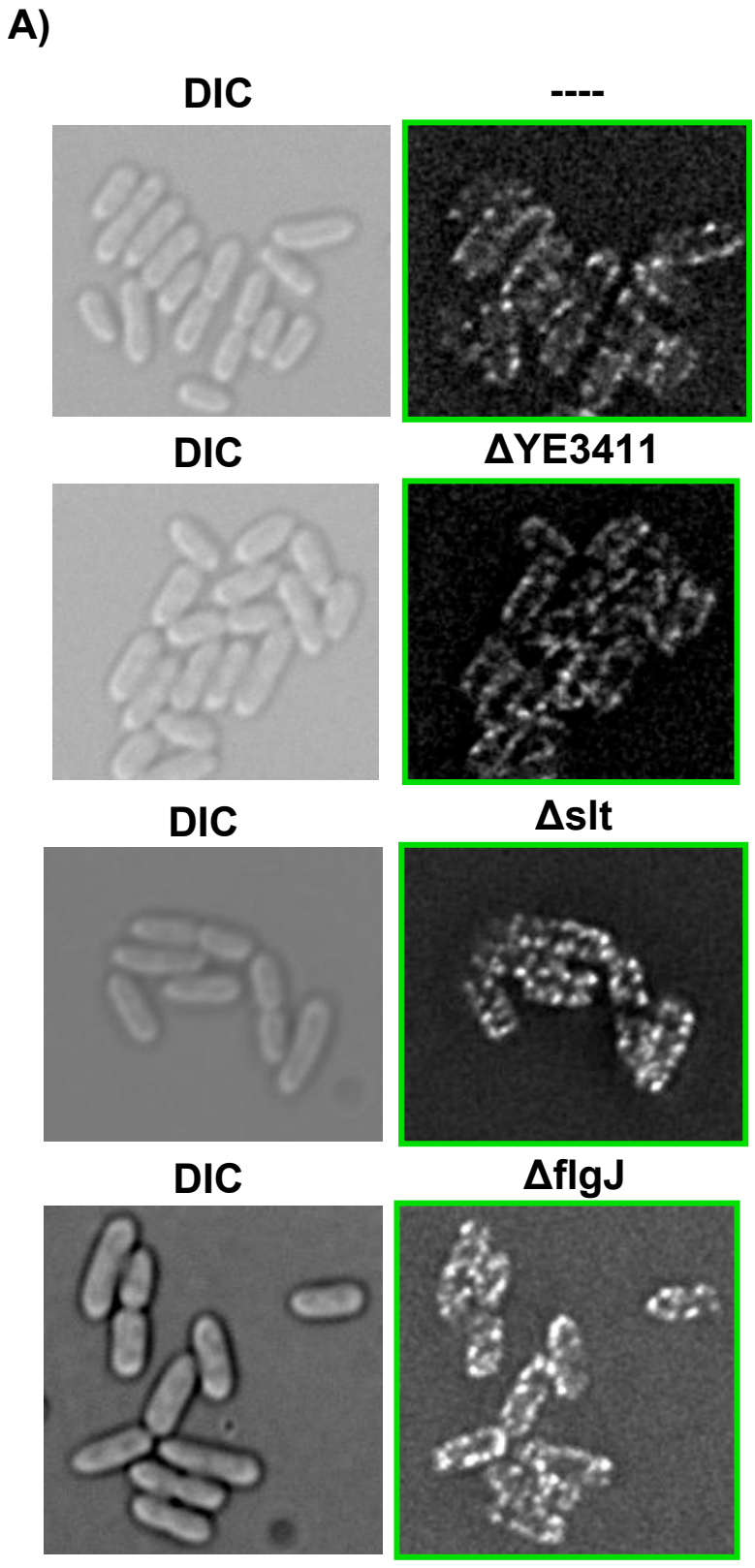

Fig. 6.5: Injectisome arrangement in muramidase deletion strains

A) left column DIC pictures; right column fluorescent pictures of EGFP-YscQ in different muramidase deletion strains. From top to bottom: --- (control strain); ΔYE3411; Δ*slt*; Δ*flgJ*

B) colonies spotted on semi-solid agar plates. Top swarming wt *Y. enterocolitica* 8081 strain; bottom non-swarming Δ*flgJ* strain.

6.3.3 Colocalization with Cytoskeleton Proteins

MreB is one of the best studied cytoskeleton proteins. Its implication in organization of different bacterial structures, e.g. the peptidoglycan synthesis machinery, has been widely proposed (White et al, 2010). Fluorescent fusions with MreB have been reported to form continuous helical filaments circumventing the cells from one pole to the other (Jones et al, 2001). Another study with fluorescent MreB constructs in *E. coli* describes distinct fluorescent foci, which seem to be arranged on a helical path (Bendezu et al, 2009). The arrangement of these foci resembles the arrangement of the fluorescent foci of the labelled injectisomes, which we have observed. Interestingly, an alignment of the nucleic acid sequences of *mreB* from *E. coli* K12 and its homologue envB in *Y. enterocolitica* 8081 shows only a moderate identity of 83 %, but an alignment of the amino acid sequences shows high similarity of more than 99% with only three different amino acids in a total of 347 aa; position 2 leucine to phenylalanine, position 221 glutamic acid to serine and position 232 arginine to leucine. Thus we decided to insert mCherry between α-helices 5 and 6 (van den Ent et al, 2001) as described by Bendezu *et al.* 2009. The *envB*-mCherry-sandwich (*envB*-mCherry$_{sw}$) construct was cloned into a medium copy plasmid under the control of the *araBAD* promotor, resulting in plasmid pMA45. This plasmid was introduced in the EGFP-YscQ strain, which still contained the wt *envB* gene. To test colocalization of these two constructs, we induced in exponentially growing bacteria the expression of EnvB-mCherry$_{sw}$ and the T3SS simultaneously by addition of arabinose and a temperature shift to 37°C. Fluorescent micrographs showed very similar foci in the green and red channel, but if the two colours were merged, no colocalization could be observed (Fig. 6.6). As a control we used strain MAAD4006 (Diepold et al, 2010), which contains EGFP-YscQ and YscC-mCherry. These two proteins colocalized almost perfectly. But as this strain still contains wt EnvB, we could not be sure if the EnvB-mCherry$_{sw}$ construct was functional and placed correctly in the cell. We used A22, which specifically acts on MreB/EnvB. Adding A22 simultaneously to the T3SS and EnvB induction did not prevent the EnvB-mCherry$_{sw}$ foci to form. If A22 was added 30 min earlier, EnvB-mCherry$_{sw}$ was not able to make foci, but it was distributed around the entire bacterial membrane (Fig. 6.6). Also the cells lost their rod shape and rounded up.

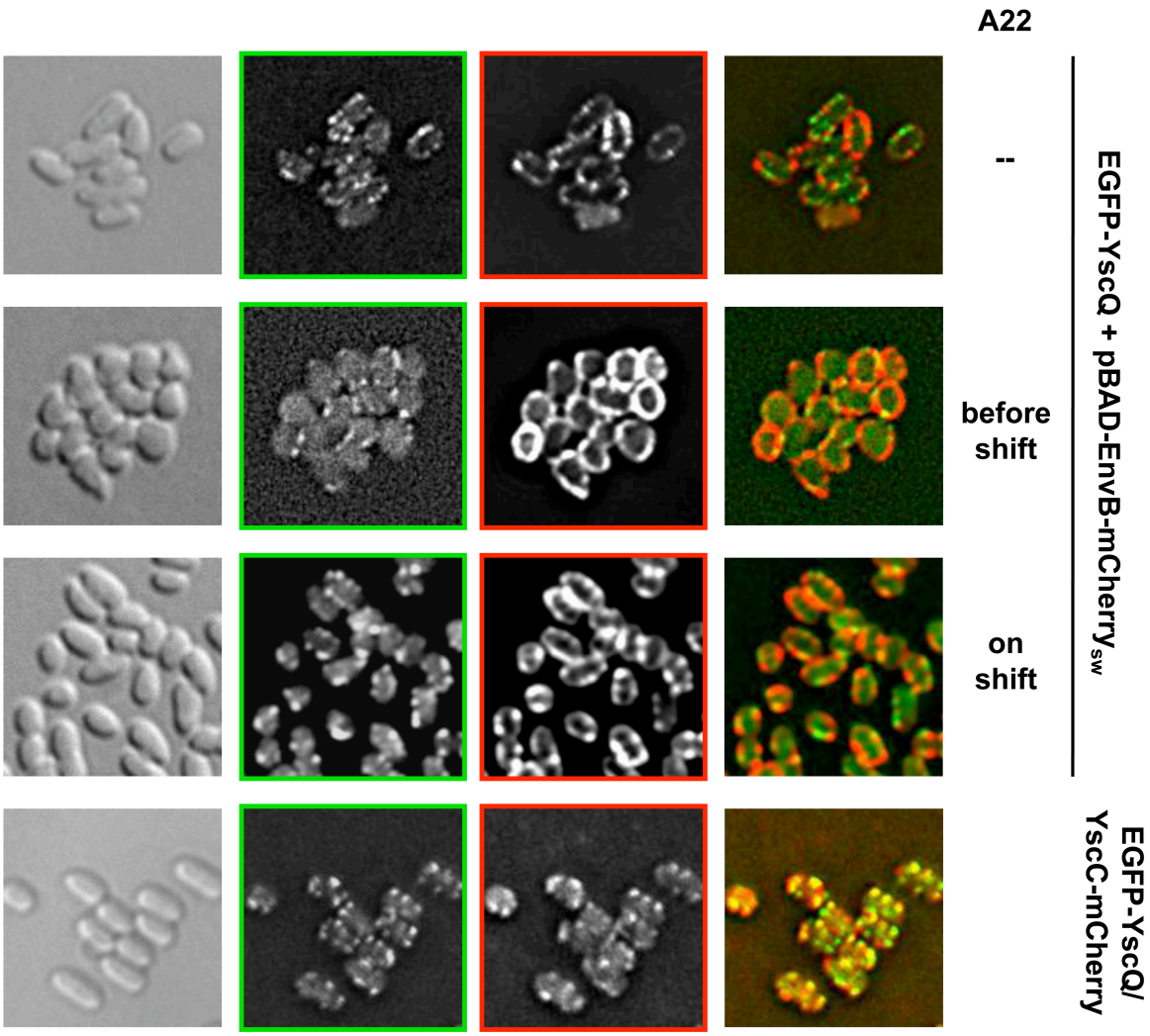

Fig. 6.6: Comparison of injectisome arrangement with EnvB arrangement

Each row contains a set of representative images, taken in the same frame with different illumination, of one condition. In the left column are DIC pictures, 2nd column pictures taken in the GFP channel, 3rd column RFP channel and latst column is a merge of the GFP image with its corresponding RFP image. First three rows show strain encoding the gene for EGFP-YscQ on the virulence plasmid and expressing EnvB-mCherry$_{sw}$ from an arabinose inducable plasmid. Top row no A22 added; second row A22 was added 30 min before induction of the T3SS and the EnvB-mCherry$_{sw}$ construct; third row A22 was added at the same moment as the T3SS and the EnvB-mCherry$_{sw}$ construct were induced. Bottom row shows control strain encoding of EGFP-YscQ and YscC-mCherry on the virulence plasmid.

These results allowed no final conclusion concerning the functionality of the EnvB-mCherry$_{sw}$ construct. Therefore we decided to make a chromosomal mutant. As *mreB*, as well as the genes downstream in the operon, *mreC* and *mreD* are essential under standard laboratory conditions, this mutant was not easy to obtain. We used an additional promoter in front of the homologous regions on the mutator plasmid to ensure the expression of the downstream proteins after the first homologous recombination, while the entire mutator plasmid is inserted into the chromosome. With this strategy we were able to insert the mCherry sequence directly into the chromosomal sequence of *envB*. This strain did not contain an additional wt version of *envB* and the protein expression is naturally regulated. Also this strain was analyzed by fluorescence microscopy and it showed the same foci arrangement, which did not colocalize with the injectisomes, as seen in the in trans expressed construct (Fig. 6.7). The cells were normally shaped, no rounding up could be observed. Thus we concluded that the construct was functional. Interestingly the pattern of the merged images of the non-colocalizing injectisomes and EnvB resemble the two independent spirals of MreC and MreB reported in *C. crescentus* (Dye et al, 2005). Hence we wanted to test if the injectisomes colocalize with the spiral made by MreC. A chromosomal mreC-mCherry mutant was constructed with the same methode as the envB mutant. In our hands MreC-mCherry did not form spirals or foci on a helical path. MreC-mCherry seemed to be recruited to the newly forming septa (Fig. 6.7). It has to be noted that only weak fluorescence could be observed. This might be due to either a rather low natural protein level or degradation of the MreC-mCherry construct. A western blot anti mCherry did however not show any degradation band (data not shown).

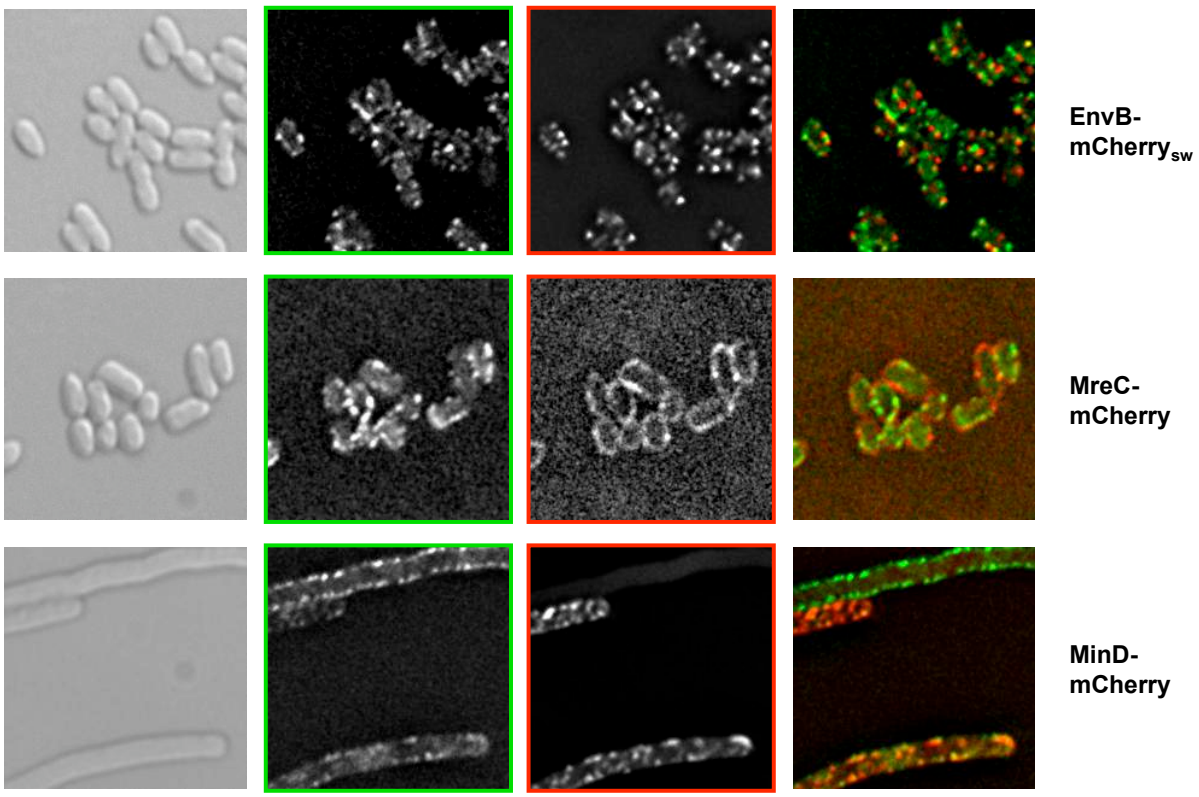

Fig. 6.7: Comparison of injectisome arrangement with different cytoskeleton components

Each row contains a set of representative images, taken in the same frame with different illumination, of one strain. In the left column are DIC pictures, 2nd column pictures taken in the GFP channel, 3rd column RFP channel and latst column is a merge of the GFP image with its corresponding RFP image. All three strains encode for EGFP-YscQ and either EnvB-mCherry$_{sw}$ (top row), MreC-mCherry (middle row) or MinD-mCherry (bottom row).

As both of the tested structures did not seem to be involved in the arrangement of the injectisomes we decided to look further for bacterial elements, especially filamentous structures, which have a similar arrangement as the injectisomes and therefore might be involved in injectisome arrangement. An interesting candidate was MinD, which has been reported to be helically arranged and which shows bright foci, when it is fused to a fluorescent protein (Shih et al, 2003). Thus we investigated, if MinD is involved in injectisome arrangement. We constructed N- and C-terminal fusions of *minD* with mCherry on the chromosome. Unfortunately, both constructs were not functional and had a defect in septum placement. Thus very long cells as well as minicells could be observed in these mutants (Fig. 6.7. and data not shown). Anyway the strains were analyzed by fluorescence microscopy and in the mutant with mCherry C-terminally fused to MinD rarely some cells were observed which showed bright foci in the red channel. Even more these red foci colocalized almost perfectly with the green foci of the injectisomes (Fig. 6.7). But MinD was not functional and it was only seen in a very low percentage of the cells, thus we could not exclude this to be an artefact. Furthermore in a *minD* deletion mutant injectisomes could form normally, the arrangement did not seem to change and secretion of the effectors into the supernatant was not affected (Fig. 6.8). This may indicate that MinD is not responsible for the arrangement of injectisomes but there is something else which makes MinD and the injectisomes take places close by each other in the cell.

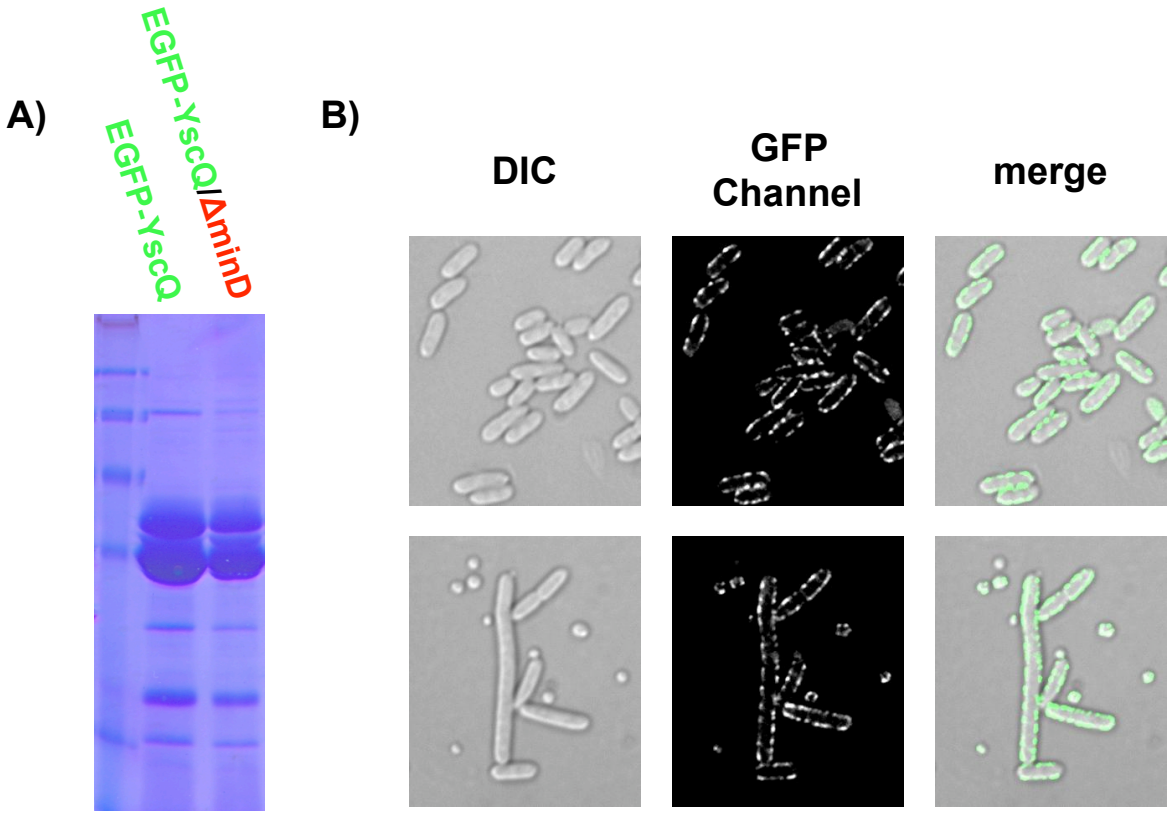

6.8 Injectisome assembly in a *minD* minus strain

A: Coomassie stained SDS-PAGE of culture supernatants containing secreted proteins. First lane: marker; second lane: EGFP-YscQ strain; third lane EGFP-YscQ/ΔminD strain.

B: Each row contains a set of representative images, taken in the same frame with different illumination, of one strain. In the left column are DIC pictures, 2nd column pictures taken in the GFP channel, 3rd column is a merge of the GFP image with its DIC picture. On top: *minD* wt strain; bottom: *minD* deletion (*ΔminD*) strain.

6.3.4 Colocalization with Special Lipid Confirmation

Barák et al. 2008 showed that in *B. subtilis* the cytoskeletal element MinD is colocalizing with a membrane spiral enriched with anionic phospholipids, which can be stained with a membrane stain called FM 4-64. This membrane spiral is forming independently of MinD, thus Barák *et. al.* 2008 are hypothesizing, that the amphipathic helix of MinD preferably binds to these anionic phospholipids enriched regions. Hence the membrane composition would be responsible for MinD arrangement. Such a lipid composition dependent arrangement is of course also possible for injectisomes. Unluckily staining of the inner membrane of Gram-negative bacteria is very difficult. The dye has to be able to pass the outer membrane and even if it does so the risk is high that the dye has as well affinity for the outer membrane. Despite these risks we decided to try membrane staining. No efficient membrane staining was obtained using FM 4-64 (data not shown). Using a different membrane dye, namely Nile Red, it was possible to stain the bacterial membranes and a few brighter foci per cell were observed. Unfortunately the fluorescent emission spectra of Nile Red appeared to be to wide and it was not only detected in the red channel, but it was shining through very bright in the green channel, masking the fluorescence of EGFP-YscQ (Fig. 6.9). As membrane staining was not feasible, we tried to identify a Flotillin like protein in *Y. enterocolitica*. To this end we performed a PSI BLAST using YuaG, the Flotillin like protein from *B. subtilis* (López & Kolter, 2010). The parameters resulting of 3 search iterations on the entire database were used for a search on the *Y. enterocolitica* 8081 genome. The only promising hit was YE3058 (E value = 10^{-13}). Thus we constructed a mCherry YE3058 hybrid and compared its localisation with the injectisome arrangement. But like EnvB, YE3058 seemed not to colocalize at all with the injectisomes (Fig. 6.10).

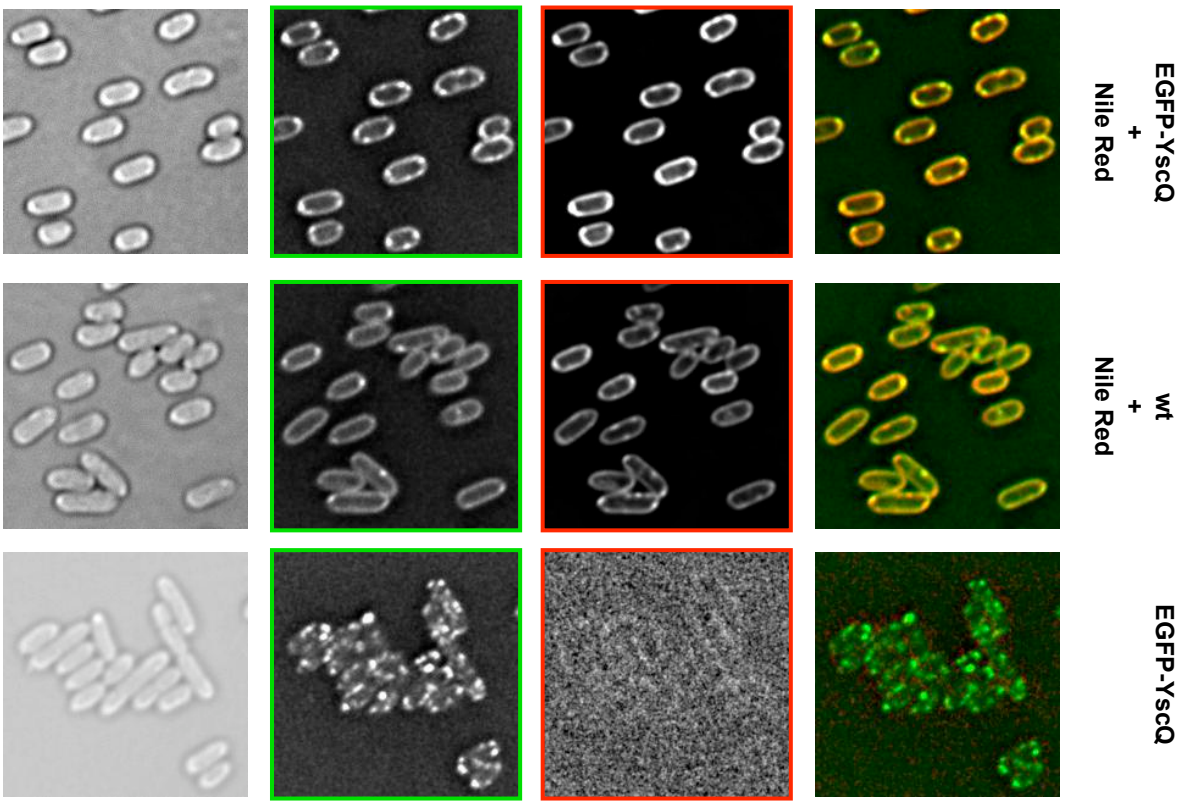

Fig. 6.9: Lipid staining

Each row contains a set of representative images, taken in the same frame with different illumination, of one condition. In the left column are DIC pictures, 2nd column pictures taken in the GFP channel, 3rd column RFP channel and latst column is a merge of the GFP image with its corresponding RFP image. Top: EGFP-YscQ strain stained with nile red; middle: wilde type strain stained with Nile Red; bottom EGFP-YscQ strain without Nile Red.

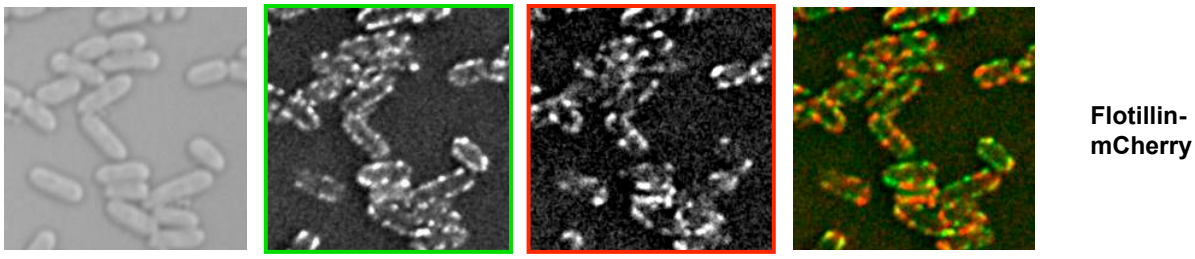

Fig. 6.10: Comparison of injectisome arrangement with the Flotillin like protein

Pictures taken in the same frame with different illumination of the strain containing Flotillin-mCherry (YE3058) and EGFP-YscQ. From left to right: DIC, GFP, mCherry and merge of GFP and mCherry.

6.4 Discussion and Conclusion

In the course of this study we tried to search for genomic factors, which facilitate the assembly of the *Yersinia* Ysc T3SS, either by helping it to pierce through the peptidoglycan layer and/or by locating it at favourable positions in the bacterial membrane. As a read-out we used a fluorescent version of the c-ring protein (EGFP-YscQ), which only assembles after the entire core of the injectisome, with YscC, YscD and YscJ spanning from the outer membrane to the inner membrane, is completely built. Thus EGFP-YscQ is an optimal read out for injectisome assembly. To facilitate the work with chromosome-encoded proteins, we decided to use the 8081 strain, the, at this time, only sequenced *Y. enterocolitica* strain. As a first step we had to knock out the restriction enzyme gene *yen*I, which otherwise would prevent the introduction of plasmids.

Unlike other T3SS or flagella, the Ysc system is missing a muramidase. This leads to the assumption that a muramidase encoded on the genome, which normally has a different role, could be used to pass the peptidoglycan layer. Therefore we executed BLAST searches with IpgF and lagB, the *Shigella* and *Salmonella* T3SS muramidases on the *Y. enterocolitica* 8081 genome. Only two hits had good E-values, a hypothetical protein YE3411 and YsaH. YsaH belongs to the second T3SS found in the 8081 strain, but is absent in the E40 strain, which led us to ignore YsaH. This might have been hasty. Recently the shotgun sequence of *Y. enterocolitica* W22703 has been published. The sequence revealed the existence of a second T3SS, different from the Ysa system, in this strain (Fuchs et al, 2011). The W22703 strain is very close to the E40 strain (Sory et al, 1995). Due to the shortness of candidates from the BLAST search we decided as well to include annotated lytic transglycosylases, as IpgF was placed in this group of muramidases (Koraimann, 2003), which were also proposed to be space-making autolysins (Scheurwater et al, 2008). First we constructed different muramidase - mCherry fusions, which we tried to co-localize with the assembled injectisomes. MltA- and MltB-mCherry seemed arranged rather opposite to EGFP-YscQ. MltC-mCherry appeared to be localized at the newly building septa and MltD- and MltF-mCherry seemed not to be expressed at the same conditions as the injectisomes. It looked as though MltF was expressed in dying bacteria. Overall, we could not observe any congruency between the EGFP-YscQ foci and the tested muramidases. A critical point in this approach is the timing. It is possible that once a path through the peptidoglycan is made, the muramidase is moving. Although this is rather unlikely as muramidases that are not tightly controlled, spatially and quantitatively, would be detrimental for bacteria. In an alternative approach we knocked out YE3411 and the soluble lytic transglycosylase and evaluated the EGFP-YscQ foci formation, which did not appear altered. We asked whether injectisomes could take over the places of the flagella, which are down

regulated at 37°C, when the T3SS is expressed. To see this we knocked out the flagellar muramidase *flgJ*. This inhibited flagella as shown by the strongly reduced swarming on semi solid agar plates. But it did not alter the EGFP-YscQ arrangement. While an *etgA* mutant in EHEC or EPEC showed significantly decreased secretion, *ipgF* and *iagB* seemed not to be essential for efficient T3S in *Shigella* and *Salmonella* under laboratory conditions. Nevertheless IpgF and IagB are evolutionary conserved and they are able to hydrolyse peptidoglycan. It is possible that fast growing bacteria can overcome the need of a muramidase by taking advantage of gaps during the peptidoglycan synthesis. If this were true, it could explain a phenomenon observed in the laboratory with *Y. enterocolitica*. If the expression of the T3SS is not made during exponential growth, but just a little later than usual, effector secretion is reduced (unpublished observation). This was always attributing to a lack of nutrition, but maybe this is due to an impeded injectisome formation in non-growing cells. In a very elegant approach, the nascent cell wall in *B. subtilis* was visualized with a fluorescent vancomycin derivate (Daniel & Errington, 2003). In Gram-negative bacteria this approach is not feasible, as the outer membrane would hinder the compound to reach its target. We tried to construct fluorescent fusions with the cell wall synthesising enzyme PBP2, but no mutants were obtained (data not shown). It was reported that the cell wall synthesizing machinery is placed by the cytoskeletal protein MreB, which was suggested to be implied in the arrangement of different cellular elements. It has to be added that over the time this study has been conducted the general view of MreB filaments has changed. Due to the reports showing *in vitro* polymerization of MreB into long filaments (van den Ent et al, 2001) and the first demonstration of continuous fluorescent helices in bacteria cells (Jones et al, 2001) the opinion was that MreB filaments are spanning from pole to pole. This view was challenged by observations of unconnected fluorescent foci made by fluorescent MreB constructs (Bendezu et al, 2009), and by a cryo electron tomography study (Swulius et al, 2011). Swulius et al. 2011 analyzed MreB filaments in six different cell types, including *C. crescentus*, *B. subtilis* and *E. coli*. They found no filament longer than 80 nm. This questions the role of MreB. Instead of being the initiation factor, which builds up a cytoskeleton and pilots cellular structures to their place of action, MreB may just be a connecting link. Still in believing MreB is forming long cell spanning helical structures, we engineered a fusion construct of mCherry and EnvB, the *Yersinia* homologue of MreB, which as expected was forming fluorescent foci in a helical looking pattern around the cell, when expressed in trans from a inducible plasmid. Although the pattern of the EnvB-mCherry$_{sw}$ construct and the fluorescent injectisomes looked strikingly similar, an overlay of the two channels revealed that both constructs were not colocalizing. But as this strain still contained the wt EnvB protein we were not sure if the hybrid construct was functional and arranged properly. Thus we were testing the influence of A22, a drug that is supposed to disassemble MreB filaments, on our hybrid constructs. When A22 was added in the same moment as EnvB-

mCherry$_{sw}$ expression was induced distinct fluorescent foci were visible 3 h later. If A22 was added 30 min before EnvB-mCherry$_{sw}$ induction, no foci but bright staining of almost the entire membrane was observed 3 h after EnvB-mCherry$_{sw}$ induction. As well under these conditions only very few foci were seen for the injectisomes. This could suggest that injectisomes depend on EnvB arrangement to assemble properly. But at this stage the cells lost already their shape, meaning all the structures depending on EnvB start to be misarranged thus the effect on the injectisomes could be very indirect. Other than expected, we could not observe any rapid disappearance of the fluorescent foci of EnvB-mCherry$_{sw}$ upon addition of A22 (data not shown). Thus we still could not be sure that the EnvB-mCherry$_{sw}$ construct was functional, hence we decided to replace the wt *envB* gene with the hybrid construct. These cells grew normally and showed wt morphology, proofing the functionality of the fluorescent EnvB. Observation of the fluorescent foci in this strain confirmed the results from the plasmid-expressed construct. However these pictures persuaded us that the injectisome arrangement is not stochastic. The chance that the fluorescent foci get close enough to overlap is high, if one of the two constructs could be placed at any place in the cell. Note, for an overlap of the fluorescent foci the proteins don't need to be in direct contact. The resolution of the fluorescence microscope is very low compared to the size of the structures we are looking at. EnvB-mCherry$_{sw}$ and the injectisomes seem to be placed on individual helical paths, reminding the independent spirals made by MreB and MreC in *C. crescentus* (Dye et al, 2005). It has to be noted that in contrast to these independent spirals in *C. crescentus*, MreB, MreC and MreD build an essential membrane bound complex in *E. coli* (Kruse et al, 2005). Anyway we tested the MreC distribution in *Y. enterocolitica*. Surprisingly the distribution pattern of MreC-mCherry did not resemble the pattern of the EnvB-mCherry$_{sw}$ construct, consequently no correlation with the injectisomes could be observed. MreC-mCherry seemed to be recruited to newly forming septa. We can only speculate why the MreC localization differs, from what was reported in other organisms. One possibility is the growth state of the cells. While most of the studies look at the cells during exponential growth, we were observing the bacteria in conditions optimized for T3S, but under these conditions growth is stalled.

As we could not see any relation between the injectisomes and the Mre system, we were looking for more structures that have been reported to be arrange in a similar pattern but are not connected to the Mre system. In literature we found another cytoskeletal element, which fulfilled the criteria, MinD. Thus we constructed mCherry fusions to MinD. Unfortunately other than the EnvB construct, chromosomal fusions to *minD* were non-functional. Fluorescence microscopy analysis showed that most of the MinD-mCherry containing cells had just a low cytosolic fluorescence but no distinct foci. But very few cells appeared to be different. They showed bright foci in the mCherry channel, which did not only strongly resemble the pattern made by the fluorescent injectisomes, but even appeared to be almost completely congruent.

Unfortunately this localization variance could be due to a loss of membrane potential in the few cells showing the spotted pattern. It has been shown, that a loss of membrane potential can mislocalize numerous cytoskeletal proteins, such as MreB, MreC and MinD (Strahl & Hamoen, 2010). Thus we cannot be sure if the colocalization of the two tagged proteins is not an artefact. It might be possible that as soon as the membrane potential gets lost, MinD, which in *E. coli* has been seen to oscillate from pole to pole (Hu & Lutkenhaus, 1999), losses its dynamic and builds artificial clusters at the injectisomes. It is thinkable that the discrepancies in literature, concerning the cellular distribution of some cytoskeletal elements, are due to artefacts in some studies. Depending on how bacteria are fixed on the microscopy slide the membrane potential could dissipate and protein localization could be disrupted. In all our experiments we have immobilized the bacteria on buffered agarose patches, which should be a very gentle method, keeping the cells as healthy as possible. Also, YscQ, the protein we are using for the read out of the injectisome arrangement, is a soluble cytosolic protein, which needs an assembled basal body to form complexes. Furthermore we now that our experimental setup does not dissociate the EGFP-YscQ from the rest of the injectisome as it can be colocalized with the outer membrane protein YscC and the needle protein YscF (Diepold et al, 2010). It is very unlikely that entire injectisomes, which are spanning both bacterial membranes and cross the rigid peptidoglycan, move upon loss of membrane potential, caused by bacteria handling, thus we believe the injectisome arrangement is no artefact.

As evidence for lipid rafts in bacteria emerged during the last few years, we were hypothesizing an influence of the lipid composition in the arrangement of the injectisomes. Not unexpectedly inner membrane staining on Gram-negative bacteria proved to be difficult. Thus we decided to indirectly stain lipid patches with a Flotillin like protein. Therefore we fused YE3058, a supposable member of the Flotillin family, to mCherry. But no colocalization between YE3058 and the injectisomes was seen. It is possible that the lipid rafts are too rigid to allow the injectisomes to form inside.

We still do not know what is causing the arrangement, but we are convinced that the arrangement is not random. More time should be invested in unravelling how this multiprotein complex can pass the peptidoglycan. However, so far the grounds seem not to be solid enough. More knowledge on the bacterial cytoskeleton and peptidoglycan assembly is clearly needed.

7 Materials and Methods

7.1 Bacterial Cultures

Y. enterocolitica strains were routinely grown shaking at room temperature in Brain Heart Infusion (BHI). *E. coli* strains for cloning were routinely grown shaking at 37°C in lysogeny broth (LB). When appropriate the media was supplemented with antibiotics; 35 µg/ml nalidixic acid (nal), 200 µg/ml ampicillin (amp), 50 µg/ml streptomycin (sm) or 50 µg/ml kanamycin (kan). The media for attenuated *Y. enterocolitica asd* mutants was always supplemented with 100 µg/ml mDAP.

7.2 Plasmid Construction

PCR products were amplified from purified pYV40 or genomic DNA using Phusion polymerase (New England BioLabs; NEB). The oligonucleotides used are listed in the table in chapter 7.8. To generate hybrid constructs or deletions, two PCR fragments were joined using overlapping PCR. Resulting inserts and plasmid vectors were digested using restrictions enzymes from NEB (see table in 7.8), ligated, transformed into *E. coli* strains by electroporation and selected on LB agar (LA) plates with the corresponding antibiotics. Constructs for expression in *Y. enterocolitica* were inserted into pBAD/myc-HisA (Invitrogen). A stop codon was inserted to prevent gene fusion to the myc-His tag. The resulting plasmids were maintained in *E. coli* Top10. Constructs for genome or pYV mutations were inserted into pKNG101 (Kaniga et al, 1991). The resulting mutator plasmids were maintained in *E. coli* BW19610 (Metcalf et al, 1994). All constructs were verified by sequencing (Microsynth AG).

7.3 *Y. enterocolitica* Mutant Generation

Mutant strains were generated by two-step allelic exchange (Kaniga et al, 1991). The *Y. enterocolitica* parent was mated on a plate with *E. coli* Sm10 λ *pir*$^{+}$ containing the corresponding mutator plasmid. To select for integration of the mutator plasmid the conjugation mix was plated on plates containing nal and sm. In a second step the streptomycin selection pressure was released during several generation times allowing the excision of the mutator plasmid. Plating on LA containing 5 % sucrose allowed selection for colonies that underwent the second recombination step and had lost the mutator plasmid. These colonies were screened for the mutant allele by colony PCR. Some mutants were made by introducing the entire plasmid into the genome (see plasmid table). To avoid wild type revertants by excision of the plasmid, constant streptomycin selection was applied.

7.4 Induction of the Ysc T3SS

Overnight pre cultures were grown as described above. Day cultures were started at an OD_{600}=0.1 in BHI either with additional 5 mM $CaCl_2$ (secretion non-permissive condition) or with 20 mM sodium-oxalate to deplete Ca^{2+} (BHI-ox; secretion permissive condition). Both kinds of media were supplemented with 20 mM $MgCl_2$ and 4 mg/ml glycerol as additional carbon source and appropriate antibiotics. After two hours of growth at RT the cultures were shifted to 37°C water baths for induction of the T3SS. If mutant strains were complemented with pBAD derived plasmids the plasmid expression was induce on time of the temperature shift with 0.2 % arabinose (unless stated differently). When mentioned A22 was used at a concentration of 10µg/ml.

7.5 Secretion/Induction Analysis

After 4 h of induction of the T3SS protein expression and secretion were analyzed. Therefore 1.5 ml culture were centrifuged in a tabletop centrifuge for 15 min at 20 000 g and 4°C. The supernatant (SN) and the total cell (TC) pellet were separated. Proteins in the SN were precipitated with 10 % (w/v) trichloroacetic acid for 1 h on ice. The precipitated proteins were centrifuged 15 min at 20 000 g and 4°C, then the pellet was washed with 1 ml of acetone followed by an additional centrifugation step and air-dried. For SDS-PAGE of TC samples 1 x 10^8 bacteria (=0.2 ODunits) were loaded. For SN samples, secreted proteins from 3 x 10^8 bacteria (=0.6 ODunits) were loaded.

7.6 Fluorescence Microscopy

Unless stated differently bacteria were used after 3 h of induction of the T3SS. Microscopy slides were layered with a patch of 2 % agarose solved in PBS. 2 µl of bacteria culture were pipetted on the agarose patch and covered with a cover slide. For Nile Red staining 100 µm of CCCP (Carbonyl cyanide 3-chlorophenylhydrazone) and 1µg/ml Nile Red were added to the culture just before the culture was pipetted on the agarose patch. Images were acquired with a DeltaVision Core (Applied Precision, USA)/Olympus IX71 microscope equipped with an UPlanSApo 100x/1.40 oil objective (Olympus, Japan) and a coolSNAP HQ-2 CCD camera (Photometrics, USA). For each set of images, DIC, mCherry and GFP channels were acquired as a Z-stack, containing 20 frames with a spacing of 150 nm. The stacks were deconvolved using softWoRx v3.3.6 (Applied Prescision, USA) with standard settings. Images were further processed with ImageJ software; all changes were applied to the entire stack of a channel.

7.7 Plasmid List

Plasmid Name	Relevant Features	Comments	Reference
pACYC184	p15A origin, *tet* (Tc^R), *cat* (Cm^R)		(Chang & Cohen, 1978)
pAD118	pKNG101 mutator *egfp-yscQ*	Contains *egfp* and two ca. 250 bp homologues regions flanking the start of *yscQ*	(Diepold et al, 2010)
pBAD/ mycHisA	amp^R, P_{BAD}, pBR322 origin		Invitrogen
pEGFP-C1	egfp	Used as template for *egfp*.	BD Biosciences Clontech
pKNG101	oriR6K, mobRK2, strAB, sacB		(Kaniga et al, 1991)
pLJM31	pKNG101 mutator *ΔyadA*	Contains a region homologues to the middle of *yadA*. Disrupts the *yadA* gene by inserting the entire plasmid.	(Mota et al, 2005)
pMA6	pBAD::*yscC*	Encodes for full-length YscC	this work
pMA8	pBAD::yscC-mCherry	Encodes for full-length YscC with a C-terminally fused mCherry. A linker sequence between the two genes encodes for Gly-Gly-Ala-Gly-Gly-Ala-Gly-Gly (GGAGGAGG)	(Diepold et al, 2010)
pMA11	pBAD::*yscD*	Encodes for full-length YscD	
pMA12	pKNG101 mutator *yscC-mCherry*	Contains *mCherry* and two ca. 250 bp homologues regions flanking the stop codon of *yscC*. To keep the ribosome binding site (RBS) of *yscD* the last 10 codons of *yscC* are repeated after *mCherry*.	(Diepold et al, 2010)

pMA25	pBAD::yscC-his	Contains full-length *yscC* with a C-terminally tag of 6 histidines. (same GGAGGAGG linker as for pMA8)	this work
pMA26	pKNG101 mutator *ΔyscC*	Contains ca. 250 bp homologues regions flanking *yscC*. This will leave just the ATG of *yscC* plus the last 10 codons to keep the RBS of *yscD*.	(Diepold et al, 2010)
pMA27	pKNG101 mutator *ΔyscC* in *flag-yscD*	Like pMA26 with an additional sequence encoding for a FLAG-tag at the N-terminus of YscD	(Diepold et al, 2010)
pMA28	pKNG101 mutator *ΔyscC* in *egfp-yscD*	Like pMA27 but with the *egfp* sequences instead of the *flag-tag*	(Diepold et al, 2010)
pMA44	pBAD::*envB*	Encodes for full-length EnvB	this work
pMA45	pBAD::envB$_{1-228}$-mCherry-envB$_{229-end}$ (envB-mCherry$_{sw}$)	Encodes for full-length EnvB with mCherry placed between amino acid (aa) 228 and aa 229.	this work
pMA51	pBAD::mCherry-mreC	Encodes for full-length MreC with an N-terminally fused mCherry.	this work
pMA52	pKNG101 mutator *mCherry-secE*	Contains the *mCherry* sequence and two ca. 250 bp homologues regions flanking the start of *secE*	this work
pMA53	pBAD::mCherry-secE	Encodes for full-length SecE with an N-terminally fused mCherry	this work
pMA54	pKNG101 mutator *mreC-mCherry* (with *yopE* promoter)	Contains *mCherry* and two homologues regions flanking the start of *mreC*. In addition the *yopE* promoter to drive the expression of the *mreC* downstream region, after the first homologues recombination.	this work

pMA55	pBAD::mreC-mCherry	Encodes for full-length MreC with an N-terminally fused mCherry	this work
pMA56	pKNG101 mutator envB$_{1-228}$-mCherry-envB$_{229-end}$ (envB-mCherry$_{sw}$) (with yopE promoter)	Contains *mCherry* and two homologues regions flanking codon 228/229 of *envB*. In addition the *yopE* promoter to drive the expression of the *envB* downstream region, after the first homologues recombination.	this work
pMA72	pKNG101 mutator *ΔflgJ*	Contains the flanking regions of *flgJ*. Deletes the entire ORF of *flgJ*	this work
pMA73	pACYC184:: *yscW*	The sequence of full-length *yscW* including ist RBS was cloned into the tetracycline resistance of pACYC184.	this work
pMA76	pBAD::yenI$_{1-663}$	Encodes for the methyltransferase part of YenI (codons 1-663).	this work
pMA77	pKNG101 mutator *ΔmtgA*	Contains the *aphA-3* cassette and the two flanking regions of *mtgA*.	this work
pMA78	pKNG101 mutator *Δslt*	Contains the *aphA-3* cassette and the two flanking regions of *slt*.	this work
pMA79	pKNG101 mutator *mltA-mCherry*	Contains the last ca. 250 bp of *mltA* followed by *mCherry*. This vector will insert itself just after *mltA* fusing *mCherry* to *mltA*.	this work
pMA80	pKNG101 mutator *mltB-mCherry*	Contains the last ca. 250 bp of *mltB* followed by *mCherry*. This vector will insert itself just after *mltB* fusing *mCherry* to *mltB*.	this work
pMA81	pKNG101 mutator *mltC-mCherry*	Contains the last ca. 250 bp of *mltC* followed by *mCherry*. This vector will insert itself just after *mltC* fusing *mCherry* to *mltC*.	this work

pMA82	pKNG101 mutator *mltD-mCherry*	Contains the last ca. 250 bp of *mltD* followed by *mCherry*. This vector will insert itself just after *mltD* fusing *mCherry* to *mltD*.	this work
pMA83	pKNG101 mutator *mltF-mCherry*	Contains the last ca. 250 bp of *mltF* followed by *mCherry*. This vector will insert itself just after *mltF* fusing *mCherry* to *mltF*.	this work
pMA84	pKNG101 mutator *YE1901-mCherry*	Contains the last ca. 250 bp of *YE1901* followed by mCherry. This vector will insert itself just after *YE1901* fusing mCherry to *YE1901*.	this work
pMA85	pKNG101 mutator *YE3411-mCherry*	Contains the last ca. 250 bp of *YE3411* followed by *mCherry*. This vector will insert itself just after *YE3411* fusing *mCherry* to *YE3411*.	this work
pMA86	pKNG101 mutator mrdA(pbp2)-mCherry	Contains the last ca. 250 bp of *mrdA* followed by *mCherry*. This vector will insert itself just after *mrdA* fusing *mCherry* to *mrdA*.	this work
pMA87	pKNG101 mutator *ΔminD*	Contains the two flanking regions of *minD*. Deletes the entire ORF of *minD*.	this work
pMA91	pKNG101 mutator *Δyen*I	Contains the two flanking regions of the restriction enzyme part of *yen*I. Deletes *yen*I from codon 663 to the stop codon.	this work
pMA91B	pKNG101 mutator *Δyen*I (without *Pst*I restriction sites)	pMA91 was digested with *Pst*I, the overhangs were filled in and the two larger fragments were ligated giving a mutator without a *Pst*I restriction site.	this work
pMA92	pKNG101 mutator *mCherry-minD*	Contains *mCherry* and the two flanking regions of the start of *minD*.	this work

pMA93	pKNG101 mutator *minD-mCherry*	Contains *mCherry* and the two flanking regions of the stop of *minD*.	this work
pMA100	pBAD::minD-mCherry	Encodes for full-length MinD with a C-terminally fused mCherry.	this work
pMA104	pKNG101 mutator *YE3058-mCherry*	Contains *mCherry* and two ca. 250 bp homologues regions flanking the stop of *YE3058.*	this work
pMA109	pKNG101 mutator *ΔYE3411*	Contains the two flanking regions of *YE3411*. Deletes the entire orf of *YE3411*.	this work
pMK3	pKNG101 mutator $asd_{\Delta 292\text{-}610}$	Deletes the aspartate-β-semialdehyde dehydrogenase (*asd*), making the strain dependant of mDAP for growth.	this work
pRVCHYN-5	*mCherry*	Used as template for *mCherry*.	(Thanbichler et al, 2007)
pUC18k	*aphA-3*	Just as template for *aphA-3*	(Ménard et al, 1993)

7.8 Oligonucleotide List

No.	Sequence	Feature	Used for	Template
3430	ATGCCATAGCATTTTTATCC		sequencing of pBAD constructs	pBAD/ mycHisA
3541	GATCGTCGACATGGTCGGCTCAGTA	*Sal*I restriction site	cloning of pMK3	gDNA E40
3542	GATCTCTAGATTCGCAGCATACGGC	*Xba*I restriction site	cloning of pMK3	gDNA E40

3543	CAGTGAATTCCGGCGTCAATCCAATA	*EcoR*I restriction site	cloning of pMK3	gDNA E40
3544	GACTGAATTCGTGACTGCGGCCACT	*EcoR*I restriction site	cloning of pMK3	gDNA E40
4760	TATTAATTGATCTGCATCAACTTAACG		sequencing of pKNG101 constructs	pKNG101
4761	GACTATACTAGTATACTCCGTCTACTGTACG		sequencing of pKNG101 constructs	pKNG101
4918	GCGTTCTGATTTAATCTGTATCAGG		sequencing of pBAD constucts	pBAD/ mycHisA
5013	GACTCCATGGCTTTTCCGCTACATTCTTTTTTC	*Nco*I restriction site	cloning of pMA6, pMA8 and pMA25	pYV40
5014	CTGAATTCACAATACGCCACGCTTAGGTGC	*EcoR*I restriction site	cloning of pMA6	pYV40
5016	CACGTCTCGAGTACCTCCGGCACCGCCTGCGCCACCCAATACGCCACGCTTAGGTGCTG	GGAGGAGG linker, *Xho*I restriction site	cloning of pMA8 and pMA12	pYV40
5017	TAAGATCTCGAGCTCCGGAGAATTCG	*Xho*I restriction site	cloning of pMA8 and pMA12	pRVCHYN-5
5018	GCATGGTACCTTACTTGTACAGCTCGTCCATGCC	*Kpn*I restriction site	cloning of pMA8, pMA55 and pMA100	pRVCHYN-5
5019	GAGGTAGCGTCTCGTCTCATTCG		sequencing of YscC	pYV40
5020	GAATACCGCAGGCCGCAAC		sequencing of YscC	pYV40

5021	GTTAACACAAGAAAATGCCCAAGC		sequencing of YscC	pYV40
5022	GTACGGCTATTTATCATCGAACCACG		sequencing of YscC	pYV40
5023	GCACCTAAGCGTGGCGTATTG		sequencing of YscC	pYV40
5024	CCATGGTCTTCTTCTGCATTACG		sequencing of mCherry	pRVCHYN-5
5025	CACCCTTGGTCACCTTCAGCTTG		sequencing of mCherry	pRVCHYN-5
5066	AGTCGTCGACCTTGAATAAGTTATTAGGTGGCTCC	*Sal*I restriction site	cloning of pMA12	pYV40
5068	AGACTCTAGAATACCTTCTTCATCGACCATCAGC	*Xba*I restriction site	cloning of pMA12, pMA26, pMA27 and pMA28	pYV40
5084	ACTGCAACATGTCTTGGGTCTGTCGTTTTTATCAAGG	*Pci*I restriction site	cloning of pMA11	pYV40
5085	ATCGAAGCTTCATCGAGGTTTACCTCCATTGAGC	*Hind*III restriction site	cloning of pMA11	pYV40
5086	CACGCAGAGAAAAGAGCCAACC		sequencing of pMA11	pYV40
5087	CCACGCTTAGGTGCTGAAACCTTGTACAGCTCGTCCATGCC		cloning of pMA12	pRVCHYN-5
5088	GGCATGGACGAGCTGTACAAGGTTTCAGCACCTAAGCGTGGCGTATTGTGAGTTGG		cloning of pMA12	pYV40

5234	GACTGAATTCAATGATGATGATGAT GATGACCTCCGGCACCGCCTGCGC CACCCAATACGCCACGCTTAGGTGC TG	*EcoR*I restriction site, His-tag	cloning of pMA25	pYV40
5235	GCATGTCGACTGGGCTAAACGTTAT CCTCAAACTTTAG	*Sal*I restriction site	cloning of pMA26, pMA27 and pMA28	pYV40
5236	CCACGCTTAGGTGCTGAAACCATAT TACTTAATTCCACCCCACGC		cloning of pMA26, pMA27 and pMA28	pYV40
5237	GCGTGGGGTGGAATTAAGTAATATG GTTTCAGCACCTAAGCGTGG		cloning of pMA26, pMA27 and pMA28	pYV40
5924	CCTCGCCCTTGCTCACCATGCTCGA GCCAGAACCAGGATAAGCAGAACC GATGC		cloning of pMA45	gDNA E40
5926	CGAACTTCAATTTCCAGAACTTCATC GCCCGGCGCGCCAGACTTGTACAG CTCGTCCATGC		cloning of pMA45	pRVCHY N-5
5927	GCATGGACGAGCTGTACAAGTCTGG CGCGCCGGGCGATGAAGTTCTGGA AATTGAAGTTCG		cloning of pMA45	gDNA E40
5932	GATCACATGTTTAAGAAATTTCGTGG CATGTTTTC	*Pci*I restriction site	cloning of pMA44, pMA45 and pMA56	gDNA E40
5933	CATGGAATTCTATTCTTCGCTGAACA AATCG	*EcoR*I restriction site	cloning of pMA44 and pMA45	gDNA E40
5938	GGTTCTGCTTATCCTGGTTCTGGCT CGAGCATGGTGAGCAAGGGCGAGG		cloning of pMA45	pRVCHY N-5

5972	CCGGCTAAAAATCGGCTTCATTCCACCTGCACCTCCCTTGTACAGCTCGTCCATGCC	GGAGG-linker	cloning of pMA51	pRVCHYN-5
5973	GGCATGGACGAGCTGTACAAGGGAGGTGCAGGTGGAATGAAGCCGATTTTTAGCCGG	GGAGG-linker	cloning of pMA51	gDNA E40
5975	CATGTCATGATCGTGAGCAAGGGCGAGGAGG	*BspH*I restriction site	cloning of pMA51 and pMA53	pRVCHYN-5
5976	CATGGAATTCATGGTGAGACTCCCGGAGC	*EcoR*I restriction site	cloning of pMA51	gDNA E40
5977	GATCGTCGACCGTTGAGATGGTGATGCCAGG	*Sal*I restriction site	cloning of pMA52	gDNA E40
5978	CCTCGCCCTTGCTCACCATAAACCAACCTGTCACTATGATTCAGAAC		cloning of pMA52	gDNA E40
5979	GTTCTGAATCATAGTGACAGGTTGGTTTATGGTGAGCAAGGGCGAGG		cloning of pMA52	pRVCHYN-5
5980	GAGCCTCGGTATTCGCACTCATTCCACCTGCACCTCCCTTGTACAGCTCGTCCATGCC	GGAGG-linker	cloning of pMA52 and pMA53	pRVCHYN-5
5981	GGCATGGACGAGCTGTACAAGGGAGGTGCAGGTGGAATGAGTGCGAATACCGAGGCTC	GGAGG-linker	cloning of pMA52 and pMA53	gDNA E40
5982	CGATATGGGCCCTTAGAACCTCAGGCCAGTAATAAATGATAC	*Apa*I restriction site	cloning of pMA52	gDNA E40
5983	CATGGAATTCTTAGAACCTCAGGCCAGTAATAAATGATAC	*EcoR*I restriction site	cloning of pMA53	gDNA E40
6120	CATGGTCGACATAACAACAAAAACAGCAGCGG	*Sal*I restriction site	cloning of pMA54 and pMA56	pYV40

6121	TGGTTCATGACTATTTATTCCCTTGG CTATTAAAAC	*BspH*I restriction site	cloning of pMA54 and pMA56	pYV40
6122	CATGTCATGAACCAGCGAGCCTATA CTGTGATTCAAGC	*BspH*I restriction site	cloning of pMA54	gDNA E40
6123	CCTCGCCCTTGCTCACCATTCCACC TGCACCTCCTGGTGAGACTCCCGGA GCAG	GGAGG-linker	cloning of pMA54 and pMA55	gDNA E40
6124	CTGCTCCGGGAGTCTCACCAGGAG GTGCAGGTGGAATGGTGAGCAAGG GCGAGG	GGAGG-linker	cloning of pMA54 and pMA55	pRVCHY N-5
6125	GGTGAGACTCCCGGAGCAGTTTACT TGTACAGCTCGTCCATGC		cloning of pMA54	pRVCHY N-5
6126	GCATGGACGAGCTGTACAAGTAAAC TGCTCCGGGAGTCTCACC		cloning of pMA54	gDNA E40
6127	CATGTCTAGACCGCACCCCGAGAGT GG	*Xba*I restriction site	cloning of pMA54	gDNA E40
6128	CATGTCATGAAGCCGATTTTTAGCC GGGGT	*BspH*I restriction site	cloning of pMA55	gDNA E40
6162	GATCTCTAGACCAGCTCCAACTGTT GGTGG	*Xba*I restriction site	cloning of pMA56	gDNA E40
6172	CATGGTCGACCCAATATCAGATGCG CTTAATGG	*Sal*I restriction site	cloning of pMA79	gDNA 8081
6173	CATACCTCCGGCACCGCCTGCGCC ACCCTGGCCTTGATTCCTGACTAAT AGTG		cloning of pMA79	gDNA 8081
6174	GGTGGCGCAGGCGGTGCCGGAGGT ATGGTGAGCAAGGGCGAGG	GGAGGAGG-linker	cloning of pMA79 - pMA86, pMA93 and pMA100	pRVCHY N-5

6175	TTACTTGTACAGCTCGTCCATGCC		cloning of pMA93	pRVCHYN-5
6178	CATGGTCGACCCGAATCTCGATAATGGCTTTAAGAC	*Sal*I restriction site	cloning of pMA80	gDNA 8081
6179	CATACCTCCGGCACCGCCTGCGCCACCACTCCGACGCGCCCGGCC		cloning of pMA80	gDNA 8081
6182	CATGGTCGACGCAAAATACCTATTTAGGCGGTATTC	*Sal*I restriction site	cloning of pMA81	gDNA 8081
6183	CATACCTCCGGCACCGCCTGCGCCACCGTGGCGGCGGTAGCTCTTC		cloning of pMA81	gDNA 8081
6186	CATGGTCGACAACAACTTAAGTACCAAGAGTACCTTAAAAGTTG	*Sal*I restriction site	cloning of pMA82	gDNA 8081
6187	CATACCTCCGGCACCGCCTGCGCCACCTGCGTCCGGGGTTGATTTG		cloning of pMA82	gDNA 8081
6190	CATGGTCGACGGCAATCCGGACAGTTGGG	*Sal*I restriction site	cloning of pMA83	gDNA 8081
6191	CATACCTCCGGCACCGCCTGCGCCACCATTATTGATTGACCAGCCGGGAC		cloning of pMA83	gDNA 8081
6194	CATGGTCGACATCAATATTTTGCAAAATCAGCAGTTAG	*Sal*I restriction site	cloning of pMA84	gDNA 8081
6195	CATACCTCCGGCACCGCCTGCGCCACCCTCTGACATCGCCCGGTAAG		cloning of pMA84	gDNA 8081
6198	CATGGTCGACACCCAGCATGAACCTGAATTAAAAAG	*Sal*I restriction site	cloning of pMA85	gDNA 8081
6199	CATACCTCCGGCACCGCCTGCGCCACCATGAGCCGCTTTTTTTTGCG		cloning of pMA85	gDNA 8081

6202	CATGGTCGACGGTACCGCGCAGGT TTATAGC	*Sal*I restriction site	cloning of pMA86	gDNA 8081
6203	CATACCTCCGGCACCGCCTGCGCC ACCGTCTGCTTCAACGCCCGGAG		cloning of pMA86	gDNA 8081
6235	CATGGTCGACTTTCGGTGGTGGTCA GACTG	*Sal*I restriction site	cloning of pMA72	gDNA 8081
6236	GCCCAATCCCAAAATAACCCATAGA TAATTTCCAATTTAGCCCGTAAG		cloning of pMA72	gDNA 8081
6237	CTTACGGGCTAAATTGGAAATTATCT ATGGGTTATTTTGGGATTGGGC		cloning of pMA72	gDNA 8081
6238	CATGTCTAGAAACCTAAGCCCCCGC ACAG	*Xba*I restriction site	cloning of pMA72	gDNA 8081
6267	CATGTCTAGATTACTTGTACAGCTC GTCCATGCC	*Xba*I restriction site	cloning of pMA79 - pMA86	pRVCHY N-5
6336	CATGTCATGAAGGGGAGACTGGCAT GAGTCG	*BspH*I restriction site	cloning of pMA73	pYV40
6337	CATGGTCGACCTATCTGGTATTAGG TGACTGGCAATTTG	*Sal*I restriction site	cloning of pMA73	pYV40
6403	CATGCCATGGGATTAGAAGAAGTTG ATGAAATC	*Nco*I restriction site	cloning of pMA76	gDNA 8081
6404	CATGGAATTCTTACATTTCACGCTTC ATGGC	*EcoR*I restriction site	cloning of pMA76	gDNA 8081
6405	GTAATGGCCCATATTACTTAC		sequencing of pMA76	gDNA 8081
6406	TGACTAACTAGGAGGAATAAATG		cloning of pMA77 and pMA78	pUC18k
6407	CATTATTCCCTCCAGGTACTA		cloning of pMA77 and pMA78	pUC18k

6408	CATGGTCGACTGACCATTGGTAACG ATCC	*Sal*I restriction site	cloning of pMA77	gDNA 8081
6409	CATTTATTCCTCCTAGTTAGTCATCG GTTAAATCCAGCACC		cloning of pMA77	gDNA 8081
6411	CATGTCTAGATGGCGAAGTGTTCCT TTTG	*Xba*I restriction site	cloning of pMA77	gDNA 8081
6412	CATGGTCGACGAAATATTTAGTCGT AATTATTGG	*Sal*I restriction site	cloning of pMA78	gDNA 8081
6413	CATTTATTCCTCCTAGTTAGTCAACT TACTGTTTCCTCACTGG		cloning of pMA78	gDNA 8081
6415	CATGTCTAGATAACTAGTACAGCAG TTTACC	*Xba*I restriction site	cloning of pMA78	gDNA 8081
6416	CATGGTCGACATTGCCGACGGCAAT ATTC	*Sal*I restriction site	cloning of pMA87 and pMA92	gDNA E40 / gDNA 8081
6417	AAAGTCTAACAAAGCCATGGTGAAA TGGATTCCTTGTCAAAAG		cloning of pMA87	gDNA E40
6418	CTTTTGACAAGGAATCCATTTCACCA TGGCTTTGTTAGACTTT		cloning of pMA87	gDNA E40
6419	CATGTCTAGACCGGTAATGTCACGT TAAG	*Xba*I restriction site	cloning of pMA87	gDNA E40
6427	GTTATCCATCAGAATGATTAATTTTA CATTTCACGCTTCATGGC		cloning of pMA91	gDNA 8081
6428	GCCATGAAGCGTGAAATGTAAAATT AATCATTCTGATGGATAAC		cloning of pMA91	gDNA 8081
6469	TAGTACCTGGAGGGAATAATGTGGT TTGATGTTTGGGATAGC		cloning of pMA77	gDNA 8081

6470	TAGTACCTGGAGGGAATAATGTCCC CTTTGTACTTGAAGC		cloning of pMA78	gDNA 8081
6482	CATGGTCGACGTGTTACTCCAATTA TGGATTG	*Sal*I restriction site	cloning of pMA91	gDNA 8081
6483	CATGTCTAGAGCGGTGTGGTTATTA ATAATATC	*Xba*I restriction site	cloning of pMA91	gDNA 8081
6484	CCTCGCCCTTGCTCACCATGAAATG GATTCCTTGTCAAAAG		cloning of pMA92	gDNA 8081
6485	ATGGTGAGCAAGGGCGAGG		cloning of pMA92 and pMA104	pRVCHY N-5
6486	ACCTCCGGCACCGCCTGCGCCACC CTTGTACAGCTCGTCCATGCC	GGAGGAGG-linker	cloning of pMA92	pRVCHY N-5
6487	GGTGGCGCAGGCGGTGCCGGAGGT ATGGCACGCATTATTGTTGTTAC	GGAGGAGG-linker	cloning of pMA92	gDNA 8081
6488	CGATATGGGCCCGAATATACAAATT ATCCGTGCG	*Xba*I restriction site	cloning of pMA92	gDNA 8081
6675	CATGGTCGACGTTAATCGCGGCGAT ATGC	*Sal*I restriction site	cloning of pMA93	gDNA 8081
6676	CATACCTCCGGCACCGCCTGCGCC ACCTCCCCCAAAAAGGCGTTTC		cloning of pMA93 and pMA100	gDNA 8081
6677	GGCATGGACGAGCTGTACAAGTAAG GGATAAACCATGGCTTTG		cloning of pMA93	gDNA 8081
6678	CATGTCTAGACGGTAATGTCACGTT AAGTTC	*Xba*I restriction site	cloning of pMA93	gDNA 8081
6771	CATGTCATGAGTGCACGCATTATTG TTGTTACATC	*BspH*I restriction site	cloning of pMA100	gDNA 8081
6883	CATGGTCGACCGTCAGTCTGCATTC TTGC	*Sal*I restriction site	cloning of pMA104	gDNA 8081

6884	CCTCGCCCTTGCTCACCATTTTACC CCGGCTGTTTTTAC		cloning of pMA104	gDNA 8081
6885	CATGGACGAGCTGTACAAGGGTAAA TAACCATGCTGGAG		cloning of pMA104	gDNA 8081
6886	CATGTCTAGAATTCAACATCGCGGG TTGC	*Xba*I restriction site	cloning of pMA104	gDNA 8081
6887	CTTGTACAGCTCGTCCATG		cloning of pMA104	pRVCHY N-5
6949	CATGGTCGACCGTATTTTTACATCAC GATATAAATT	*Sal*I restriction site	cloning of pMA109	gDNA 8081
6950	GCAGTCTGAGCGGCTCAACTGCAAA TAAGCCTCTCAC		cloning of pMA109	gDNA 8081
6951	GTGAGAGGCTTATTTGCAGTTGAGC CGCTCAGACTGC		cloning of pMA109	gDNA 8081
6952	CATGTCTAGAAGTGCAAATGCAGTG CCTG	*Xba*I restriction site	cloning of pMA109	gDNA 8081

7.9 Y. enterocolitica Strain List

Name	Relevant Genotype	Mutator Plasmid	Parental Strain	Reference
E40	wilde type			(Sory et al, 1995)
MRS40	*Δbla*		E40	(Sarker et al, 1998)
8081	wilde type			(Portnoy et al, 1981)
IML421	*yopH*$_{1-352}$, *yopO*$_{65-55}$, *yopP*$_{238}$, *yopE*$_{21}$, *yopM*$_{23}$, *yopT*$_{135}$ *(ΔyopHOPEMT)*		MRS40	(Iriarte & Cornelis, 1998)
IML421asd	ΔyopHOPEMT/Δasd (biosafety level 1 strain)	pMK3	IML421	this work
ISOA4015	*ΔyscQ*		MRS40	(Diepold et al, 2010)
AD4016	*egfp-yscQ*		MRS40	(Diepold et al, 2010)
AD4020	*egfp-yscQ/ΔyscF*		ISO4006	(Diepold et al, 2010)
AD4085	*egfp-yscQ/ΔyopHOPEMT/Δasd*		IML421	(Diepold et al, 2010)
MA4005	*yscC-mCherry*	pMA12	MRS40	(Diepold et al, 2010)
MAAD4006	*yscC-mCherry/egfp-yscQ*	pMA12	AD4016	(Diepold et al, 2010)
MA4007	*yscC-mCherry/ΔyscQ*	pMA12	ISOA4015	{Diepold

MAAD4016	yscC-mCherry/egfp-yscQ/ΔyscF	pMA12	AD4020	(Diepold et al, 2010)
MAAD4018	*ΔyscC/egfp-yscD*	pMA28	MRS40	(Diepold et al, 2010)
MAAD4019	*yscC-mCherry/egfp-yscQ/ ΔyopHOPEMT/Δasd*	pMA12	AD4085	this work
MAAD4028	*yscC-mCherry/egfp-yscQ/ ΔyopHOPEMT/Δasd/ΔyadA*	pLJM31	MAAD4019	this work
MA4030	*egfp-yscQ/mreC-mCherry*	pMA54	AD4016	this work
MA4031	*egfp-yscQ/envB-mCherry*$_{sw}$	pMA56	AD4016	this work
MA4039	*egfp-yscQ/ΔyopHOPEMT/ Δasd/ΔminD*	pMA87	AD4085	this work
MA8040	mutant *yenI*	pMA91B	8081	this work
MA8041	*yscC-mCherry*	pMA12	MA8040	this work
MA8042	*egfp-yscQ*	pAD118	MA8040	this work
MA8043	*egfp-yscQ/ΔflgJ*	pMA72	MA8042	this work
MA8044	*egfp-yscQ/mltA-mCherry*	pMA79	MA8042	this work
MA8045	*egfp-yscQ/mltB-mCherry*	pMA80	MA8042	this work
MA8046	*egfp-yscQ/mltC-mCherry*	pMA81	MA8042	this work
MA8047	*egfp-yscQ/mltD-mCherry*	pMA82	MA8042	this work
MA8048	*egfp-yscQ/mltF-mCherry*	pMA83	MA8042	this work
MA8049	*egfp-yscQ/YE1901-mCherry*	pMA84	MA8042	this work
MA8050	*egfp-yscQ/YE3411-mCherry*	pMA85	MA8042	this work
MA8051	*egfp-yscQ/mrdA(pbp2)-mCherry*	pMA86	MA8042	this work

MA8052	*egfp-yscQ/mCherry-minD*	pMA92	MA8042	this work
MA4053	*ΔyopHOPEMT/Δasd/ΔminD*	pMA87	IML421asd	this work
MA4055	*egfp-yscQ/ΔyopHOPEMT/Δasd/ ΔminD/ΔyadA*	pLJM31	MA4039	this work
MA4056	*ΔyopHOPEMT/Δasd/ΔminD/ΔyadA*	pLJM31	MA4053	this work
MA8057	*egfp-yscQ/mtgA::apha3*	pMA77	MA8042	this work
MA8058	*egfp-yscQ/slt::apha3*	pMA78	MA8042	this work
MA8059	*egfp-yscQ/minD-mCherry*	pMA93	MA8042	this work
MA8068	*flotillin-mCherry/egfp-yscQ*	pMA104	MA8042	this work
MA8073	*egfp-yscQ/ΔYE3411*	pMA109	MA8042	this work

8 Abbreviations

A22	S-(3,4-dichlorobenzyl)isothiourea
amp	Ampicillin
asd	aspartate semi-aldehyde dehydrogenase
B. subtilis	*Bacillus subtilis*
BHI	Brain heart infusion
BHI-ox	Brain heart infusion with sodium oxalate
DIC	Differential interference contrast
EGFP	Enhanced green fluorescent protein
EHEC	Enterohemorrhagic *E. coli*
EPEC	Enteropathogenic *E. coli*
GalNac	N-acetylglucosamine
gDNA	genomic DNA
GFP	Green fluorescent protein
kan	Kanamycin
LB	Lysogeny broth
LT	lytic transglycosylase
mCherry	Monomeric red fluorescent protein
mDAP	meso Diaminopimelic acid
mlt	Membrane bound lytic transglycosylase
MurNac	N-acetylmuramic acid
nal	Nalidixic acid
OD_{600}	Optical density at 600nm
orf	Open reading frame
PBP	Penicillin binding protein
PBS	Phosphate buffered saline
RT	Room temperature
S. aureus	*Staphylococcus aureus*
S. flexneri	*Shigella flexneri*
S. enterica	*Salmonella enterica* serovar *thyphimurium*
slt	Soluble lytic transgycosylase
sm	Streptomycin
SN	Supernatant
T3SS	Type three secretion system
T4P	Type 4 pili

T4SS	Type 4 secretion system
TC	Total cell
tet	Tetracycline
Y. enterocolitica	*Yersinia enterocolitica*
yop	*Yersinia* outer protein

9 References

1. Adler HI, Fisher WD, Cohen A, Hardigree AA (1967) MINIATURE *escherichia coli* CELLS DEFICIENT IN DNA. *Proc Natl Acad Sci USA* **57**(2)**:** 321-326
2. Aizawa SI (1996) Flagellar assembly in *Salmonella typhimurium*. *Mol Microbiol* **19**(1)**:** 1-5
3. Akeda Y, Galan JE (2004) Genetic analysis of the *Salmonella enterica* type III secretion-associated ATPase InvC defines discrete functional domains. *J Bacteriol* **186**(8)**:** 2402-2412
4. Allaoui A, Ménard R, Sansonetti PJ, Parsot C (1993) Characterization of the *Shigella flexneri ipgD* and *ipgF* genes, which are located in the proximal part of the mxi locus. *Infect Immun* **61**(5)**:** 1707-1714
5. Allaoui A, Sansonetti PJ, Menard R, Barzu S, Mounier J, Phalipon A, Parsot C (1995) MxiG, a membrane protein required for secretion of *Shigella* spp. Ipa invasins: involvement in entry into epithelial cells and in intercellular dissemination. *Mol Microbiol* **17**(3)**:** 461-470
6. Allaoui A, Woestyn S, Sluiters C, Cornelis GR (1994) YscU, a *Yersinia enterocolitica* inner membrane protein involved in Yop secretion. *J Bacteriol* **176**(15)**:** 4534-4542
7. Andrade A, Pardo JP, Espinosa N, Perez-Hernandez G, Gonzalez-Pedrajo B (2007) Enzymatic characterization of the enteropathogenic *Escherichia coli* type III secretion ATPase EscN. *Arch Biochem Biophys* **468**(1)**:** 121-127
8. Bange G, Kummerer N, Engel C, Bozkurt G, Wild K, Sinning I (2010) FlhA provides the adaptor for coordinated delivery of late flagella building blocks to the type III secretion system. *Proc Natl Acad Sci U S A* **107**(25)**:** 11295-11300
9. Barák I, Muchová K, Wilkinson AJ, O'Toole PJ, Pavlendová N (2008) Lipid spirals in *Bacillus subtilis* and their role in cell division. *Mol Microbiol* **68**(5)**:** 1315-1327
10. Barreteau H, Kovac A, Boniface A, Sova M, Gobec S, Blanot D (2008) Cytoplasmic steps of peptidoglycan biosynthesis. *FEMS Microbiol Rev* **32**(2)**:** 168-207
11. Bendezu FO, Hale CA, Bernhardt TG, de Boer PAJ (2009) RodZ (YfgA) is required for proper assembly of the MreB actin cytoskeleton and cell shape in *E. coli*. *The EMBO Journal* **28**(3)**:** 193-204
12. Biemans-Oldehinkel E, Sal-Man N, Deng W, Foster LJ, Finlay BB (2011) Quantitative Proteomic Analysis Reveals Formation of an EscL-EscQ-EscN Type III Complex in Enteropathogenic E. coli. *Journal of Bacteriology***:** 1-20
13. Blaylock B, Riordan KE, Missiakas DM, Schneewind O (2006) Characterization of the *Yersinia enterocolitica* type III secretion ATPase YscN and its regulator, YscL. *J Bacteriol* **188**(10)**:** 3525-3534

14. Blocker A, Gounon P, Larquet E, Niebuhr K, Cabiaux V, Parsot C, Sansonetti P (1999) The tripartite type III secreton of *Shigella flexneri* inserts IpaB and IpaC into host membranes. *J Cell Biol* **147**(3)**:** 683-693
15. Blocker AJ, Jouihri N, Larquet E, Gounon P, Ebel F, Parsot C, Sansonetti PJ, Allaoui A (2001) Structure and composition of the *Shigella flexneri* "needle complex", a part of its type III secreton. *Mol Microbiol* **39**(3)**:** 652-663
16. Bouhss A, Trunkfield AE, Bugg TD, Mengin-Lecreulx D (2008) The biosynthesis of peptidoglycan lipid-linked intermediates. *FEMS Microbiol Rev* **32**(2)**:** 208-233
17. Chang AC, Cohen SN (1978) Construction and characterization of amplifiable multicopy DNA cloning vehicles derived from the P15A cryptic miniplasmid. *J Bacteriol* **134**(3)**:** 1141-1156
18. Chen S, Beeby M, Murphy GE, Leadbetter JR, Hendrixson DR, Briegel A, Li Z, Shi J, Tocheva EI, Müller A, Dobro MJ, Jensen GJ (2011) Structural diversity of bacterial flagellar motors. *The EMBO Journal*
19. Cordes FS, Komoriya K, Larquet E, Yang S, Egelman EH, Blocker A, Lea SM (2003) Helical structure of the needle of the type III secretion system of *Shigella flexneri*. *J Biol Chem* **278**(19)**:** 17103-17107
20. Cornelis GR (2006) The type III secretion injectisome. *Nat Rev Microbiol* **4**(11)**:** 811-825
21. Cornelis GR, Van Gijsegem F (2000) Assembly and Function of Type III Secretory Systems. *Annual Review of Microbiology*
22. Cornelis GR, Wolf-Watz H (1997) The *Yersinia* Yop virulon: a bacterial system for subverting eukaryotic cells. *Mol Microbiol* **23**(5)**:** 861-867
23. Crago AM, Koronakis V (1998) *Salmonella* InvG forms a ring-like multimer that requires the InvH lipoprotein for outer membrane localization. *Mol Microbiol* **30**(1)**:** 47-56
24. Creasey EA, Delahay RM, Daniell SJ, Frankel G (2003) Yeast two-hybrid system survey of interactions between LEE-encoded proteins of enteropathogenic *Escherichia coli*. *Microbiology (Reading, Engl)* **149**(Pt 8)**:** 2093-2106
25. Crepin VF, Prasannan S, Shaw RK, Wilson RK, Creasey E, Abe CM, Knutton S, Frankel G, Matthews S (2005) Structural and functional studies of the enteropathogenic *Escherichia coli* type III needle complex protein EscJ. *Mol Microbiol* **55**(6)**:** 1658-1670
26. Daefler S, Guilvout I, Hardie KR, Pugsley AP, Russel M (1997) The C-terminal domain of the secretin PulD contains the binding site for its cognate chaperone, PulS, and confers PulS dependence on pIVf1 function. *Mol Microbiol* **24**(3)**:** 465-475
27. Daefler S, Russel M (1998) The *Salmonella typhimurium* InvH protein is an outer membrane lipoprotein required for the proper localization of InvG. *Molecular Microbiology* **28**(6)**:** 1367-1380

28. Daniel RA, Errington J (2003) Control of cell morphogenesis in bacteria: two distinct ways to make a rod-shaped cell. *Cell* **113**(6)**:** 767-776
29. Demchick P, Koch AL (1996) The permeability of the wall fabric of *Escherichia coli* and Bacillus subtilis. *Journal of Bacteriology* **178**(3)**:** 768-773
30. Diepold A, Amstutz M, Abel S, Sorg I, Jenal U, Cornelis GR (2010) Deciphering the assembly of the Yersinia type III secretion injectisome. *The EMBO Journal* **29**(11)**:** 1928-1940
31. Divakaruni AV, Baida C, White CL, Gober JW (2007) The cell shape proteins MreB and MreC control cell morphogenesis by positioning cell wall synthetic complexes. *Mol Microbiol* **66**(1)**:** 174-188
32. Divakaruni AV, Loo RRO, Xie Y, Loo JA, Gober JW (2005) The cell-shape protein MreC interacts with extracytoplasmic proteins including cell wall assembly complexes in *Caulobacter crescentus*. *Proc Natl Acad Sci USA* **102**(51)**:** 18602-18607
33. Dye NA, Pincus Z, Theriot JA, Shapiro L, Gitai Z (2005) Two independent spiral structures control cell shape in *Caulobacter*. *Proc Natl Acad Sci USA* **102**(51)**:** 18608-18613
34. Edqvist PJ, Olsson J, Lavander M, Sundberg L, Forsberg A, Wolf-Watz H, Lloyd SA (2003) YscP and YscU regulate substrate specificity of the *Yersinia* type III secretion system. *J Bacteriol* **185**(7)**:** 2259-2266
35. Eichelberg K, Ginocchio CC, Galan JE (1994) Molecular and functional characterization of the *Salmonella typhimurium* invasion genes invB and invC: homology of InvC to the F0F1 ATPase family of proteins. *J Bacteriol* **176**(15)**:** 4501-4510
36. Fadouloglou VE, Tampakaki AP, Glykos NM, Bastaki MN, Hadden JM, Phillips SE, Panopoulos NJ, Kokkinidis M (2004) Structure of HrcQB-C, a conserved component of the bacterial type III secretion systems. *Proc Natl Acad Sci U S A* **101**(1)**:** 70-75
37. Ferris HU, Minamino T (2006) Flipping the switch: bringing order to flagellar assembly. *Trends Microbiol* **14**(12)**:** 519-526
38. Figge RM, Divakaruni AV, Gober JW (2004) MreB, the cell shape-determining bacterial actin homologue, co-ordinates cell wall morphogenesis in *Caulobacter crescentus*. *Mol Microbiol* **51**(5)**:** 1321-1332
39. Francis NR, Sosinsky GE, Thomas D, DeRosier DJ (1994) Isolation, characterization and structure of bacterial flagellar motors containing the switch complex. *J Mol Biol* **235**(4)**:** 1261-1270
40. Fraser GM, Hirano T, Ferris HU, Devgan LL, Kihara M, Macnab RM (2003) Substrate specificity of type III flagellar protein export in *Salmonella* is controlled by subdomain interactions in FlhB. *Mol Microbiol* **48**(4)**:** 1043-1057

41. Fuchs TM, Brandt K, Starke M, Rattei T (2011) Shotgun sequencing of *Yersinia enterocolitica* strain W22703 (biotype 2, serotype O:9): genomic evidence for oscillation between invertebrates and mammals. *BMC Genomics* **12:** 168
42. Galan JE, Collmer A (1999) Type III secretion machines: bacterial devices for protein delivery into host cells. *Science* **284**(5418)**:** 1322-1328
43. García-Gómez E, Espinosa N, de la Mora J, Dreyfus G, González-Pedrajo B (2011) The muramidase EtgA from enteropathogenic *Escherichia coli* is required for efficient type III secretion. *Microbiology (Reading, Engl)* **157**(Pt 4)**:** 1145-1160
44. Genin S, Boucher CA (1994) A superfamily of proteins involved in different secretion pathways in gram-negative bacteria: modular structure and specificity of the N-terminal domain. *Mol Gen Genet* **243**(1)**:** 112-118
45. Ghosh P (2004) Process of protein transport by the type III secretion system. *Microbiol Mol Biol Rev* **68**(4)**:** 771-795
46. Gitai Z, Dye NA, Reisenauer A, Wachi M, Shapiro L (2005) MreB actin-mediated segregation of a specific region of a bacterial chromosome. *Cell* **120**(3)**:** 329-341
47. Grimm R, Typke D, Barmann M, Baumeister W (1996) Determination of the inelastic mean free path in ice by examination of tilted vesicles and automated most probable loss imaging. *Ultramicroscopy* **63**(3-4)**:** 169-179
48. Hakansson S, Bergman T, Vanooteghem JC, Cornelis G, Wolf-Watz H (1993) YopB and YopD constitute a novel class of Yersinia Yop proteins. *Infect Immun* **61**(1)**:** 71-80
49. Haller JC, Carlson S, Pederson KJ, Pierson DE (2000) A chromosomally encoded type III secretion pathway in *Yersinia enterocolitica* is important in virulence. *Mol Microbiol* **36**(6)**:** 1436-1446
50. Hardie KR, Lory S, Pugsley AP (1996) Insertion of an outer membrane protein in *Escherichia coli* requires a chaperone-like protein. *The EMBO Journal* **15**(5)**:** 978-988
51. Hodgkinson J, Horsley A, Stabat D, Simon M, Johnson S, da Fonseca P, Morris E, Wall J, Lea SM, Blocker AJ (2009) Three-dimensional reconstruction of the *Shigella* T3SS transmembrane regions reveals 12-fold symmetry and novel features throughout. *Nat Struct Mol Biol*
52. Hoiczyk E, Blobel G (2001) Polymerization of a single protein of the pathogen *Yersinia enterocolitica* into needles punctures eukaryotic cells. *Proc Natl Acad Sci USA* **98**(8)**:** 4669-4674
53. Hu Z, Lutkenhaus J (1999) Topological regulation of cell division in *Escherichia coli* involves rapid pole to pole oscillation of the division inhibitor MinC under the control of MinD and MinE. *Mol Microbiol* **34**(1)**:** 82-90
54. Iriarte M, Cornelis GR (1998) YopT, a new Yersinia Yop effector protein, affects the cytoskeleton of host cells. *Molecular Microbiology*

55. Iriarte M, Cornelis GR (1999) The 70-Kilobase Virulence Plasmid of *Yersiniae*. In *Pathogenicity islands and other mobile virulence elements*, Kaper JB, Hacker J (eds), Chapter 6, pp 91-126. Washington, D.C.: ASM Press
56. Izoré T, Job V, Dessen A (2011) Biogenesis, Regulation, and Targeting of the Type III Secretion System. *Structure* **19**(5)**:** 603-612
57. Jackson MW, Plano GV (2000) Interactions between type III secretion apparatus components from *Yersinia pestis* detected using the yeast two-hybrid system. *FEMS Microbiology Letters* **186**(1)**:** 85-90
58. Johnson S, Blocker AJ (2008) Characterization of soluble complexes of the *Shigella flexneri* type III secretion system ATPase. *FEMS Microbiology Letters* **286**(2)**:** 274-278
59. Jones LJ, Carballido-López R, Errington J (2001) Control of cell shape in bacteria: helical, actin-like filaments in *Bacillus subtilis*. *Cell* **104**(6)**:** 913-922
60. Jouihri N, Sory M-P, Page A-L, Gounon P, Parsot C, Allaoui A (2003) MxiK and MxiN interact with the Spa47 ATPase and are required for transit of the needle components MxiH and MxiI, but not of Ipa proteins, through the type III secretion apparatus of *Shigella flexneri*. *Mol Microbiol* **49**(3)**:** 755-767
61. Journet L, Agrain C, Broz P, Cornelis GR (2003) The needle length of bacterial injectisomes is determined by a molecular ruler. *Science* **302**(5651)**:** 1757-1760
62. Kaniga K, Delor I, Cornelis GR (1991) A wide-host-range suicide vector for improving reverse genetics in gram-negative bacteria: inactivation of the blaA gene of *Yersinia enterocolitica*. *Gene* **109**(1)**:** 137-141
63. Kawagishi I, Homma M, Williams AW, Macnab RM (1996) Characterization of the flagellar hook length control protein fliK of Salmonella typhimurium and *Escherichia coli*. *J Bacteriol* **178**(10)**:** 2954-2959
64. Khan IH, Reese TS, Khan S (1992) The cytoplasmic component of the bacterial flagellar motor. *Proc Natl Acad Sci U S A* **89**(13)**:** 5956-5960
65. Kimbrough TG, Miller SI (2000) Contribution of *Salmonella typhimurium* type III secretion components to needle complex formation. *Proc Natl Acad Sci USA* **97**(20)**:** 11008-11013
66. Kimbrough TG, Miller SI (2002) Assembly of the type III secretion needle complex of *Salmonella typhimurium*. *Microbes Infect* **4**(1)**:** 75-82
67. Knutton S, Rosenshine I, Pallen MJ, Nisan I, Neves BC, Bain C, Wolff C, Dougan G, Frankel G (1998) A novel EspA-associated surface organelle of enteropathogenic *Escherichia coli* involved in protein translocation into epithelial cells. *EMBO J* **17**(8)**:** 2166-2176
68. Koffler H, Kobayashi T (1957) Purification of flagella and flagellin with ammonium sulfate. *Arch Biochem Biophys* **67**(1)**:** 246-248

69. Koraimann G (2003) Lytic transglycosylases in macromolecular transport systems of Gram-negative bacteria. *Cellular and molecular life sciences : CMLS* **60**(11)**:** 2371-2388
70. Koster M, Bitter W, de Cock H, Allaoui A, Cornelis GR, Tommassen J (1997) The outer membrane component, YscC, of the Yop secretion machinery of *Yersinia enterocolitica* forms a ring-shaped multimeric complex. *Mol Microbiol* **26**(4)**:** 789-797
71. Kruse T, Bork-Jensen J, Gerdes K (2005) The morphogenetic MreBCD proteins of *Escherichia coli* form an essential membrane-bound complex. *Mol Microbiol* **55**(1)**:** 78-89
72. Kubori T, Matsushima Y, Nakamura D, Uralil J, Lara-Tejero M, Sukhan A, Galán JE, Aizawa S-I (1998) Supramolecular structure of the *Salmonella typhimurium* type III protein secretion system. *Science* **280**(5363)**:** 602-605
73. Kubori T, Shimamoto N, Yamaguchi S, Namba K, Aizawa S (1992) Morphological pathway of flagellar assembly in *Salmonella typhimurium*. *J Mol Biol* **226**(2)**:** 433-446
74. Kubori T, Sukhan A, Aizawa S-I, Galán JE (2000) Molecular characterization and assembly of the needle complex of the *Salmonella typhimurium* type III protein secretion system. *Proc Natl Acad Sci USA* **97**(18)**:** 10225-10230
75. Kudryashev M, Cyrklaff M, Wallich R, Baumeister W, Frischknecht F (2010) Distinct in situ structures of the *Borrelia* flagellar motor. *J Struct Biol* **169**(1)**:** 54-61
76. Kutsukake K, Minamino T, Yokoseki T (1994) Isolation and characterization of FliK-independent flagellation mutants from *Salmonella typhimurium*. *J Bacteriol* **176**(24)**:** 7625-7629
77. Langhorst MF, Reuter A, Stuermer CA (2005) Scaffolding microdomains and beyond: the function of reggie/flotillin proteins. *Cell Mol Life Sci* **62**(19-20)**:** 2228-2240
78. Lavander M, Sundberg L, Edqvist PJ, Lloyd SA, Wolf-Watz H, Forsberg A (2002) Proteolytic cleavage of the FlhB homologue YscU of *Yersinia pseudotuberculosis* is essential for bacterial survival but not for type III secretion. *J Bacteriol* **184**(16)**:** 4500-4509
79. Lilic M, Quezada CM, Stebbins CE (2010) A conserved domain in type III secretion links the cytoplasmic domain of InvA to elements of the basal body. *Acta Crystallogr D Biol Crystallogr* **66**(Pt 6)**:** 709-713
80. López D, Kolter R (2010) Functional microdomains in bacterial membranes. *Genes Dev* **24**(17)**:** 1893-1902
81. Macnab RM (2003) How bacteria assemble flagella. *Annual Review of Microbiology* **57:** 77-100
82. Marlovits TC, Kubori T, Lara-Tejero M, Thomas DR, Unger VM, Galán JE (2006) Assembly of the inner rod determines needle length in the type III secretion injectisome. *Nature* **441**(7093)**:** 637-640

83. Marlovits TC, Kubori T, Sukhan A, Thomas DR, Galán JE, Unger VM (2004) Structural insights into the assembly of the type III secretion needle complex. *Science* **306**(5698)**:** 1040-1042
84. Marlovits TC, Stebbins CE (2009) Type III secretion systems shape up as they ship out. *Curr Opin Microbiol*
85. Matias VR, Al-Amoudi A, Dubochet J, Beveridge TJ (2003) Cryo-transmission electron microscopy of frozen-hydrated sections of *Escherichia coli* and *Pseudomonas aeruginosa. J Bacteriol* **185**(20)**:** 6112-6118
86. McDowell MA, Johnson S, Deane JE, Cheung M, Roehrich AD, Blocker AJ, McDonnell JM, Lea SM (2011) Structural and functional studies on the N-terminal domain of the *Shigella* type III secretion protein MxiG. *J Biol Chem*
87. Ménard R, Sansonetti PJ, Parsot C (1993) Nonpolar mutagenesis of the ipa genes defines IpaB, IpaC, and IpaD as effectors of *Shigella flexneri* entry into epithelial cells. *Journal of Bacteriology* **175**(18)**:** 5899-5906
88. Metcalf WW, Jiang W, Wanner BL (1994) Use of the rep technique for allele replacement to construct new *Escherichia coli* hosts for maintenance of R6K gamma origin plasmids at different copy numbers. *Gene* **138**(1-2)**:** 1-7
89. Michiels T, Vanooteghem JC, Lambert de Rouvroit C, China B, Gustin A, Boudry P, Cornelis GR (1991) Analysis of virC, an operon involved in the secretion of Yop proteins by *Yersinia enterocolitica*. *J Bacteriol* **173**(16)**:** 4994-5009
90. Milne JLS, Subramaniam S (2009) Cryo-electron tomography of bacteria: progress, challenges and future prospects. *Nat Rev Microbiol* **7**(9)**:** 666-675
91. Minamino T, Macnab RM (2000) Domain structure of *Salmonella* FlhB, a flagellar export component responsible for substrate specificity switching. *J Bacteriol* **182**(17)**:** 4906-4914
92. Miyahara M, Maruyama T, Wake A, Mise K (1988) Widespread occurrence of the restriction endonuclease YenI, an isoschizomer of PstI, in *Yersinia enterocolitica* serotype O8. *Appl Environ Microbiol* **54**(2)**:** 577-580
93. Moore SA, Jia Y (2010) Structure of the cytoplasmic domain of the flagellar secretion apparatus component FlhA from *Helicobacter pylori*. *J Biol Chem* **285**(27)**:** 21060-21069
94. Morita-Ishihara T, Ogawa M, Sagara H, Yoshida M, Katayama E, Sasakawa C (2006) *Shigella* Spa33 is an essential C-ring component of type III secretion machinery. *J Biol Chem* **281**(1)**:** 599-607
95. Mota LJ, Journet L, Sorg I, Agrain C, Cornelis GR (2005) Bacterial Injectisomes: Needle Length Does Matter. *Science*

96. Mueller CA, Broz P, Müller SA, Ringler P, F Erne-Brand F, Sorg I, Kuhn M, Engel A, Cornelis GR (2005) The V-antigen of *Yersinia* forms a distinct structure at the tip of injectisome needles. *Science* **310**(5748)**:** 674-676
97. Müller SA, Pozidis C, Stone R, Meesters C, Chami M, Engel A, Economou A, Stahlberg H (2006) Double hexameric ring assembly of the type III protein translocase ATPase HrcN. *Mol Microbiol* **61**(1)**:** 119-125
98. Murphy GE, Leadbetter JR, Jensen GJ (2006) In situ structure of the complete *Treponema primitia* flagellar motor. *Nature* **442**(7106)**:** 1062-1064
99. Nambu T, Minamino T, Macnab RM, Kutsukake K (1999) Peptidoglycan-hydrolyzing activity of the FlgJ protein, essential for flagellar rod formation in *Salmonella typhimurium*. *Journal of Bacteriology* **181**(5)**:** 1555-1561
100. Pallen M, Chaudhuri R, Khan A (2002) Bacterial FHA domains: neglected players in the phospho-threonine signalling game? *Trends Microbiol* **10**(12)**:** 556-563
101. Pallen MJ, Bailey CM, Beatson SA (2006) Evolutionary links between FliH/YscL-like proteins from bacterial type III secretion systems and second-stalk components of the FoF1 and vacuolar ATPases. *Protein Sci* **15**(4)**:** 935-941
102. Pallen MJ, Beatson SA, Bailey CM (2005) Bioinformatics, genomics and evolution of non-flagellar type-III secretion systems: a Darwinian perspective. *FEMS Microbiol Rev* **29**(2)**:** 201-229
103. Plano GV, Barve SS, Straley SC (1991) LcrD, a membrane-bound regulator of the *Yersinia pestis* low-calcium response. *J Bacteriol* **173**(22)**:** 7293-7303
104. Portnoy DA, Moseley SL, Falkow S (1981) Characterization of plasmids and plasmid-associated determinants of *Yersinia enterocolitica* pathogenesis. *Infect Immun* **31**(2)**:** 775-782
105. Pozidis C, Chalkiadaki A, Gomez-Serrano A, Stahlberg H, Brown I, Tampakaki AP, Lustig A, Sianidis G, Politou AS, Engel A, Panopoulos NJ, Mansfield J, Pugsley AP, Karamanou S, Economou A (2003) Type III protein translocase: HrcN is a peripheral ATPase that is activated by oligomerization. *J Biol Chem* **278**(28)**:** 25816-25824
106. Quinaud M, Chabert J, Faudry E, Neumann E, Lemaire D, Pastor A, Elsen S, Dessen A, Attree I (2005) The PscE-PscF-PscG complex controls type III secretion needle biogenesis in *Pseudomonas aeruginosa*. *J Biol Chem* **280**(43)**:** 36293-36300
107. Quinaud M, Ple S, Job V, Contreras-Martel C, Simorre JP, Attree I, Dessen A (2007) Structure of the heterotrimeric complex that regulates type III secretion needle formation. *Proc Natl Acad Sci U S A* **104**(19)**:** 7803-7808
108. Rothfield L, Taghbalout A, Shih Y-L (2005) Spatial control of bacterial division-site placement. *Nat Rev Microbiol* **3**(12)**:** 959-968

109. Sanowar S, Singh P, Pfuetzner RA, Andre I, Zheng H, Spreter T, Strynadka NCJ, Gonen T, Baker D, Goodlett DR, Miller SI (2010) Interactions of the Transmembrane Polymeric Rings of the *Salmonella enterica* Serovar Typhimurium Type III Secretion System. *mBio* **1**(3)**:** e00158-00110-e00158-00117
110. Sarker M, Sory M-P, Boyd AP, Iriarte M, Cornelis GR (1998) LcrG is Required for Efficient Translocation of *Yersinia* Yop Effector Proteins into Eukaryotic Cells. *Infection and Immunity*
111. Scheurwater E, Reid CW, Clarke AJ (2008) Lytic transglycosylases: bacterial space-making autolysins. *Int J Biochem Cell Biol* **40**(4)**:** 586-591
112. Scheurwater EM, Burrows LL Maintaining network security: how macromolecular structures cross the peptidoglycan layer. *FEMS Microbiol Lett* **318**(1)**:** 1-9
113. Schraidt O, Marlovits TC (2011) Three-dimensional model of *Salmonella*'s needle complex at subnanometer resolution. *Science* **331**(6021)**:** 1192-1195
114. Schuster SC, Baeuerlein E (1992) Location of the basal disk and a ringlike cytoplasmic structure, two additional structures of the flagellar apparatus of *Wolinella succinogenes*. *J Bacteriol* **174**(1)**:** 263-268
115. Sekiya K, Ohishi M, Ogino T, Tamano K, Sasakawa C, Abe A (2001) Supermolecular structure of the enteropathogenic *Escherichia coli* type III secretion system and its direct interaction with the EspA-sheath-like structure. *Proc Natl Acad Sci USA* **98**(20)**:** 11638-11643
116. Shih YL, Le T, Rothfield L (2003) Division site selection in *Escherichia coli* involves dynamic redistribution of Min proteins within coiled structures that extend between the two cell poles. *Proc Natl Acad Sci U S A* **100**(13)**:** 7865-7870
117. Sorg I, Wagner S, Amstutz M, Müller SA, Broz P, Lussi Y, Engel A, Cornelis GR (2007) YscU recognizes translocators as export substrates of the *Yersinia* injectisome. *EMBO J* **26**(12)**:** 3015-3024
118. Sory M-P, Boland A, Lambermont I, Cornelis GR (1995) Identification of the YopE and YopH domains required for secretion and internalization into the cytosol of macrophages, using the cyaA gene fusion approach. *Proc Natl Acad Sci USA* **92**(26)**:** 11998-12002
119. Spreter T, Yip C, Sanowar S, André I, Kimbrough TG, Vuckovic M, Pfuetzner R, Deng W, Yu A, Finlay BB, Baker D, Miller S, Strynadka NCJ (2009) A conserved structural motif mediates formation of the periplasmic rings in the type III secretion system. *Nat Struct Mol Biol*
120. Strahl H, Hamoen LW (2010) Membrane potential is important for bacterial cell division. *Proc Natl Acad Sci USA* **107**(27)**:** 12281-12286

121. Suefuji K, Valluzzi R, RayChaudhuri D (2002) Dynamic assembly of MinD into filament bundles modulated by ATP, phospholipids, and MinE. *Proc Natl Acad Sci U S A* **99**(26)**:** 16776-16781
122. Sukhan A, Kubori T, Wilson J, Galán JE (2001) Genetic analysis of assembly of the *Salmonella enterica* serovar Typhimurium type III secretion-associated needle complex. *Journal of Bacteriology* **183**(4)**:** 1159-1167
123. Sun P, Tropea JE, Austin BP, Cherry S, Waugh DS (2008) Structural characterization of the *Yersinia pestis* type III secretion system needle protein YscF in complex with its heterodimeric chaperone YscE/YscG. *J Mol Biol* **377**(3)**:** 819-830
124. Suzuki T, Iino T, Horiguchi T, Yamaguchi S (1978) Incomplete flagellar structures in nonflagellate mutants of *Salmonella typhimurium*. *J Bacteriol* **133**(2)**:** 904-915
125. Swulius MT, Chen S, Jane Ding H, Li Z, Briegel A, Pilhofer M, Tocheva EI, Lybarger SR, Johnson TL, Sandkvist M, Jensen GJ (2011) Long helical filaments are not seen encircling cells in electron cryotomograms of rod-shaped bacteria. *Biochem Biophys Res Commun*
126. Szeto TH, Rowland SL, Rothfield LI, King GF (2002) Membrane localization of MinD is mediated by a C-terminal motif that is conserved across eubacteria, archaea, and chloroplasts. *Proc Natl Acad Sci U S A* **99**(24)**:** 15693-15698
127. Tamano K, Aizawa S, Katayama E, Nonaka T, Imajoh-Ohmi S, Kuwae A, Nagai S, Sasakawa C (2000) Supramolecular structure of the *Shigella* type III secretion machinery: the needle part is changeable in length and essential for delivery of effectors. *The EMBO Journal* **19**(15)**:** 3876-3887
128. Thanbichler M, Iniesta AA, Shapiro L (2007) A comprehensive set of plasmids for vanillate- and xylose-inducible gene expression in *Caulobacter crescentus*. *Nucleic Acids Res* **35**(20)**:** e137
129. Troisfontaines P, Cornelis GR (2005) Type III secretion: more systems than you think. *Physiology (Bethesda, Md)* **20:** 326-339
130. Typas A, Banzhaf M, Gross CA, Vollmer W (2012) From the regulation of peptidoglycan synthesis to bacterial growth and morphology. *Nat Rev Microbiol* **10**(2)**:** 123-136
131. Van Arnam JS, McMurry JL, Kihara M, Macnab RM (2004) Analysis of an engineered *Salmonella* flagellar fusion protein, FliR-FlhB. *J Bacteriol* **186**(8)**:** 2495-2498
132. van den Ent F, Amos LA, Löwe J (2001) Prokaryotic origin of the actin cytoskeleton. *Nature* **413**(6851)**:** 39-44
133. Wagner S, Sorg I, Degiacomi M, Journet L, Dal Peraro M, Cornelis GR (2009) The helical content of the YscP molecular ruler determines the length of the *Yersinia* injectisome. *Molecular Microbiology* **71**(3)**:** 692-701

134. White CL, Kitich A, Gober JW (2010) Positioning cell wall synthetic complexes by the bacterial morphogenetic proteins MreB and MreD. *Mol Microbiol*
135. Williams AW, Yamaguchi S, Togashi F, Aizawa SI, Kawagishi I, Macnab RM (1996) Mutations in *fliK* and *flhB* affecting flagellar hook and filament assembly in *Salmonella typhimurium*. *J Bacteriol* **178**(10)**:** 2960-2970
136. Woestyn S, Allaoui A, Wattiau P, Cornelis GR (1994) YscN, the putative energizer of the *Yersinia* Yop secretion machinery. *Journal of Bacteriology* **176**(6)**:** 1561-1569
137. Worrall LJ, Lameignere E, Strynadka NC (2011) Structural overview of the bacterial injectisome. *Curr Opin Microbiol* **14**(1)**:** 3-8
138. Worrall LJ, Vuckovic M, Strynadka NCJ (2010) Crystal structure of the C-terminal domain of the *Salmonella* type III secretion system export apparatus protein InvA. *Protein Sci* **19**(5)**:** 1091-1096
139. Yip CK, Kimbrough TG, Felise HB, Vuckovic M, Thomas NA, Pfuetzner RA, Frey EA, Finlay BB, Miller SI, Strynadka NCJ (2005) Structural characterization of the molecular platform for type III secretion system assembly. *Nature* **435**(7042)**:** 702-707
140. Yu Y-C, Lin C-N, Wang S-H, Ng S-C, Hu WS, Syu W-J (2010) A putative lytic transglycosylase tightly regulated and critical for the EHEC type three secretion. *Journal of biomedical science* **17**(1)**:** 52
141. Zahrl D, Wagner M, Bischof K, Bayer M, Zavecz B, Beranek A, Ruckenstuhl C, Zarfel GE, Koraimann G (2005) Peptidoglycan degradation by specialized lytic transglycosylases associated with type III and type IV secretion systems. *Microbiology (Reading, Engl)* **151**(Pt 11)**:** 3455-3467
142. Zarivach R, Vuckovic M, Deng W, Finlay BB, Strynadka NCJ (2007) Structural analysis of a prototypical ATPase from the type III secretion system. *Nat Struct Mol Biol* **14**(2)**:** 131-137
143. Zhang L, Wang Y, Picking WL, Picking WD, De Guzman RN (2006) Solution structure of monomeric BsaL, the type III secretion needle protein of *Burkholderia pseudomallei*. *J Mol Biol* **359**(2)**:** 322-330

10 Acknowledgments

Finally I would like to thank the numerous persons who supported me during my work and without their help this would not have been possible:

Isabel Sorg, she was a good teacher and introduced me well into the T3S field. She did not just teach me the experimental procedures but also to work accurate and to do all the proper controls. To work hand in hand with **Andreas Diepold** was very energizing, we had lots of stimulating scientific discussions and solved several little "puzzles". Many thanks to **Misha Kudryashev,** with whom collaboration actually was a benefit for both sides, although or maybe because, we come out of two different scientific worlds. **Sören Abel** my saviour. Whenever I had any trouble with the microscope, which was not rarely, he would always find time to help me.

The technical and administrative staff: **Michaela Hanisch** for great organisation skills, **Marina Kuhn** for excellent lab and floor management, **Roger Sauder** for his "McGyver" skills. **Roland Gut** and **Verena Heusner** for media preparation.

All the present and former lab members for a great working atmosphere, interesting discussions, inputs and support: **Christian Arquint**, **Petr Broz**, **Claudio Cadel**, **Salome Casutt-Meyer**, **Cédric Cattin**, **Yaniv Cohen**, **Fabian Commichau**, **Gottfried Eisner**, **Chantal Fiechter**, **Catherine Haberthür-Müller**, **Simon Ittig**, **Kristina Kolygo**, **Frédéric Lauber**, **Michel Letzelter**, **Manuela Mally**, **Pablo Manfredi**, **Oliver Märki**, **Lisa Metzger**, **Cecile Pfaff**, **Francesco Renzi**, **Anna Rozhkova**, **Loïc Sauteur**, **Hwain Shin**, **Steffi Wagner** and **Ulrich Wiesand**.

Last but not least many thanks to **Guy Cornelis,** who supported and guided me during my thesis.